A THEORETICAL FORMULATION OF INITIAL STATE WAVEFUNCTIONS FOR PHOTOEMISSION CALCULATIONS

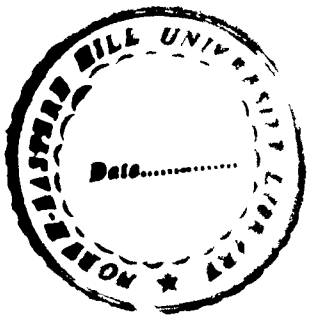

By

B. Zoliana

Department of Physics

Submitted

in fulfilment of the requirement of the

Degree of Doctor of Philosophy in Physics of

North-Eastern Hill University, Shillong.

Thesis

DS
537.54
ZOL;1

In loving memory of my parents, who encouraged, supported and loved me throughout their lives.

Declaration of the Candidate

The North-Eastern Hill University

July 2004

I, B. Zoliana, hereby declare that the subject matter of this thesis is the record of the work done by me, that the contents of this thesis did not form basis of the award of any previous degree to me or to the best of my knowledge to anybody else, and that the thesis has not been submitted by me for any research degree in any other University/Institute.

This is being submitted to the North-Eastern Hill University for the degree of Doctor of Philosophy in Physics.

(B. ZOLIANA)
Candidate

Countersigned 30.7.04

(DR. M. K. PARIDA)
Professor & Head
Department of Physics
North-Eastern Hill University
Shillong- 793 022.

Prof. & Head
Department,
NEHU Shillong-793022

(DR. D. T. KHATHING)
Professor
Department of Physics
North-Eastern Hill University
Shillong- 793 022.
Supervisor

(DR. R. K. THAPA)
Reader
Department of Physics
Pachhunga University College
Mizoram University
Aizawl, Mizoram.
Joint Supervisor.

ACKNOWLEDGEMENT

I shall be failing in my duty if I did not unreservedly acknowledge my indebtedness to important people on completion of my research works for my Ph.D. degree. First of all, I would like to thank Prof. D.T. Khathing, Department of Physics, North-Eastern Hill University, Shillong, my research Supervisor for his guidance, understanding and help during my works related to this thesis. I would like to give my special thanks to my Joint Supervisor Dr. R.K. Thapa, Reader, Department of Physics, Pachhunga University College, Mizoram University, Aizawl, Mizoram for his untiring guidance, help and constant support. It was him who initiated the research topic of investigation for this Ph.D. works and had always been encouraging me to go ahead, sparing his precious time for my works without which I could not have completed my research works.

I am deeply grateful to Dr. P. K. Patra, Science Centre, North-Eastern Hill University, Shillong for his invaluable help and suggestions in my research works and sparing his time for discussions which were very beneficial. I would also like to thank Dr. Zaithanzauva Pachuau, Department of Physics, Govt. Zirtiri Residential Science College, Aizawl and Ms. Lalthakimi Zadeng, Condensed Matter Theory Research Group, Pachhunga University College, Mizoram University, Aizawl for their great help and cooperation.

Cooperation and encouragement received from the Faculty Members of the Department of Physics, North-Eastern Hill University, Shillong is also highly appreciated.

I would like to express thanks and appreciation to the Department of Higher and Technical Education, Govt. of Mizoram for the financial support through Senior Research Fellowship awarded to me.

Thanks are also due to Prof. S.G. Davison and Mrs. Prue Davison, University of Waterloo, Ontario, Canada for providing books and journals related to my research works.

My thanks are no less due to Mrs. K. Thapa, for her hospitality and kindness.

Last but not the least, I would like to express my deep sense of gratitude to my wife Vanlalsangi, my children and to those special people, for their constant prayers and moral supports for which this work could have been completed. I thank God once again, for giving me good health and all these beloved ones, who contributed in different ways for the completion of my research works.

Dated: 24th July, 2004

Department of Physics
North-Eastern Hill University
Shillong - 793 022.

(B. Zoliana)

CONTENTS

Chapter		Topic	Page
		Declaration of the candidate	
		Acknowledgement	
		List of Figures	viii
		Synopsis of Ph.D. Thesis	xi
1	:	Introduction	1
2	:	Calculation of Electromagnetic Fields	15
	2. 1:	Dielectric Model and Calculation of Electromagnetic Fields	17
	2. 2:	Evaluation of Electromagnetic Fields.	32
3	:	Photocurrent Calculations using Mathieu Potential Model.	46
	3. 1:	Formalism Used	48
	3. 2:	Results and Discussions	50
4	:	A Theoretical Formulation of Initial State Wavefunction for Photoemission Calculation by using Projection Operator Method of Group Theory	62
	4. 1:	Application of Projection Operator Method to Deduce the Basis Function	65
	4. 2:	Formulation of Initial State Wavefunction by using Basis Functions Derived by Projection Operator Method	67
5	:	Conclusion	90

APPENDIX -I:	Surface State Photoemission Calculations by using Mathieu Potential Model (the case of Strong Potential).	95
APPENDIX -II:	FORTRAN Programme for Surface State Photoemission Calculations by using Mathieu Potential Model (Strong Potential case).	98
APPENDIX -III:	Derivation of Basis Function by Using Projection Operator Method of Group Theory for Development of Initial State Wavefunction for Photoemission Calculations.	102
APPENDIX -IV:	FORTRAN Programme for Calculation of Photocurrent by using Projection Operator Technique applied to an Empty Potential case.	111
APPENDIX -V:	FORTRAN Programme to Calculate Photocurrent by using Projection Operator Technique applied to Crystal defined by Kronig-Penney δ - Potential.	116
	References	121
	Biodata	126

LIST OF FIGURES

Figures			Page
1.1	:	Schematic diagram of Angle Resolved Ultraviolet Photoemission Spectroscopy (ARUPS).	5
2.1	:	Dielectric model used for the calculation of vector potential.	18
2.2	:	Plot of variation of square of electromagnetic field $\left\|\tilde{A}_{\omega}(z)\right\|^2$ against photon energy in the case of Ag for locationof surface plane at z = - *d* (bulk), z = - 0.5 *d* (surface) andz = 0 (vacuum).	34
2.3	:	Plot of variation of $\left\|\tilde{A}_{\omega}(z)\right\|^2$ against the distance *z/d* for Ag.	35
2.4	:	Variation of square of electromagnetic field plotted against photon energy in the case of Al for location of surface plane at z = -*d* (bulk), z = - 0.5 *d* (surface) and z = 0 (vacuum).	36
2.5	:	Plot of square of electromagnetic field against distance for Al.	37
2.6	:	Plot of $\frac{d\tilde{A}_{\omega}}{dz}$ against distance from the surface for photon energies 9 eV, 11 eV and 13 eV in Al.	38
2.7	:	Variation of square of electromagnetic field plotted against photon energy in the case of Cr for location of surface plane at z = -*d* (bulk), z = - 0.5 *d* (surface) and z = 0 (vacuum).	40
2.8	:	Plot of square of electromagnetic field against photon energy for location of surface planes at z = - *d* (bulk), z = -0.5 *d* (surface) and z = 0 (vacuum) in the case of GaAs.	42

2.9	:	Plot of square of electromagnetic field against photon energy for location of surface planes at z = - d (bulk), z = -0.5d (surface) and z = 0 (vacuum) in the case of InAs.	44
3.1	:	Plot of photocurrent against photon energy with ψ_i defined by Mathieu potential in the case of Ag.	53
3.2	:	Plot of photocurrent against photon energy with ψ_i defined by Mathieu potential in the case of Fe.	54
3.3	:	Plot of photocurrent against photon energy with ψ_i defined by Mathieu potential in the case of Ni.	55
3.4	:	Plot of photocurrent against photon energy with ψ_i defined by Mathieu potential in the case of Pd.	56
3.5	:	Plot of photocurrent against photon energy with ψ_i defined by Mathieu potential in the case of GaAs.	58
3.6	:	Plot of photocurrent against photon energy with ψ_i defined by Mathieu potential in the case of PbSe.	59
4.1	:	Model Potential diagram for calculating initial state wavefunction ψ_i for the case of an empty potential crystal.	68
4.2	:	Plot of photocurrent as a function of photon energy for Cu for surface state located at 2.72 eV below Fermi level with surface width d= 10 a.u.	71
4.3	:	Schematic representation of Kronig-Penney δ-potential model for calculating the initial state wave function by using projection operator method of Group Theory.	73

4.4	:	Plot of photocurrent variation against photon energy in the case of Al, for surface width d= 10 a.u.and d= 0 by employing Kronig-Penney δ -potential with inset showing the experimental results.	79
4.5	:	Plot of photocurrent against photon energy for surface widths d= 10 a.u and d= 0 in Be using Kronig-Penney δ -potential where ψ_i is derived by projection operator methodof Group Theory.	81
4.6	:	Plot of variation of photocurrent with photon energy for surface widths d= 10 a.u and d= 0 in Cu using Kronig-Penney δ -potential where ψ_i is derived by projection operator methodof Group Theory.	82
4.7	:	Plot of photocurrent variation with photon energy for two surface widths d= 10 a.u and d= 0 in W using Kronig-Penney δ -potential with experimental data in the inset.	84
4.8	:	Plot of photocurrent variation with photon energy in GaAs for surface widths d= 10 a.u. and d= 0 using Kronig-Penney δ -potential where ψ_i is derived by projection operator method of Group Theory.	86
4.9	:	Plot of photocurrent variation with photon energy for surface widths d= 10 a.u and d= 0 in Si. Kronig-Penney δ -potential model is employed and the initial state wavefunction is calculated by using projection operator method of Group Theory.	88

SYNOPSIS OF Ph.D. THESIS

A THEORETICAL FORMULATION OF INITIAL STATE WAVEFUNCTIONS FOR PHOTOEMISSION CALCULATIONS.

Introduction :

Over the last few years interests in a detailed understanding of physical properties of condensed materials and their surfaces has grown enormously for many reasons. Catalytic reactions, for example, which are of great technical importance, strongly depend on the electronic and geometric structure of a solid surface. Furthermore, the miniaturization in microelectronics has reached a point where surface properties become dominant. Also great progress has been made in the production of nearly two-dimensional structures like multilayers or thin films, which have new and fascinating features. For investigating the electronic properties of clean and adsorbate-covered surfaces and thin films, angle-resolved ultraviolet photoelectron spectroscopy (ARUPS) has become important tools, because these experimental techniques allows measuring the dispersion of occupied bands as well the unoccupied bands in and around Fermi level. More detailed informations about the ARUPS has been provided by Feuerbacher *et. al.*[1], Inglesfield[2], Willis *et. al.*[3], Dose[4], Glasser *et. al.*[5] , Plummer and Eberhardt[6], Kar[7], Schattke[8], Braun[9] etc.

Photoemission is concerned with the emission of electrons from the surface/bulk of metals by the reaction of incident photon radiation with the electrons. The high absorption coefficient of the ultra-violet (U.V.) radiation and the small escape depth of the electrons emitted from the solid gives U.V. spectroscopy a big

advantage over the other methods of investigating the electronic states on the surface of solids. Basically, the understanding of the electronic structure of solids and solid surfaces depends on the quality of the photoemission results. Therefore, a steady improvement and growing amount of data will be necessary to put the actual *ab-initio* results of electronic structure calculations into a physically realistic context. The knowledge of the electronic energy spectrum is fundamental to many equilibrium and transport properties and thereby photoemission deserves high interest from basic research as well as from technical application. The interplay between band structure calculation and photoemission measurement is controlled by the interpretation schemes to extract the information about the electronic states and their energies from the spectra. There are a lot of more or less heuristic methods which allow a quick access to a part of the physical content in the experimental data. However, all of them lack the accuracy required if the actual high quality of measurement and the actual state of the art of *ab-initio* calculations should make sense. As in many other techniques the spectra cannot be formally inverted to yield the electronic structure but have to be brought to convergence with theory by trial and error procedures.

In its simplest version the golden rule formula contains the matrix elements between the initial bound states and the final states which are scattering solutions of the same hamiltonian for the dipole operator of the electromagnetic field, and the delta function for energy conservation. The numerical evaluation of golden rule formula yields the photocurrent at the detector which has to be compared with the experimental value. As even *ab-initio* electronic structure calculations are not free of parameters, one can only minimize the disagreement between experiment and theory in choosing the available quantities appropriately. There may be various

approximations in the evaluation of the wavefunctions according to the specific intentions. In the best case one can selfconsistently construct one particle potential adapted to the real surface. Bloch states or equivalently the Green functions for the valence band part as well as the scattering states for conduction bands are calculated. The latter are equivalent to the time inverse states of a low energy electron diffraction (LEED) system representing the final states accepted by the photoemission detector. The transfer of these ideas into a working numerical programme is far from being trivial and has been first accomplished in a closed form by neglecting the relativistic effects and choosing muffin-tin potential[10] obtained from atomic calculations. However, this does not guarantee that the agreement with the experiment is splendid. Especially, semiconductors with their reconstructed surfaces[1, 11] still represent a challenge to the theoretical photoemission.

2. **Research design and Methodology** :

The golden rule formula for calculating the photocurrent density is given by,

$$\frac{dj(E)}{d\Omega} = \frac{2\pi}{\hbar} \sum |< \psi_f | \Delta | \psi_i >|^2 \, \delta(E - E_f) \delta(E_f - E_i - \hbar\omega) \, f_o(E - \hbar\omega)[1 - f_o(E)] \ldots (1)$$

where Δ is the perturbation responsible for photoemission by radiation of frequency ω and $\psi_i(\psi_f)$ refers to the initial (final) state wavefunction, $E_i(E_f)$ the initial (final) state energy, $f_o(E)$ denotes the Fermi occupation function. We are considering the photoemission to take place along z - axis which is normal to the surface. We may therefore write Δ as

$$\Delta \approx \frac{e}{mc}\left[\tilde{A}_\omega(z)\frac{d}{dz}+\frac{1}{2}\frac{d}{dz}\tilde{A}_\omega(z)\right] \qquad \ldots \quad (2)$$

where $\tilde{A}_\omega(z)=\frac{A_\omega^z(z)}{A_o}$ is the component of vector potential along z -axis, A_o is the amplitude of the incident beam. The model of Bagchi and Kar[12] is employed for the computation $\tilde{A}_\omega(z)$. We assume the z-direction to be perpendicular to the surface which is chosen as z = 0 plane. The response of the electromagnetic field is bulk-like every where except in the surface region defined by $-a \le z \le 0$ In this region, the model dielectric function is chosen to be local one which interpolates linearly between the bulk value inside the metal and the vacuum value (unity) outside. The model frequency-dependent dielectric function is therefore given by,

$$\varepsilon(\omega,z)=\begin{cases}\varepsilon(\omega)\equiv\varepsilon_1(\omega)+i\varepsilon_2(\omega), & z\le -a\\ 1+[1-\varepsilon(\omega)]\frac{z}{a}, & -a\le z\le 0\\ 1, & z\ge 0\end{cases} \qquad \ldots \quad (3)$$

For the complex dielectric function $\varepsilon(\omega,z)$, we use the experimentally determined values. We consider a p-polarized light to be incident on the surface plane making an angle θ_i with the z-axis. The vector potential of interest in the long wavelength $(\omega a/c)\to 0$ is given by

$$\tilde{A}_\omega(z)=\begin{cases}-\dfrac{\sin 2\theta_i}{[\varepsilon(\omega-\sin^2\theta_i]^{\frac{1}{2}}+\varepsilon(\omega)\cos\theta_i}, & z\le -a\\ -\dfrac{\sin 2\theta_i}{[\varepsilon(\omega-\sin^2\theta_i]^{\frac{1}{2}}+\varepsilon(\omega)\cos\theta_i}\cdot\dfrac{a\,\varepsilon(\omega)}{[1-\varepsilon(\omega)]z+a}, & -a\le z\le 0\\ -\dfrac{\varepsilon(\omega)\sin 2\theta_i}{[\varepsilon(\omega-\sin^2\theta_i]^{\frac{1}{2}}+\varepsilon(\omega)\cos\theta_i}, & z\ge 0.\end{cases} \qquad \ldots\ldots \quad (4)$$

We plan in this thesis to develop formalism for calculating ψ_i which will describe the electron states in the surface and the bulk regions.

3. **Review of works done**:

The formulation of the initial state wavefunction by choosing the exact potential model for the surface and the bulk regions of the solid is very important and complex too. There are various approaches to surface and bulk photoemission calculations which had been applied to real cases. Feibelman[13] was perhaps the first one to report the surface photocurrents in which the surface potential barrier was used to solve Schrödinger's equation for deriving ψ_i and ψ_f. However, his calculations were restricted to jellium models only and were complex too. Weng *et. al.*[14] have done the surface studies of (100) faces of *W* and *Mo*. To explain the photoemission spectra, they have used the Wannier type localized wavefunction to define the orbital basis. Smith[15] has also presented surface state calculations from various faces of *Cu* but by using a simple type of wavefunctions. Pendry[10] has given a detailed method of photoemission calculations by employing multiple-scattering formalism and this has been the most widely accepted technique. The method of Levinson *et. al.*[16] was restricted to only free electron type of metals but however could explain the effect of spatial variation of vector potential on photoemission. With their very simple approach, Thapa *et. al.* have used the free electron[17] and Kronig-Penney[18] model potentials to calculate photocurrent from metals and semiconductors. Behaviour of photocurrent in the U.V. range for the values of photon energy below and above the plasmon energy showed interesting features. Pachuau *et. al.*[19] have recently used the

sinusoidal Mathieu potential to derive the ψ_i, and used it to the case of photoemission from metals.

4. **Proposed work of investigation:**

The purpose of the proposed Ph.D. programme is to develop a formalism for calculating $|\psi_i>$ which will be calculated in such a manner that it should be able to describe both the electronic states at the surface and the bulk regions of the metal. For this purpose, one has to first define the crystal potential. To begin with, we will consider at first the free electron type of potential, then a potential which will be periodic with the periodicity of the lattice namely, the muffin-tin type of potential and sinusoidal Mathieu potential. We propose to explore the symmetry properties of the surface states. The LCAO procedure will be used to obtain the symmetry-adapted surface state wavefunctions which are very convenient for visualizing the surface state wavefunctions[20], analyzing their symmetry and in interpreting the experimental results. Our primary objective then would be to derive the atomic orbitals in terms of appropriate basis functions. These basis functions will be deduced by using the projection operator techniques of group theory[20, 21]. By identifying the point groups to which the metal under investigation belongs, we can then construct the atomic orbitals which will enable one to develop appropriately the initial state wavefunction ψ_i .

The final state wavefunction ψ_f will be the scattering state[12] of the step potential existing at the surface. We can now expand the matrix element in Eq. (1) to calculate photocurrent into a number of integrals. As these integrals cannot be solved analytically, hence FORTRAN programs will be developed to evaluate them for computing the photocurrent. Photocurrent will be calculated as a function of a number

of parameters like photon energy, surface width, width of the potential, scattering factor, potential strength etc. The behaviour of photocurrent especially near the plasmon energy of crystals would be of our interest. The photoemission data thus obtained will be compared with other models.

References :

1. B. Feuerbacher, B. Fitton and R. F. Willis, *Photoemission and the Electronic Properties of Surfaces*, (Wiley, New York, 1978).
2. J. E. Inglesfield, *Rep. Prog. Phys.* **45**, 223 (1982).
3. R. H. Willis, G. P. Srivastava and I. T. Mcgovern, *Rep. Prog. Phys.* **43**, 83 (1980).
4. V. Dose, *Prog. Surf. Sci.* **13**, 225 (1983).
5. M. L. Glasser and A. Bagchi, *Prog. Surf. Sci.* **7**, 113 (1976).
6. E. W. Plummer and W. Eberhardt, *Advances in Chemical Phys.* **49**, 533 (1982).
7. N. Kar, *Proc. Nuclear and Solid State Phys. Symposium*, **26A**, 383 (1983).
8. W. Schattke, *Prog. Surf. Sci.* **54**, 211 (1997).
9. J. Braun, *Rep. Prog. Phys.* **59**, 1267 (1996).
10. J. B. Pendry, Surf. Sci. 57, 679 (1976), *Low Energy Electron Diffraction* (Academic, 1974).
11. A. Zangwill, *Physics at Surfaces* (Cambridge University Press, 1989).
12. A. Bagchi and N. Kar, *Phys. Rev.* **B18**, 5648 (1978).
13. P. J. Feibelman, *Phys. Rev. Lett.* **34**, 1092 (1975).
14. S. L. Weng, E. W. Plummer and T. Gustafsson, *Phys. Rev.* **B18**, 1718 (1978).
15. N. V. Smith, *Phys. Rev.* **B32**, 3549 (1985).

16. H. J. Levinson, E. W. Plummer and P. J. Feibelman, *Phys. Rev. Lett.* **43,** 952 (1979).

17. R. K. Thapa and N. Kar, *Phys. Rev.* **B51**, 17980 (1995).

18. R. K. Thapa and N. Kar, *Surf. Sci.* **338,** 138 (1995), R. K. Thapa, *Phys. Stat. Sol.***B179**, 391 (1993).

19. Zaithanzauva Pachuau, B. Zoliana, D. T. Khating, P. K. Patra and R. K. Thapa, *Phys. Letts.***A 294**, 52 (2002).

20. E. Bertel, *Phys. Rev.* **B50,** 4925 (1994).

21. J. F. Cornwell, *Group Theory and Electronic Energy Bands in Solids* (North-Holland, 1969).

CHAPTER 1

INTRODUCTION

Electronic structure is an important ingredient in the understanding of a solid and the photoemission spectroscopy has been used as an investigative method for the conceptual understanding of the behaviour of electrons in the surface and bulk of a solid. The Ultraviolet Photoemission Spectroscopy (UPS) is a versatile and flexible tool in the study of electronic states on the surface of a solid. The ultraviolet radiation in the range of 10 to about 300 eV brings the excitation of electrons within a small value of escape depth which can come out of solid and make photoemission a useful technique for study of surfaces. Beside this, the variation of photon energy leads to a variation in escape depth of the electrons by means of which its relative importance to the surface and the bulk effects can be varied. The X-ray Photoelectron Spectroscopy (XPS) in the range of 1000 eV or more has also been used to study the inner core level of the solid due to its highly penetrating characteristic. The excitation of electrons in deep lying level produces the collective electron oscillations (plasmon) which involves complex type of photoemission. Both UPS and XPS are surface sensitive techniques. However, the high absorption coefficient of ultra-violet radiation and small escape depth of the electron photoemitted from solids gives the UPS a greater advantage over other method of investigations of electronic structure of solids.

The measurement of energy distributions of the emitted electrons allows the determination of the energy and momentum of the photoemitted electrons which gives information on the electronic structure of the surface and bulk of the solids. There are two types of energy analysers for the emitted electrons. In one method, electrons emitted in all angles are collected in a hemispherical analyser which is known as Angle-integrated Ultraviolet Spectroscopy. The other method, which is known as

Angle-Resolved Ultraviolet Spectroscopy (ARUPS) can analyse the energy of the electrons emitted at a fixed angle which gives rise to the energy distribution curve. By determining the momentum of electrons which shows maximum on the curve and by measuring the change in energy position of the maxima on the curve with the change of momentum, one can determine the energy-wave vector relationship. The absolute value of the momentum (k) of the electron can be determined from the relation $E = \frac{\hbar^2 k^2}{2m}$. The method of ARUPS is illustrated in Fig. (1. 1). The incoming UV radiation is incident on the solid at an angle θ_i with respect to normal. The electron energy analyser can be varied between 0^o and 90^o. The azimuthal angle can be set to any desired value. The energy and angular distribution of the emitted electrons can be determined as a function of energy, polarization and angle of incidence (θ_i) of the applied radiation.

The UPS serves as a bridge between photocurrent measurements and corresponding electronic structure calculations. Therefore, it directly probes the quality of theoretically investigated band dispersion for crystalline materials. The experimental facts showed that the electrons with kinetic energy in the range 10 -100 eV have a very short mean free path in solids (< 10 Å), and the binding energy of a core electron is a sensitive function of atomic identity. Therefore, measurements of kinetic energy of electrons ejected from a solid after photon or electron bombardment can provide surface-specific elemental information. But the detailed interpretation of photoemission data requires the use of theory which should be able to incorporate appropriately the initial and final state wavefunctions of the electrons, and also a

suitable form of the vector potential which is involved in the matrix element for photoemission calculations. The photoemission calculation for self-consistent wavefunctions corresponding to electron states below vacuum level has been done by Appelbaum *et. al.*[1] and Alldrege *et. al*[2]. Reliable techniques have been developed for the calculation of electron wavefunctions at energy 30-300 eV above the vacuum level. But the surface effect where the electrons have a very short mean free path cannot be clearly mentioned at such energy since these techniques have drawbacks for calculation of electromagnetic field which excites the photoelectrons from the surface of solids. The inclusion of surface photoelectric effect necessitates the treatment of variation of the electromagnetic fields near surface very carefully. The vector potential is usually assumed to be constant to make the calculation easier. The inclusion of photon field variation in certain conditions results in good agreement with the experimental data.

A simple calculation of photocurrent involves the evaluation of the matrix element $\langle \psi_f | \mathcal{H}' | \psi_i \rangle$ where ψ_i and ψ_f are the initial and final one-electron states whose energies are related by $E_f = E_i - \hbar\omega$. The perturbation in the Hamiltonian responsible for the photoexcitation of the electron is given by

$$\mathcal{H}' = \frac{e}{2mc} (\boldsymbol{p}.\boldsymbol{A} + \boldsymbol{A}.\boldsymbol{p}) \qquad (1.1)$$

where $\boldsymbol{p}$ is the one electron momentum operator and $\boldsymbol{A}$ is the vector potential. We are considering the photoemission to take place along z-axis which is normal to the surface. The perturbation $\mathcal{H}'$ in one dimensional case may be written as

$$\mathcal{H}' = \frac{e}{mc}\left[\tilde{A}_\omega(z)\frac{d}{dz} + \frac{1}{2}\frac{d}{dz}\tilde{A}_\omega(z)\right] \qquad (1.2)$$

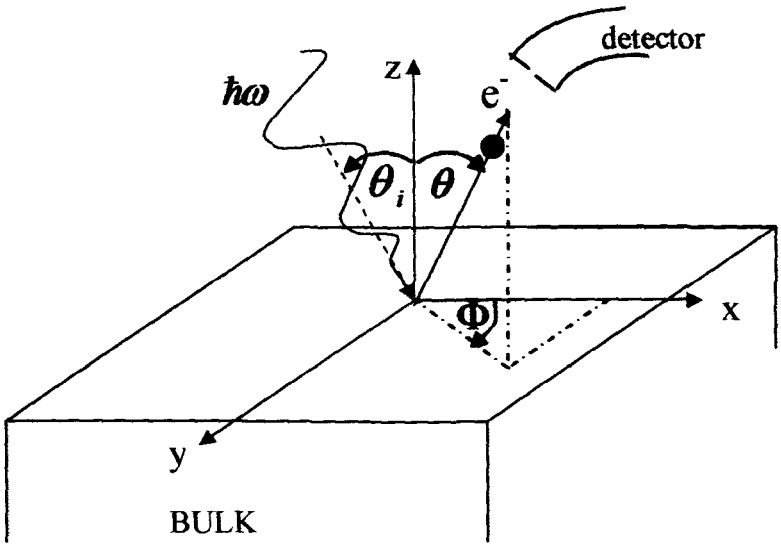

Figure 1. 1: Schematic diagram of Angle Resolved Ultraviolet Photoemission Spectroscopy (ARUPS), in which the photoemission takes place along *z*- direction.

where $\tilde{A}_\omega(z) = \frac{A_\omega^z(z)}{A_o}$, $A_\omega^z(z)$ is the z-component of vector potential along z-axis, A_o is the amplitude of the vector potential associated with the incident radiation. In the standard photoemission calculation, the one electron states are calculated with a high degree of accuracy but the variation of the photon field is generally neglected. In the case where one looks at the photoemission current as a function of the photon energy with the constant initial state, the photon field variation in the surface region needs to be considered more carefully which is evident from Eq. (1. 2). But calculation of the electromagnetic field in the presence of the surface is an extremely complex problem. Hence the calculation of the vector potential in the surface region therefore needs a detailed microscopic analysis of the surface in terms of the dielectric response function. This is because the usual theory of refraction breaks down at a microscopic level which therefore calls for the consideration of the factors like surface discontinuity, non-locality, etc.

The photocurrent arising from the interaction of the electromagnetic field with the solid has been derived by a number of authors[3-6]. The photocurrent density formula may be written with the help of Golden Rule formula[7] as

$$\frac{d\,j(E)}{d\Omega} = \frac{2\pi}{\hbar}\sum_f \left|\langle \psi_f \left| \mathcal{H}' \right| \psi_i \rangle\right|^2 \delta(E - E_f)\delta(E_f - E_i - \hbar\omega)\, f_o(E - \hbar\omega)\left[1 - f_o(E)\right] \quad \ldots (1.3)$$

In Eq. (1. 3), E_i and E_f are the initial and final state of energy, f_o represents the fermi occupation function and δ - function describes the energy conservation. The formula for photoemission cross-section can be written as

$$\frac{d\sigma}{d\Omega} = \frac{k^2}{\omega}\left|\left\langle \psi_f \left| \tilde{A}_\omega(z)\frac{d}{dz} + \frac{1}{2}\frac{d}{dz}\tilde{A}_\omega(z) \right| \psi_i \right\rangle\right|^2 \qquad \ldots \quad (1.4)$$

Thus we see that the calculation of photocurrent density is based on the evaluation of the matrix element $\langle \psi_f | \mathcal{H}' | \psi_i \rangle$.

Several authors have done photocurrent calculations by using various methods. For example, Endriz[8] has used the modified form of the Mitchell-Makinson time dependent perturbation calculation of the surface photo effect. He calculated the photocurrent by using hydrodynamic approximation and applied it to the case of aluminium and other alkali metals where the results for photon energy at plasmon energy ($\hbar\omega_p$) agreed with the experimental data. However the model of Endriz did not reproduce the experimental data of Petersen and Hagstrom[9] which showed a maximum at 12 eV in photoemission cross-section. Schaich and Ashcroft[4] had also developed a model theory of photoemission on the basis of quadratic response and independent particle formalism but had not discussed the electrodynamics of the dielectric response function for the surface. They used a computationally simple model to study the electronic structure in solids and surfaces to understand photoemission. To incorporate the band structure effects, the model of Kronig-Penney potential was used. In this model spatial dependence of vector potential was neglected and throughout the calculation it was assumed to be a constant. The approach of Mahan[5] was to extend the wave mechanical scattering theory originally proposed by Adawi[10]which regards the emitted electron wavefunction as equivalent to the time reversed form of an incident electron along with the scattered part.

The evaluation of matrix element $\langle \psi_f | \mathcal{H}' | \psi_i \rangle$ requires the knowledge of ψ_i and ψ_f. Liebsch[11] and Pendry[12,13] have recognised that the calculation of ψ_i and ψ_f was similar in principle to Low Energy Electron Diffraction (LEED) calculation. Their approach was to consider the solid to be a stack of identical layers terminated at the surface. The final state which had an electron going into the detector was shown to be a time-reversed LEED state. The initial state can also be constructed similarly. The detailed computational programme developed by them was quite standard and successful in application to real system. The photoemission calculation of Pendry[12] gave accurate computational results for initial and final electronic states but the vector potential was taken to be a constant. Pendry recognised that the vector potential would vary in the surface region but, taking the exact account of spatial variation was a complex problem. Again, taking $A_\omega(z)$ to be constant simplified the calculation of the matrix element by using a convenient gauge for $A_\omega(z)$.

Several model calculations have been proposed to calculate electromagnetic fields and to interpret the photoemission experimental data. A realistic model called Random Phase Approximation (RPA) was proposed by Feibelman[14] for a model surface assuming a jellium metal. He took care to get the correct responses of the external field in the presence of the surface as the probing of the outer few layers of a solid takes place. In fact, that was the motivation for constructing an RPA dielectric tensor to study the plasmon dispersion and the microscopic refraction problems. Feibelman gave an assumption of a smooth surface and the dielectric function was determined by the effect of electron 'spill-out' in the region of the dipole layer. The simplicity of this model includes that it has only two inputs- the electron gas radius r_s

and a single–electron surface potential barrier. The potential barrier completely determines the electronic structure of the surface. This can be taken to be the output of a self- consistent jellium ground state calculation. But it can also be varied at will to test the similarity of the aspect of surface responses to various features of the ground state. The RPA model incorporates many features that are expected to be important. The dielectric function is non-local and interpolates smoothly from unity in the vacuum to ε_B in the bulk. It includes the single-electron excitation spectrum and it gives rise to bulk and surface plasma oscillations and satisfies the requirement of charge conservation. The prediction of RPA agrees well with the photoemission experiments that describe the nature of electromagnetic field in the case of free electron metal surfaces. Feibelman assumed that spatial variation parallel to surface is negligible compared to those perpendiculars to surface. He evaluated $A_\omega^z(z)$ within RPA using $r_s = 2$ and calculated the photocurrent matrix using Lang-Kohn potential for the initial and the final state. It was found that his calculated data of jellium was in good agreement with the measured data of Levinson *et. al*[15]. RPA applied to surface is exact within the surface only. Mukhopadhyay and Lundqvist[16] and Bagchi[17] have also developed similar methods for calculating the electromagnetic fields near the surfaces.

The semi-classical infinite barrier (SCIB) model of Kliewer[18] describes the surface very crudely but the phenomena of particle–hole and plasmon excitation are included. The SCIB model apparently violates the nature of the surface from its very assumption as the infinite barrier is not an accurate approximation to the potential existing at the surface. In this model, the electron cannot tunnel out of the solid,

therefore, SCIB power absorptance is assumed to represent the photocurrent emitted. For example, the photocurrent is larger above the plasmon energy $\hbar\omega_p$ and below it is completely in disagreement with the experimental data of Levinson *et.al.*[15] The SCIB model did not reproduce the Friedel oscillations that extend tens of angstroms into the solid, but these appear to have a small effect on photoemission cross section.

The model calculation of Forstmann and Stenschke[19] is based on the hydrodynamic approximation and will therefore not take into account the particle-hole excitations in the surface region which is a very important physical feature affecting the absorption of the electromagnetic radiation. However, the dielectric function used is very simple so that one can easily evaluate the photon field. The detailed calculations of the electromagnetic field using the hydrodynamical model were performed by Kempa and Forstmann[20] and had incorporated the fields in calculating photoyields. This was applied to the case of aluminium and was found that the frequency dependence of the surface photoemission yield is due to the behaviour of the electric field and does not depend very much on the initial and final state wavefunctions. Photoyield results obtained by them showed similar experimental behaviour as found by Levinson *et.al.*[15] The hydrodynamical screening of photofield was also used by Barberan and Inglesfield[21] for the calculation of photoemission. They had shown that the constant vector potential and the Fresnel field are inadequate to explain the photoemission results arising out of the screened electromagnetic field inside the metal. They found that below plasmon frequency (ω_p), $A_\omega^z(z)$ rises rapidly near the surface due to the polarisation charge but at ω_p , there are plasma oscillations. $A_\omega^z(z)$ is almost zero inside the metal at ω_p which means that normal

component of electric field E_z is also zero inside the metal. These results of Barberan and Inglesfield[21] are in good agreement with that of Feibelman *et.al.*[14] for the case of aluminium, apart from the oscillations in $A_\omega^z(z)$ below ω_p . This had been attributed to the excitations in $A_\omega^z(z)$ below ω_p which has arisen due to Friedel type of oscillations from the electron-holes excitations which were not included in the hydrodynamic calculations. Maniv and Matieu[6] have also achieved a considerable progress in the calculations of the electromagnetic field in metal-vacuum interfacial region. They primarily considered the near fields in the immediate vicinity of the interface. They developed a scheme for a more general solution of the Feibelman's model[14] and were able to determine a dielectric response functions in the interfacial region. The plot of the photofield versus the photon energy did not show the behaviour as obtained by Feibelman[14] and Levinson *et.al.*[15] in the case of aluminium. They found that the model was true for photon energy larger than plasmon energy and was applicable only to free electron type of solids.

Thapa[22] using the dielectric model developed by Bagchi and Kar[23] made a detail investigation of variation of electromagnetic fields and applied to various metals like aluminium, nickel, silver, etc. Thapa and others[24,25] have also calculated photocurrent in the case of aluminium using the dielectric model of Bagchi and Kar[23] which showed good agreement with the experimental results[15] . The photocurrent calculations using the Kronig-Penney[26] model in case of a number of metals and semiconductors have been also reported by Thapa *et.al*[24,25] .

Surface state calculations using Mathieu potential[27] was done by Levine[28]. Davison and Levine[29], Slater and Koster[30] and Carver[31] also used this model to describe the energy bands in a realistic crystal. A detailed calculation of

photoemission incorporating photon field variation and initial state wavefunction derivation using Mathieu potential model was done by Pachuau[32] and applied to metals like Al, Be , W, Mo and Si. Pachuau *et. al.*[33] applied this potential model as described by Davison and Steslicka[34] to find the photocurrent which reproduces qualitatively the behaviour of the experimental results as reported by Bartynski *et. al*[35].

An electronic state of a crystal is defined by a Bloch wavefunction. Hence there may be generally two types of electron states namely , incident-reflected pair of bulk Bloch waves which are propagating within the crystal but evanescent in the vacuum and surface electron wave which are propagating along the boundary with $\boldsymbol{k}$ parallel to the surface/interface. This wave is concentrated in the surface and is evanescent both in the bulk and vacuum regions. The identification of such states being that their energy lies in the band gap and hence has complex wave vector. These states pertain to surface states. The formulation of initial state wavefunction defining such states consists of the solution of Schrödinger's equation both in the bulk and surface region of the metal. One general approach is to calculate the wavefunction in the two regions and make sure that it matches properly as regards ψ and $\frac{d\psi}{dz}$ on the boundary plane[29] $z = 0$.

Surface electronic structures always pertain to a particular kind of symmetry, even if it is only a mirror plane, and often there is an axis of symmetry perpendicular to the surface. If the incident beam of the photon is made parallel to the mirror plane, or to the axis of symmetry so that it does not spoil the symmetry, beams diffracted from this configuration must have the same symmetry as the surface. Tinkham[36] has

made a full exposition of the group theoretical approach of symmetry and applied to quantum mechanics. Bertel[37] has studied the symmetry properties of surface states and calculated the basis functions belonging to the irreducible representation of the symmetry point group. These basis functions were generated by Projection Operator[38] technique. Since the location of the electron in the energy band gap[39] of the bulk solid was identified as the surface state, the linear combination of atomic orbital (LCAO) represented surface state wavefunction in terms of atomic orbital centred at the lattice sites. Bertel[37] showed that it was sufficient to consider the effect of the projection operators on the atomic orbital to find out the symmetry of the wavefunctions of surface states. This method is then applied to Cu (110) and a symmetrised basis functions are obtained.

The formulation of initial state wave function in this thesis is performed under two steps: firstly, assuming empty lattice potentials and considering the electronic states of surface pertaining to the symmetrised basis function, an initial wavefunction is formulated using which photocurrent from Cu (110) were calculated. Secondly, Kronig-Penney δ -potential barrier[34] is used instead of empty lattice potential and we employ Green's function technique to solve Schrödinger equation,. In both the cases, the dielectric model is the modified version as used by Bagchi and Kar[23]. Photocurrent is calculated for free electron type of metals (Be,Al,), d-band metals (Cu,W) and for semiconductor material like Si and GaAs.

The material in this thesis is organised as follows: In chapter 2, we shall discuss the basic theory involved in the deduction of vector potential of interest $\tilde{A}_{\omega}(\omega, z)$. $\tilde{A}_{\omega}(\omega, z)$ versus $\hbar\omega$ and z will be calculated from metals like Ag, Al, Cr and semiconductors like GaAs and InAs. In chapter 3, a brief description of

the surface state photoemission calculation by using Mathieu potential model is given with application to the case of strong potential metals like Ag, Fe, Ni, Pd and semiconductors like GaAs and PbSe. In chapter 4, we shall deal with the theoretical formulation of the initial state wavefunction under the following steps:

1. Deductions of the symmetrised basis functions by using Projection operator technique of group theory. Initial state wavefunction will be formulated incorporating the basis function and will be applied to the case of Cu to calculate the photocurrent but with empty potential case.

2. Derivation of initial state wavefunction as the solution of Schrödinger's equation for δ - potential (Kronig-Penney potential model) by using Green function formalism.

3. Application of the wavefunctions deduced above to photoemission calculations from W, Cu, Be, Al, Si and GaAs, and compare the results with the previous theoretical models and experimental results.

CHAPTER 2

CALCULATION OF ELECTROMAGNETIC FIELDS

The photoemission current intensity depends strongly upon the nature of the incident radiation field in the surface region. The discontinuity in the electromagnetic field which appears at the vacuum-solid interface in a macroscopic model of the dielectric response becomes continuous but rapidly varying field. This spatially varying electromagnetic field induced by the dielectric response function of the surface region can be the major contributor to the surface photoeffect. However, for the bulk photoemission, the bulk potential has an effect on the transition from one state to another thereby causing either direct or indirect photoemission.

The dielectric response in the surface region considered is one of the most important factors during photoemission and is of fundamental importance as the dielectric behaviour of the surface region is different from that within the bulk region. Feibelman[14] using the Lang-Kohn (sinusoidal) type of potential had calculated the photoemission intensity incorporating the initial and final wavefunctions. However, the spatial variation of vector potential at the surface was applicable to only free electron metals, in which dielectric response was represented only by jellium model. Mukhopadhyay and Lundqvist[40] have also derived vector potential for the surface, bulk and vacuum regions of the solids which involved an appropriate description of the charge density of the electron. Given a well defined charge density profile, one can evaluate the vector potential. However this model has not yet been used in the photoemission calculations. In this chapter, we shall give the detailed description of the dielectric model which is a modified version of the type as used by Bagchi and Kar[23] to derive the electromagnetic field. Bagchi and Kar[23] defined the surface width extending from $z = -\frac{d}{2}$ to $z = +\frac{d}{2}$, where d is the width of the surface, and $z = 0$

plane is the nominal surface plane. In this thesis, we will consider all throughout the surface to be extending from $z = 0$ to $z = -d$, as shown in Fig. (2.1). We will discuss the detail derivation of the vector potential in this chapter. Vector potential derived will be used to calculate electromagnetic fields from metals and semiconductors for regions located in the vacuum, surface and bulk portion of the solids.

2. 1 Dielectric model and Calculation of Electromagnetic Fields:

For calculation of electromagnetic field the dielectric model is shown in Fig. (2.1). The metal is assumed to occupy the space to the left of $z = 0$ plane. The dielectric constant varies linearly over the surface region $-d \le z \le 0$, where it is a locally varying function of z interpolating linearly between the bulk value inside the metal and the vacuum value (unity) outside. The frequency-dependent dielectric function is given by:

$$\left.\begin{aligned} \varepsilon_1(z) &= \varepsilon_1 && z \le -d \\ &= 1 + \frac{(1-\varepsilon_1)}{d} z && -d \le z \le 0 \\ &= 1 && z \ge 0 \end{aligned}\right\} \quad \ldots \ (2.1a)$$

and

$$\left.\begin{aligned} \varepsilon_2(z) &= \varepsilon_2 && z \le -d \\ &= \frac{-\varepsilon_2}{d} z && -d \le z \le 0 \\ &= 0 && z \ge 0 \end{aligned}\right\} \quad \ldots \ (2.1b)$$

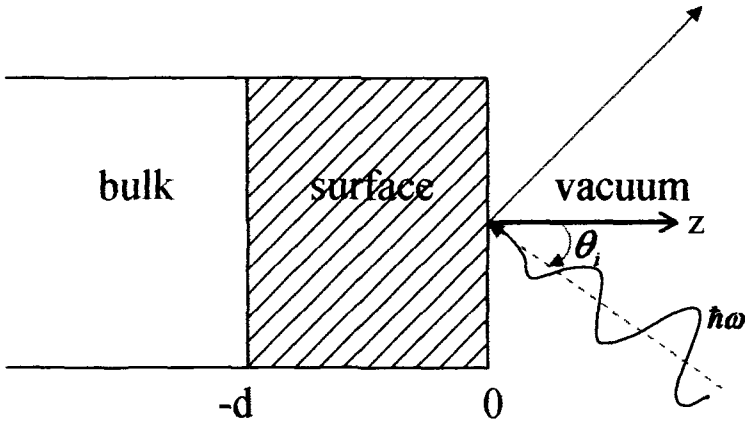

Figure 2. 1: Dielectric model used for the calculation of vector potential. Here *d* is the width of the surface.

such that

$$\varepsilon(\omega,z)\begin{cases}\varepsilon(\omega)\cong\varepsilon_1(\omega)+i\varepsilon_2(\omega), & \textit{for bulk} \quad (z\le -d)\\ 1+[1-\varepsilon(\omega)]\frac{z}{d}, & \textit{for surface} \quad (-d\le z\le 0)\\ 1, & \textit{for vacuum} \quad (z\ge 0)\end{cases} \quad \ldots \text{ (2.1c)}$$

where d is the width of the surface, and $\varepsilon(\omega)$ is a complex dielectric function. The refractive index of the bulk metal $\hat{n}$ is also complex such that $\hat{n}=\sqrt{\varepsilon_1+i\varepsilon_2}=n+ik$. The real part $\varepsilon_1(\omega)$ and imaginary part $\varepsilon_2(\omega)$ of the dielectric constants are defined in the following way to simplify the calculation:

$$\alpha_1=1\ ; \qquad \beta_1=\frac{(1-\varepsilon_1)}{d}$$

$$\alpha_2=0; \qquad \beta_2=\frac{-\varepsilon_2}{d}$$

such that $\varepsilon_1(z)=\alpha_1+\beta_1 z$ ... (2. 2a)

$\varepsilon_2(z)=\alpha_2+\beta_2 z$ ... (2. 2b)

The incident radiation is considered to be a light of angular frequency ω with θ_i as the angle of incidence on the metal surface which is defined by the x-y plane. A gauge was chosen in which the scalar potential is set equal to zero i.e. $\varphi(\vec{r},t)=0$, such that the electromagnetic field $\boldsymbol{E}(\boldsymbol{K},\omega,z)$ can be expressed in terms of the vector potential as

$$\boldsymbol{E}(\boldsymbol{K},\omega,z)=-\frac{i\omega}{c}\boldsymbol{A}(\boldsymbol{K},\omega,z) \quad \ldots \quad \text{(2. 3a)}$$

where $\boldsymbol{K}=\frac{\omega}{c}\sin\theta_i$ is the parallel component of wave vector.

The magnetic field is related to vector potential by the formula

$$\boldsymbol{B} = \nabla \times \boldsymbol{A} \qquad \ldots \quad (2.3b)$$

Let $\boldsymbol{A}(\mathbf{r},t) = \boldsymbol{A}(z).e^{i(\boldsymbol{K}\cdot\boldsymbol{\rho}-\omega t)}$, where $\boldsymbol{\rho} = x\hat{x} + y\hat{y}$ and $\boldsymbol{K} = K\hat{x} = \hat{x}(\frac{\omega}{c}\sin\theta_t)$

Therefore, $\frac{\partial}{\partial t}\boldsymbol{A}(\mathbf{r},t) = \boldsymbol{A}(z).e^{i(\boldsymbol{K}\cdot\boldsymbol{\rho}-\omega t)}(-i\omega) = -i\omega\boldsymbol{A}(\mathbf{r},t)$

$$\text{i.e } \frac{\partial}{\partial t} \leftrightarrow -i\omega \qquad \ldots \quad (2.4a)$$

Also, $\nabla \boldsymbol{A}(\mathbf{r},t) = \nabla \boldsymbol{A}(z)e^{i[K\hat{x}(x\hat{x}+y\hat{y})-\omega t]}$

$$= \left(\hat{x}\frac{\partial}{\partial x} + \hat{y}\frac{\partial}{\partial y} + \hat{z}\frac{\partial}{\partial z}\right)\left[\boldsymbol{A}(z)e^{i(Kx-\omega t)}\right]$$

$$= \left(iK\hat{x} + \hat{z}\frac{\partial}{\partial z}\right)\boldsymbol{A}(\mathbf{r},t)$$

Therefore, $\nabla \leftrightarrow \left(iK\hat{x} + \hat{z}\frac{\partial}{\partial z}\right)$. $\qquad \ldots \quad (2.4b)$

From Maxwell's equations

$$\left.\begin{aligned} &\nabla.\boldsymbol{D} = 0, \qquad \nabla.\boldsymbol{B} = 0 \\ &\nabla\times\boldsymbol{E} = -\frac{1}{c}\frac{\partial \boldsymbol{B}}{\partial t} \\ &\nabla\times\boldsymbol{B} = \frac{1}{c}\frac{\partial \boldsymbol{E}}{\partial t} + \frac{4\pi}{c}\boldsymbol{J} \end{aligned}\right\} \qquad \ldots \quad (2.5)$$

We assume $\mu = 1 \Rightarrow \boldsymbol{B} = \boldsymbol{H}$. Also, $\boldsymbol{J}_{ext} = 0$, i.e. there are no external currents and charges. Since $\boldsymbol{J} = \boldsymbol{J}_{ind} = \sigma\boldsymbol{E}$, the last of Maxwell's equations gives

$$\nabla\times\boldsymbol{B} = \frac{1}{c}\frac{\partial \boldsymbol{E}}{\partial t} + \frac{4\pi\sigma}{c}\boldsymbol{E}$$

$$= \frac{1}{c}\frac{\partial \boldsymbol{E}}{\partial t} + \frac{4\pi\sigma}{c}\frac{1}{(-i\omega)}\frac{\partial \boldsymbol{E}}{\partial t}, \qquad \left(\because \frac{\partial \boldsymbol{E}}{\partial t} = -i\omega\boldsymbol{E}\right)$$

$$= \frac{1}{c}(1+\frac{4\pi\sigma i}{\omega})\frac{\partial \boldsymbol{E}}{\partial t} = \frac{\varepsilon}{c}\frac{\partial \boldsymbol{E}}{\partial t} \qquad \ldots \quad (2.6)$$

where $\varepsilon = 1+\frac{4\pi i\sigma}{\omega}$.

In terms of the vector potential, Eq. (2. 3b) can be written as

$$\nabla \mathrm{x} \nabla \mathrm{x} \boldsymbol{A} = \nabla\,(\nabla.\boldsymbol{A}) - \nabla^2 \boldsymbol{A} = -\frac{\varepsilon}{c^2}\frac{\partial^2 \boldsymbol{A}}{\partial t^2} \qquad \ldots \quad (2.7)$$

Substituting (2. 4a) and (2. 4b) in (2. 7) we have,

$$(-\boldsymbol{K}^2+\frac{\partial^2}{\partial z^2})\,\boldsymbol{A}(z)+\frac{\varepsilon\omega^2}{c^2}\boldsymbol{A}(z)-(i\boldsymbol{K}+\hat{z}\frac{\partial}{\partial z})\,[(i\boldsymbol{K}+\hat{z}\frac{\partial}{\partial z}).\boldsymbol{A}(z)]=0 \qquad \ldots \quad (2.8)$$

Now we consider two distinct cases of polarisation.

(i) *s-polarisation* : In this case $\boldsymbol{A} \parallel \mathbf{y}$ and so $\boldsymbol{E} \parallel \mathbf{y}$. Thus $\boldsymbol{A}(\mathrm{z}) \equiv A^y(z)\hat{y}$,

such that $\left(i K\hat{x}+\hat{z}\frac{\partial}{\partial z}\right).\boldsymbol{A}(\mathbf{r},t) = iK(\hat{x}.\hat{y})A^y(z)+\frac{\partial}{\partial z}A^y(z)(\hat{z}.\hat{y})=0$

Now Eq. (2. 8) becomes

$$\frac{d^2}{dz^2}A^y(z)+(\frac{\varepsilon\omega^2}{c^2}-K^2)A^y(z)=0$$

$$\text{or} \quad \frac{d^2}{dz^2}A^y(z)+\frac{\omega^2}{c^2}(\varepsilon-\sin^2\theta_i)A^y(z)=0 \qquad \ldots \quad (2.9)$$

To solve this equation, we introduce the following labels. Let $\mathrm{k} = \frac{\omega}{c}$, $\mathrm{k_x} = \mathrm{K} = \mathrm{k}\sin\theta_i$ and $\mathrm{k_z} = \mathrm{k}\cos\theta_i$. Then Eq. (2. 9) takes different forms for different region of the metal.

For outside the metal in the vacuum i.e. for $z \geq 0$, $\varepsilon(\omega)=1$ and

$$\frac{d^2}{dz^2}A^y(z)+\frac{\omega^2}{c^2}\cos^2\theta_i A^y(z)=0 \qquad \ldots \quad (2.10a)$$

The solution is $A^y(z) = A_o e^{-ik_z z} + A_o'' e^{ik_z z}$, ... (2.10b)

where A_0 and A_o'' are the amplitudes of the incident and the reflected vector potential respectively whose ratio is related to the reflection coefficient $R_\perp$ through the

formula $$\frac{A_0''}{A_0} = R_\perp^{1/2} e^{i\delta_\perp}$$ .... (2.11)

where $$R_\perp = \frac{[\cos\theta i - \alpha]^2 + \beta^2}{[\cos\theta_i + \alpha]^2 + \beta^2}$$ ... (2.11a)

and $$\tan\delta_\perp = \frac{2\beta\cos\theta_i}{\alpha^2 + \beta^2 - \cos^2\theta_i}$$ ... (2.11b)

On the other hand, for $z \le -d$, i.e. inside the metal, $\varepsilon = \varepsilon_1 + i\varepsilon_2$.

Let $\varepsilon_1 + i\varepsilon_2 = \hat{n}^2 = (n^2 + ik)^2$

$\Rightarrow$ $\varepsilon_1 = n^2 - k^2$; $\varepsilon_2 = 2nk$

We define a complex angle of refraction γ through the relation

$$\hat{n}\sin\gamma = \sin\theta_i$$ ... (2.12a)

therefore, $$\hat{n}\cos\gamma = \sqrt{\hat{n}^2 - \sin^2\theta_i} = \alpha + i\beta$$ ... (2.12b)

where variables α and β are defined by

$$\begin{Bmatrix}\alpha^2 \\ \beta^2\end{Bmatrix} = \frac{1}{2}[(n^2 - k^2 - \sin^2\theta_i)^2 + 4n^2k^2]^{1/2}\begin{Bmatrix}+ \\ -\end{Bmatrix}\frac{1}{2}(n^2 - k^2 - \sin^2\theta_i)$$

Then Eq. (2. 9) for $z \le -d$ gives

$$\frac{d^2}{dz^2}A^y(z) + k^2(\hat{n}^2 - \sin^2\theta_i)A^y(z) = 0$$ ... (2.13a)

The solution corresponding to a single refracted wave is

$$A^y(z) = A_0' e^{-ik(\hat{n}\cos\gamma)z}$$

$$= A_0' e^{-ik\alpha z} e^{k\beta z} \qquad \ldots \qquad (2.13b)$$

where A_0' naturally is the amplitude of the refracted vector potential.

Now for the surface region i.e. $-d \le z \le 0$, Eq. (2. 9) becomes

$$\frac{d^2}{dz^2} A^y(z) + k^2[(\alpha_1 + i\alpha_2) + (\beta_1 + i\beta_2)z - \sin^2\theta_i]A^y(z) = 0$$

whose solution is

$$\left|\frac{A^y(z)}{A_0}\right| \cong [1 + R_\perp + 2R_\perp^{1/2}\cos\delta_\perp]^{1/2} \qquad \ldots \quad (2.14a)$$

where $$\cos\delta_\perp = \frac{\cos^2\theta_i - \alpha^2 - \beta^2}{[(\cos^2\theta_i - \alpha^2 - \beta^2)^2 + 4\beta^2\cos^2\theta_i]^{1/2}} \qquad \ldots \quad (2.14b)$$

(ii) *p - polarization*: In this case, $\boldsymbol{A}$ is in the xz-plane and $\boldsymbol{B} \| \mathrm{y}$ ($\equiv \mathrm{B}\hat{\mathbf{y}}$).

The equation for $\boldsymbol{B}$ can be derived from Maxwell's equations[41] as shown below:

Consider the Maxwell's equations

$$\nabla \times \boldsymbol{B} = \frac{\varepsilon}{c}\frac{\partial \boldsymbol{E}}{\partial t}, \qquad \ldots \quad (2.15a)$$

$$\nabla \times \boldsymbol{E} = \frac{1}{c}\frac{\partial \boldsymbol{B}}{\partial t}. \qquad \ldots \quad (2.15b)$$

For time dependence of the form $\boldsymbol{E} \sim e^{-i\omega t}$, above take the form,

$$\nabla \times \boldsymbol{B} = -\frac{i\omega\varepsilon}{c}\frac{\partial \boldsymbol{E}}{\partial t} \qquad \ldots \quad (2.16a)$$

$$\nabla \times \boldsymbol{E} = \frac{i\omega}{c}\frac{\partial \boldsymbol{B}}{\partial t} \qquad \ldots \quad (2.16b)$$

From Eq. (2. 16a),

$$\nabla\times(\nabla\times\boldsymbol{B}) = -\frac{i\omega\varepsilon}{c}\nabla\times(\varepsilon\boldsymbol{E}),$$

$$\text{or} \qquad \nabla(\nabla\cdot\boldsymbol{B}) - \nabla^2\boldsymbol{B} = -\frac{i\omega}{c}\nabla\times(\varepsilon\boldsymbol{E}),$$

$$\text{or} \qquad \nabla^2\boldsymbol{B} - \frac{i\omega}{c}\nabla\times(\varepsilon\boldsymbol{B}) = 0 \qquad \ldots \quad (2.\ 16c)$$

since $\nabla\cdot\boldsymbol{B} = 0$,

Now using the identity

$$\nabla\times(\varepsilon\boldsymbol{E}) = \varepsilon\nabla\times\boldsymbol{E} + (\nabla\varepsilon)\times\boldsymbol{E},$$

so that,

$$\nabla\times(\varepsilon\boldsymbol{E}) = \frac{(i\omega\varepsilon)}{c}\boldsymbol{B} + \frac{c}{(-i\omega\varepsilon)}(\nabla\varepsilon)\times(\nabla\times\boldsymbol{B}), \ldots (2.\ 16d)$$

using Eq. (2. 16b) for $\nabla\times\boldsymbol{E}$, and Eq. (2. 16a) for $\boldsymbol{E}$.

From Eqs. (2. 16c) and (2. 16d), one then gets

$$\nabla^2\boldsymbol{B} + \frac{\omega^2\varepsilon}{c^2}\boldsymbol{B} + \frac{1}{\varepsilon}(\nabla\varepsilon)\times(\nabla\times\boldsymbol{B}) = 0, \qquad \ldots \quad (2.\ 16e)$$

which is the required equation for $\boldsymbol{B}$.

As an application to *p*-polarised radiation incident on a planar surface (*xy*-plane) consider $\boldsymbol{B} = B\,\hat{y}$, and $B \equiv B(z)e^{i(\mathrm{K}x-\omega t)}$, and note that

$$\nabla \equiv (iK\hat{x} + \hat{z}\frac{d}{dz}), \text{ and } \nabla^2 \equiv -K^2 + \frac{d^2}{dz^2},$$

so that in local approximation (i.e., $\varepsilon \equiv \varepsilon(z,\omega)$),

$$\nabla\varepsilon = \hat{z}\frac{d\varepsilon}{dz},\ \nabla\times\boldsymbol{B} = iKB\hat{z} - \hat{x}\frac{dB}{dz},$$

and therefore,

$$\frac{1}{\varepsilon}(\nabla\varepsilon)\times(\nabla\times\boldsymbol{B}) = -\left[\frac{1}{\varepsilon}\frac{d\varepsilon}{dz}\frac{dB}{dz}\right]\hat{y} \qquad \ldots \quad (2.16f)$$

From Eqs. (2.16c) and (2.16f), one gets

$$\frac{\partial^2 B}{\partial z^2} + \left[\frac{\omega^2\varepsilon}{c^2} - K^2\right]B - \frac{1}{\varepsilon}\frac{\partial\varepsilon}{\partial z}\frac{\partial B}{\partial z} = 0,$$

or

$$\frac{\partial}{\partial z}\left[\frac{1}{\varepsilon}\frac{\partial B}{\partial z}\right] + \left[\frac{\omega^2}{c^2} - \frac{K^2}{\varepsilon}\right]B = 0, \qquad \ldots \quad (2.17)$$

which is the required equation for B.

We must solve this equation under the boundary condition that both B and $\frac{\partial B}{\partial z}$ are continuous. Once B is known, the electric field components can be found by using Maxwell's equation, i.e.

$$-i\omega\boldsymbol{E} = \frac{c}{\varepsilon}(\nabla\times\boldsymbol{B})$$

$$= \frac{c}{\varepsilon}\left\{\left(iK\hat{x} + \hat{z}\frac{\partial}{\partial z}\right)\times\left(B\hat{y}\right)\right\}$$

In terms of Cartesian components,

$$\left.\begin{aligned} E_x &= \frac{1}{ik\varepsilon}\frac{\partial B}{\partial z} \\ E_z &= -\frac{K}{k\varepsilon}B = -\frac{\sin\theta_i}{\varepsilon}B \end{aligned}\right\} \qquad \ldots \quad (2.18)$$

To solve Eq. (2. 17), we follow the prescription of Landau and Lifshitz and use the substitution $B(z) = u(z)\sqrt{\varepsilon(z)}$ and by substituting $\frac{\omega^2}{c^2} = k^2$ and $K = k\sin\theta_i$, we obtain

$$\frac{\partial}{\partial z}(\frac{1}{\varepsilon})(\frac{\partial B}{\partial z})+\frac{\partial^2 B}{\partial z^2}\frac{1}{\varepsilon}+\frac{k^2}{\varepsilon}(\varepsilon-\sin^2\theta_i)B=0$$

or $$-\frac{1}{\varepsilon}\frac{\partial\varepsilon}{\partial z}\frac{\partial}{\partial z}(u\sqrt{\varepsilon})+\frac{\partial}{\partial z}(\frac{\partial u\sqrt{\varepsilon}}{\partial z})+k^2(\varepsilon-\sin^2\theta_i)u\sqrt{\varepsilon}=0$$

The final result gives

$$\frac{d^2u}{dz^2}+k^2(\varepsilon-\sin^2\theta_i)u+[\frac{1}{2\varepsilon}\frac{d^2\varepsilon}{dz^2}-\frac{3}{4}\frac{1}{\varepsilon^2}(\frac{d\varepsilon}{dz})^2]u=0 \qquad \ldots \quad (2.19)$$

In Eq. (2. 19), clearly $\frac{d^2\varepsilon}{dz^2}=0$ everywhere except for $z=-d$ and 0, where it blows up.

Now substituting the values of dielectric constants for each regions in Eq. (2. 19), we can obtain the expression for the magnetic field for the three regions of the metal.

In the first region, $z\geq 0$ (vacuum), where ε=1, we have

$$\frac{d^2u}{dz^2}+k^2\cos^2\theta_i u=0 \qquad \ldots \quad (2.20a)$$

whose solution is $\mathrm{B}=B_0e^{-ik_z z}+B_0^{''}e^{ik_z z}$ $\qquad \ldots \quad (2.20b)$

In the second region, $z\leq -d$ and $\varepsilon \equiv \varepsilon_1+\mathrm{i}\varepsilon_2=\hat{n}$

$$\frac{d^2u}{dz^2}+k^2\hat{n}^2\cos^2\gamma\, u=0 \qquad \ldots \quad (2.21a)$$

The solution is (absorbing $\hat{n}$ into the constant coefficient)

$$B=B_o^{'}e^{-ik(\hat{n}\cos\gamma)z} \qquad \ldots \quad (2.21b)$$

For the third region, $-d\leq z\leq 0$ (surface),

$$\frac{d^2u}{dz^2}+k^2(\varepsilon-\sin^2\theta_i)u-\frac{3}{4}\frac{1}{\varepsilon^2}(\frac{d\varepsilon}{dz})^2]u=0 \qquad \ldots \quad (2.22a)$$

Recalling Eqs. (2. 2a) and (2. 2b), Eq.(2. 22a) becomes

$$\frac{d^2u}{dz^2} + k^2(b+cz)u - \frac{3}{4}\frac{1}{(b'+cz)^2}c^2u = 0 \qquad \ldots (2.\ 22b)$$

where $b' = \alpha_1 + i\alpha_2 = b + \sin^2\theta_i$ is a short hand notation introduced purely for convenience.

Eq. (2. 22b) has the solution $u(z) = Az'^{3/2} + Bz'^{-1/2}$

But $\varepsilon(z) = b' + cz = cz'$ .Therefore, $B(z) = Cz'^2 + D$

$$= C[z + \frac{(\alpha_1 + i\alpha_2)}{\beta_1 + i\beta_2}]^2 + D,$$

$$\text{i.e.} \qquad B(z) = C[z + \frac{b'}{c}]^2 + D, \quad -d \le z \le 0 \qquad \ldots (2.\ 22c)$$

The constants C and D are determined by matching the boundary conditions at z = $-d$ and z = 0.

At z = 0, from Eqs. (2. 20b) and (2. 22c) we have,

$$\left.\begin{aligned} B_0 + B_0'' &= C(\frac{b'}{c})^2 + D \\ ik\cos\theta_i[-B_0 + B_0''] &= 2C(\frac{b'}{c}) \end{aligned}\right\} \qquad \ldots (2.\ 23a)$$

At z = - d, from Eqs. (2. 21b) and (2. 22c) we have,

$$\left.\begin{aligned} C(-d + \frac{b'}{c})^2 + D &= B_0' e^{ik(\alpha+i\beta)d} \\ 2C(-d + \frac{b'}{c}) &= -ik(\alpha+i\beta)B_0' e^{-ik(\alpha+i\beta)(-d)} \end{aligned}\right\} \qquad \ldots (2.\ 23b)$$

Calculations from Eqs. (2. 23a) and (2. 23b) shows the results as:

$$\frac{B_0''}{B_o} = \frac{-1 + \cos\theta_i\{\frac{\varepsilon}{\alpha+i\beta} - \frac{ikd}{2}(1+\varepsilon)\}}{1 + \cos\theta_i\{\frac{\varepsilon}{\alpha+i\beta} - \frac{ikd}{2}(1+\varepsilon)\}} \qquad \ldots (2.24a)$$

$$\frac{C}{B_0} = \frac{ik\cos\theta_t}{d}(1-\varepsilon)\frac{1}{1+\cos\theta_t\{\frac{\varepsilon}{\alpha+i\beta}-\frac{ikd}{2}(1-\varepsilon)\}} \quad \ldots (2.24b)$$

$$\frac{D}{B_0} = \varepsilon\cos\theta_t \frac{[\frac{2}{(\alpha+i\beta)}+ikd(\frac{\varepsilon}{1-\varepsilon})]}{1+\cos\theta_t\{\frac{\varepsilon}{\alpha+i\beta}-\frac{ikd}{2}(1+\varepsilon)\}} \quad \ldots (2.24c)$$

$$\& \quad \frac{B_0'}{B_0} = \frac{2\varepsilon\cos\theta_t}{\alpha+i\beta}\frac{e^{-ikd(\alpha+i\beta)/2}}{1+\cos\theta_t\left\{\frac{\varepsilon}{\alpha+i\beta}-\frac{ikd}{2}(1+\varepsilon)\right\}} \quad \ldots (2.24d)$$

Therefore, the expression for magnetic field can be obtained as

$$\frac{B(z)}{B_0} = e^{-ik\cos\theta_t z} + \frac{B_0''}{B_0}e^{ik\cos\theta_t z}, \qquad z \geq 0 \quad \ldots (2.25a)$$

$$= (\frac{C}{B_0})[z+\frac{d}{1-\varepsilon}]^2 + \frac{D}{B_0}, \qquad -d \leq z \leq 0 \quad \ldots (2.25b)$$

$$= \frac{B_0'}{B_0}e^{-ik(\alpha+i\beta)z}, \qquad z \leq -d \quad \ldots (2.25c)$$

where B_0 = amplitude of the magnetic field.

We now compute the electric field from Eq. (2. 25) using Eq. (2. 18). Recall that for the incident electromagnetic wave in vacuum, *the amplitude of the electric field is the same as the amplitude of the magnetic field, ie* $E_0 = B_0$. We also recall our model of linear dielectric variation,

$$\varepsilon(z) = 1, \qquad z \geq 0$$

$$= 1 + \frac{(1-\varepsilon)}{d}z, \qquad -d \leq z \leq 0$$

$$= \varepsilon \equiv \varepsilon_1 + i\varepsilon_2, \qquad z \leq -d$$

Therefore, the x-component of electric field are given as

$$\frac{E_x(z)}{E_0} = [-e^{-ik\cos\theta_t(z)} + (\frac{B_0''}{B_0})e^{ik\cos\theta_t(z)}]\cos\theta_t, \qquad z \geq 0 \qquad \ldots \text{(2. 26a)}$$

$$= \frac{1}{ik[1+\frac{(1-\varepsilon)}{d}z]}(\frac{C}{B_0}) \cdot 2\,[z+\frac{d}{1-\varepsilon}]$$

$$= \frac{-2\cos\theta_t}{1+\cos\theta_t\left\{\frac{\varepsilon}{\alpha+i\beta}-\frac{dki}{2}(1+\varepsilon)\right\}}, \qquad -d \leq z \leq 0 \qquad \ldots \text{(2. 26b)}$$

$$= -ik\,(\alpha+i\beta)\,(\frac{B'}{B_0})e^{-ik(\alpha+i\beta)z}, \qquad z \leq -d \qquad \ldots \text{(2. 26c)}$$

Notice that the x component of the electric field in the interface region ($-d \leq z \leq 0$) is a constant quantity and is independent of z. On the other hand, for the z-component of the electric field, we obtain electric field for different regions as follows:

For vacuum region, i.e. $z \geq 0$,

$$\frac{E_z(z)}{E_0} = -\sin\theta_t[e^{-ik\cos\theta_t(z)} + \frac{B_0''}{B_0}e^{ik\cos\theta_t(z)}],$$

$$= -\sin\theta_t[e^{-ik\cos\theta_t(z)} + e^{ik\cos\theta_t(z)}\frac{-1+\cos\theta_t\left\{\frac{\varepsilon}{\alpha+i\beta}-\frac{dki(1+\varepsilon)}{2}\right\}}{1+\cos\theta_t\left\{\frac{\varepsilon}{\alpha+i\beta}-\frac{dki(1+\varepsilon)}{2}\right\}}]$$

In the long wavelength limit, kd<<1, and $z \geq 0$,

$$\frac{E_z(z)}{E_0} = -\sin\theta_t[1+\frac{-1+\frac{\varepsilon\cos\theta_t}{\alpha+i\beta}}{1+\frac{\varepsilon\cos\theta_t}{\alpha+i\beta}}]$$

$$= - \frac{\varepsilon \sin 2\theta_t}{\left[\varepsilon - \sin^2 \theta_t\right]^{\frac{1}{2}} + \varepsilon \cos \theta_t}, \qquad \text{for } z \geq 0 \qquad \ldots \text{ (2. 27a)}$$

For the surface region, i.e. $-d \leq z \leq 0$,

$$\frac{E_z(z)}{E_0} = \frac{-\sin \theta_t}{1 + (1-\varepsilon)\frac{z}{d}} \left[\frac{C}{B_0} \left(z + \frac{d}{1-\varepsilon} \right)^2 + \frac{D}{B_0} \right],$$

$$= \frac{-\sin \theta_t d}{1 + (1-\varepsilon)\frac{z}{d}} \left\{ - \frac{ik \cos \theta_t}{d} \frac{(1-\varepsilon)[z + \frac{d}{2}(\frac{1+\varepsilon}{1-\varepsilon})]^2}{1 + \cos \theta_t \{ \frac{\varepsilon}{\alpha + i\beta} - \frac{ikd}{2}(1+\varepsilon) \}} + \varepsilon \cos \theta_t \right.$$

$$\left. \times \left\{ \frac{[\frac{2}{\alpha + i\beta} + ikd(\frac{\varepsilon}{1-\varepsilon})]}{1 + \cos \theta_t \{ \frac{\varepsilon}{\alpha + i\beta} - \frac{ikd}{2}(1+\varepsilon) \}} \right\} \right.$$

Let us consider when the wavelength of light is much larger than d, then $kd \ll 1$,

$$\frac{E_z(z)}{E_0} \underset{kd \to 0}{\cong} \frac{-d}{1 + (1-\varepsilon)\frac{z}{d}} \frac{2 \sin \theta_t \cos \theta_t}{1 + \cos \theta_t \frac{\varepsilon}{\alpha + i\beta}} \frac{\varepsilon}{\alpha + i\beta}$$

$$= - \frac{\sin 2\theta_t}{(\alpha + i\beta) + \varepsilon \cos \theta_t} \frac{\varepsilon d}{d + (1-\varepsilon)z}$$

Noting that $\alpha + i\beta = \hat{n} \cos \gamma = \sqrt{\varepsilon - \sin^2 \theta_t}$, we obtain

$$\frac{E_z(z)}{E_0} \underset{kd \to 0}{\cong} - \frac{\sin 2\theta_t}{\left[\varepsilon - \sin^2 \theta_t\right]^{\frac{1}{2}} + \varepsilon \cos \theta_t} \frac{\varepsilon d}{d + (1-\varepsilon)z}, \qquad \text{for } -d \leq z \leq 0 \ldots \text{ (2. 27b)}$$

Again in the bulk region, i.e., $z \leq -d$,

$$\frac{E_z(z)}{E_0} = \frac{-\sin \theta_t}{\varepsilon} \left[\left(\frac{B_0'}{B_0} \right) e^{-ik(\alpha + i\beta)z} \right]$$

$$= \frac{\sin\theta_i}{\varepsilon}\left[\frac{2\varepsilon\cos\theta_i}{(\alpha+i\beta)}\frac{e^{-ik(\alpha+i\beta)d}\,e^{-ik(\alpha+i\beta)z}}{1+\cos\theta_i\left\{\frac{\varepsilon}{\alpha+i\beta}-\frac{dki(1+\varepsilon)}{2}\right\}}\right]$$

In the long wavelength limit, k d<<1, i.e. ($\frac{\omega}{c}\to\infty$), and for $z\le -d$

$$\therefore \quad \frac{E_z(z)}{E_0} = \frac{-\sin 2\theta_i}{(\alpha+i\beta)}\frac{1}{1+\frac{\varepsilon\cos\theta_i}{(\alpha+i\beta)}}$$

$$= -\frac{\sin 2\theta_i}{\left[\varepsilon-\sin^2\theta_i\right]^{\frac{1}{2}}+\varepsilon\cos\theta_i}, \qquad \text{for } z\le -d \qquad \ldots \text{ (2. 27c).}$$

Thus the z component of the electric field in the long wavelength limit ($\frac{\omega d}{c}\to\infty$) is given by:

$$\tilde{A}_\omega(z) = \frac{E_z(z)}{E_0} = \begin{cases} -\dfrac{\varepsilon(\omega).\sin 2\theta_i}{\left[\varepsilon(\omega)-\sin^2\theta_i\right]^{\frac{1}{2}}+\varepsilon(\omega).\cos\theta_i} & z\ge 0 \\ -\dfrac{\sin 2\theta_i}{\left[\varepsilon(\omega)-\sin^2\theta_i\right]^{\frac{1}{2}}+\varepsilon(\omega).\cos\theta_i}\,\dfrac{\varepsilon(\omega).d}{d+[1-\varepsilon(\omega)]z}, & -d\le z\le 0 \\ -\dfrac{\sin 2\theta_i}{\left[\varepsilon(\omega)-\sin^2\theta_i\right]^{\frac{1}{2}}+\varepsilon(\omega).\cos\theta_i}, & z\le -d \end{cases}$$

$$\ldots \quad (2.28)$$

The electromagnetic fields had been calculated as a function of photon energy for three locations of surface plane i.e. z = 0, $-\frac{d}{2}$ and $-d$. The value of the dielectric constant $\varepsilon(\omega)$ is unity for vacuum region whereas for the bulk and the surface region, we have used the experimental data as given by Weaver[42] and Edwards[43] for metals and semiconductors respectively. We have calculated the frequency dependence of

$\tilde{A}_\omega(z)$ and $\left|\tilde{A}_\omega(z)\right|^2$ for a number of cases. $\left|\tilde{A}_\omega(z)\right|^2$ has been plotted against photon energy $(\hbar\omega)$ as it occurs in the matrix element for photoemission cross-section calculation and is a quadratic function of $\tilde{A}_\omega(z)$. The solids for which fields have been evaluated are silver, aluminium and chromium, and semiconductors like gallium arsenide and indium arsenide. The thickness is a parameter in our calculation. However, it has been found by Appelbaum[44] that for most metals, the surface width d ~ 15 $\overset{0}{\text{A}}$ with respect to the last plane of the atoms beyond which the electronic properties are independent of the presence of the surface and hence we take the value of d~ 5.292 $\overset{0}{\text{A}}$.

2. 2 Evaluation of the Electromagnetic Fields:

The plot of electromagnetic fields against the photon energy $(\hbar\omega)$ in the case of *s*-polarisation did not give any interesting features[45]. This indicates that *s*-polarised light do not play important role in photoemission which is also evident from the calculation of Weng *et.al*[46] in the case of W and Mo. In this section, we show the results of electromagnetic fields for *p*-polarised light calculated in the case of metals like Ag, Al, Cr and semiconductors GaAs and InAs by using the formula given in Eq. (2. 28). We have plotted $\left|\tilde{A}_\omega(z)\right|^2$ as a function of photon energy $(\hbar\omega)$ and distance (z/d) from the surface of the solids under consideration.

(a) Silver:

In Fig. (2. 2), we show for Ag the plot of the variation of $\left|\tilde{A}_\omega(z)\right|^2$ against photon energy $(\hbar\omega)$ for the values of z = - d (bulk), -0.5 d (surface) and z = 0.0

(vacuum). We note that there is a sharp peak in the curve corresponding to z = - 0.5 d at 3.5 eV photon energy followed by a minimum at $\hbar\omega$ = 4.5 eV. For z = 0 and – d, we do not observe such behaviour in the field plot as seen at z = - 0.5 d. To show that peak at $\hbar\omega$ = 3.5 eV for z = - 0.5 d is surface related we also plotted $\left|\tilde{A}_\omega(z)\right|^2$ against z for $\hbar\omega$ = 1 eV, 3.5 eV and 5 eV as shown in (Fig. 2.3). We find that for $\hbar\omega$ = 3.5 eV, peak in $\left|\tilde{A}_\omega(z)\right|^2$ is observed near z = 0.5 d. For other values of photon energies i.e. at $\hbar\omega$ = 1 eV and 5 eV, no such peaks are observed. This implies that origin of peak at $\hbar\omega$ = 3.5 eV for z = - 0.5 d is a surface related phenomena.

(b) Aluminium:

In Fig. (2. 4) we have shown for Al the results of $\left|\tilde{A}_\omega(z)\right|^2$ plotted against the photon energy $(\hbar\omega)$ for three locations of the surface plane, for example at z = - d (bulk), z = - 0.5 d (surface) and z = 0 (vacuum). We find that the peak in $\left|\tilde{A}_\omega(z)\right|^2$ occurs at $\hbar\omega$ = 11 eV and decreases to a minimum at 15 eV photon energy which is close to the plasmon energy $(\hbar\omega)$ of Al, that is, $\hbar\omega_p$ = 15.75 eV. The peak value in $\left|\tilde{A}_\omega(z)\right|^2$ at $\hbar\omega$ =11 eV is due to the excitations of surface plasmon which is related to bulk plasmon by $\hbar\omega_s = \hbar\omega_p / \sqrt{2}$.

We have also plotted $\left|\tilde{A}_\omega(z)\right|^2$ as a function of distance (z) for values of photon energy at $\hbar\omega$ = 9 eV, 11 eV and 13 eV as shown in Fig. (2. 5). It is seen that highest peak is obtained for $\hbar\omega$ = 11 eV at z = -0.5 d. This indicates that occurrence

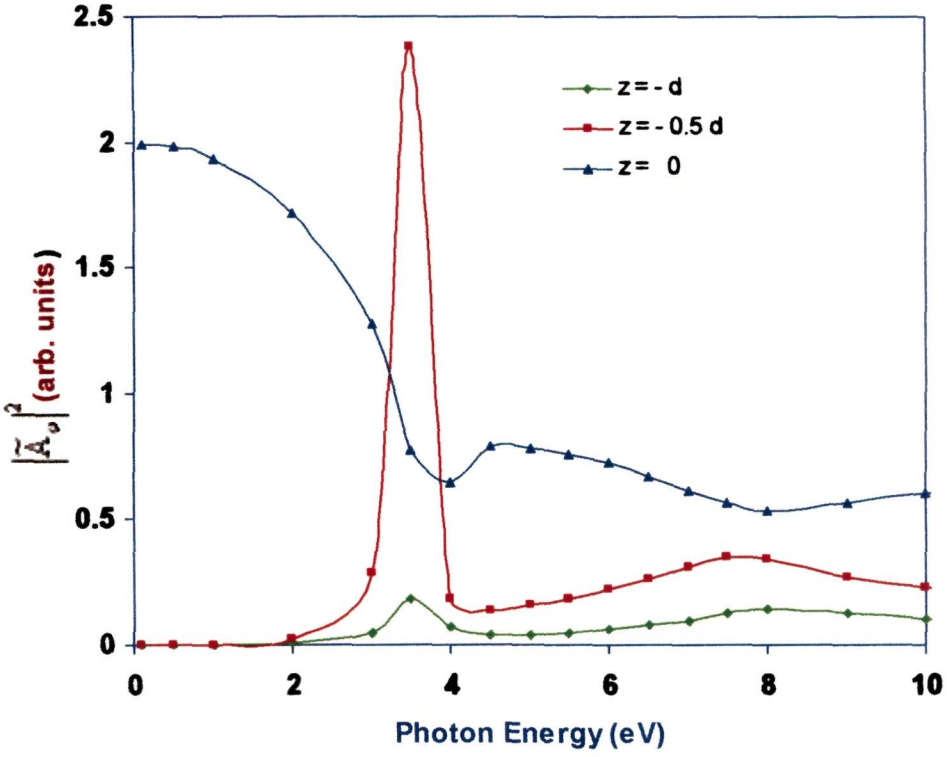

Figure 2. 2: Plot of variation of square of electromagnetic field $\left|\tilde{A}_\omega(z)\right|^2$ against photon energy in the case of Ag for location of surface plane at z = - *d* (bulk), z = - 0.5 *d* (surface) and z = 0 (vacuum).

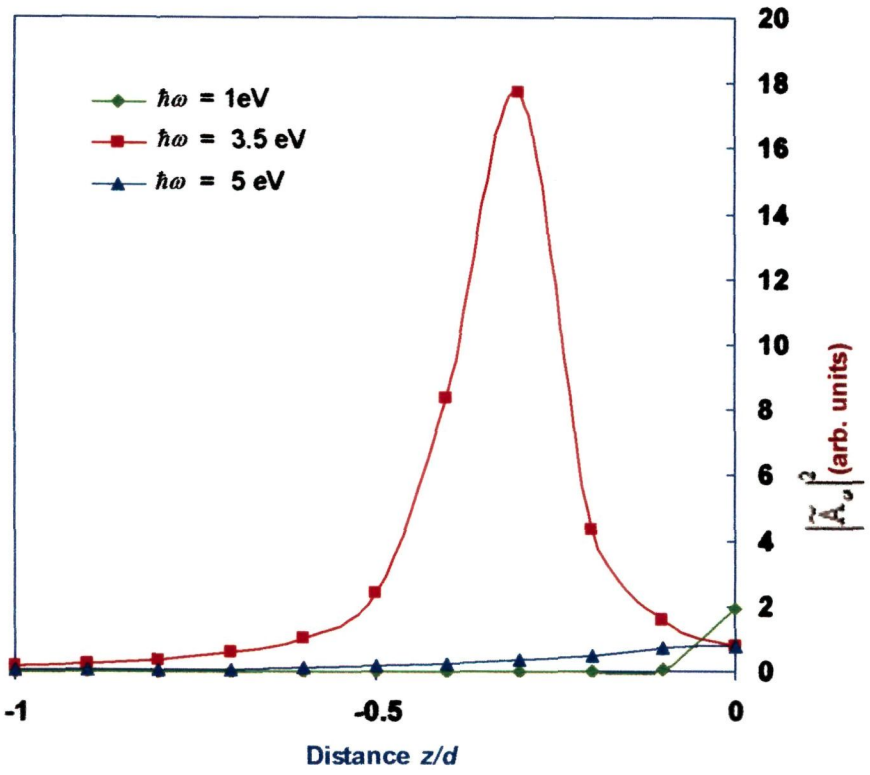

Figure 2. 3: Plot of variation of $\left|\tilde{A}_\omega(z)\right|^2$ against the distance *z/d* for Ag.

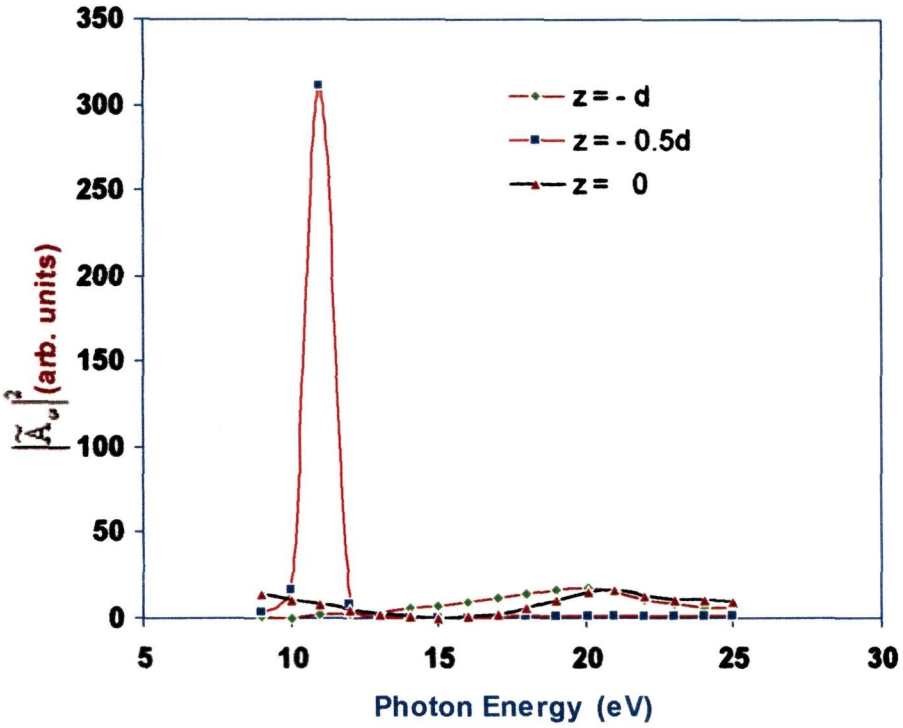

Figure 2. 4: Variation of square of electromagnetic field plotted against photon energy in the case of Al for location of surface plane at z = -*d* (bulk), z = - 0.5 *d* (surface) and z = 0 (vacuum).

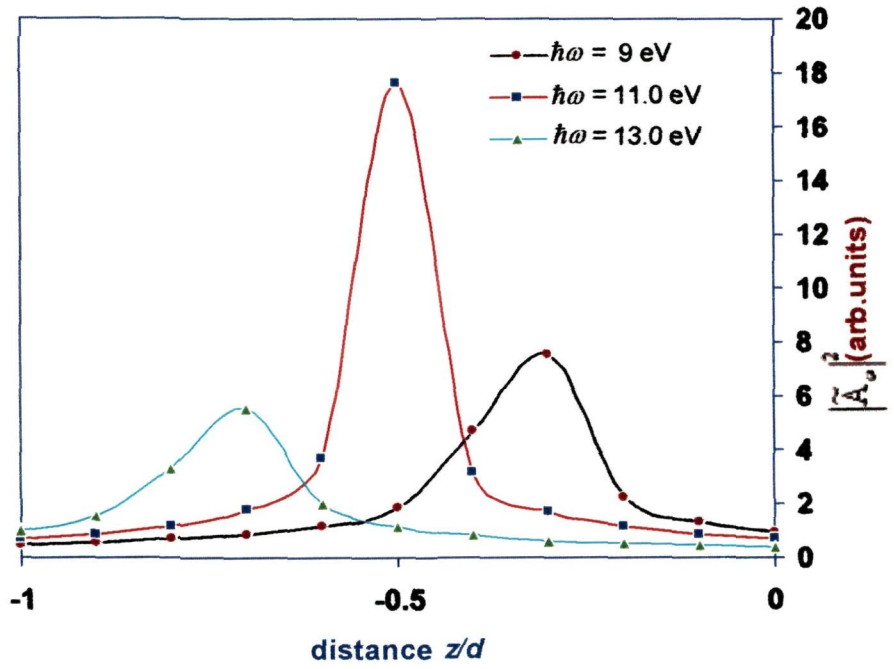

Figure 2. 5: Plot of square of electromagnetic field against distance for Al.

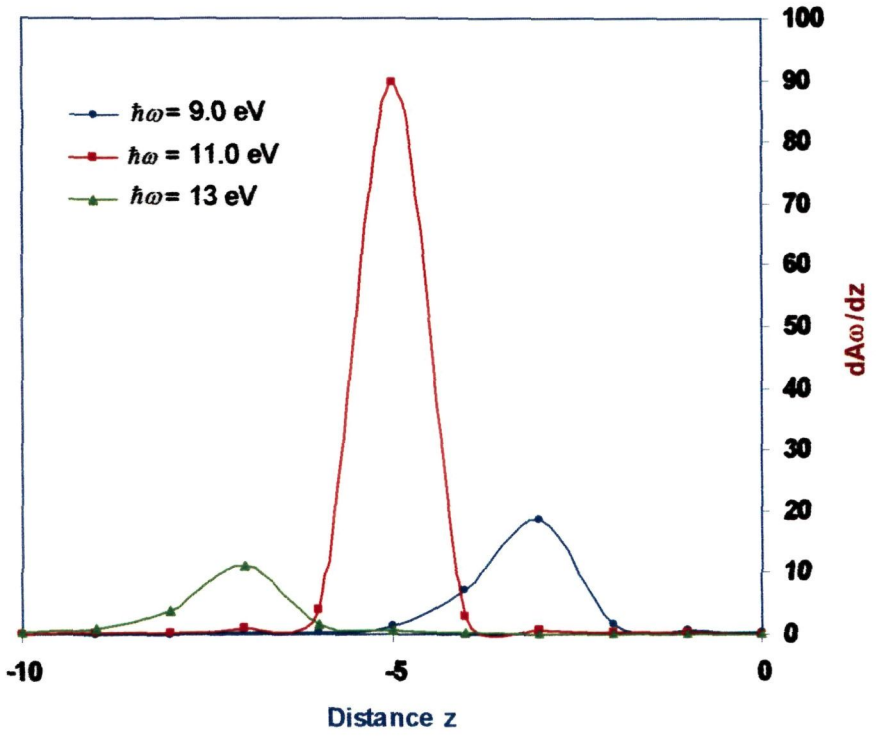

Figure 2. 6: Plot of $\frac{d\tilde{A}_{\omega}}{dz}$ against distance from the surface for photon energies 9 eV, 11 eV and 13 eV in Al.

of maxima in the field is a surface related phenomena. Further there is a strong evidence[15] that it is the spatial variation of $\tilde{A}_{\omega}(z)$ which causes the occurrence of peak in the surface region. Fig. (2. 6) shows the plot of spatial variation of electromagnetic field ($\frac{d\tilde{A}_{\omega}}{dz}$) against the location of the surface plane (z) for three different values of photon energy. It is seen that $\frac{d\tilde{A}_{\omega}}{dz}$ is maximum in the middle of surface region for $\hbar\omega$ = 11 eV, whereas for other photon energies 9 eV and 13 eV respectively, peak values in $\frac{d\tilde{A}_{\omega}}{dz}$ is smaller in magnitude and is shifted away from the middle of the surface region.

(c) Chromium:

Fig. (2. 7) shows the plot of variation of $\left|\tilde{A}_{\omega}(z)\right|^2$ against the photon energy ($\hbar\omega$) for three location of surface planes of chromium. In the case of chromium, we find that peak in $\left|\tilde{A}_{\omega}(z)\right|^2$ was obtained at $\hbar\omega \sim$ 8 eV for z = - 0.5d (surface region) which decreased to minimum at $\hbar\omega$ = 12.5 eV. It further increased and showed a second peak at $\hbar\omega$ = 20 eV whose height was smaller than at $\hbar\omega$ = 8 eV. The variation in the behaviour of $\left|\tilde{A}_{\omega}(z)\right|^2$ for vacuum (z = 0) and bulk (z = -d) was completely different than in the surface region.

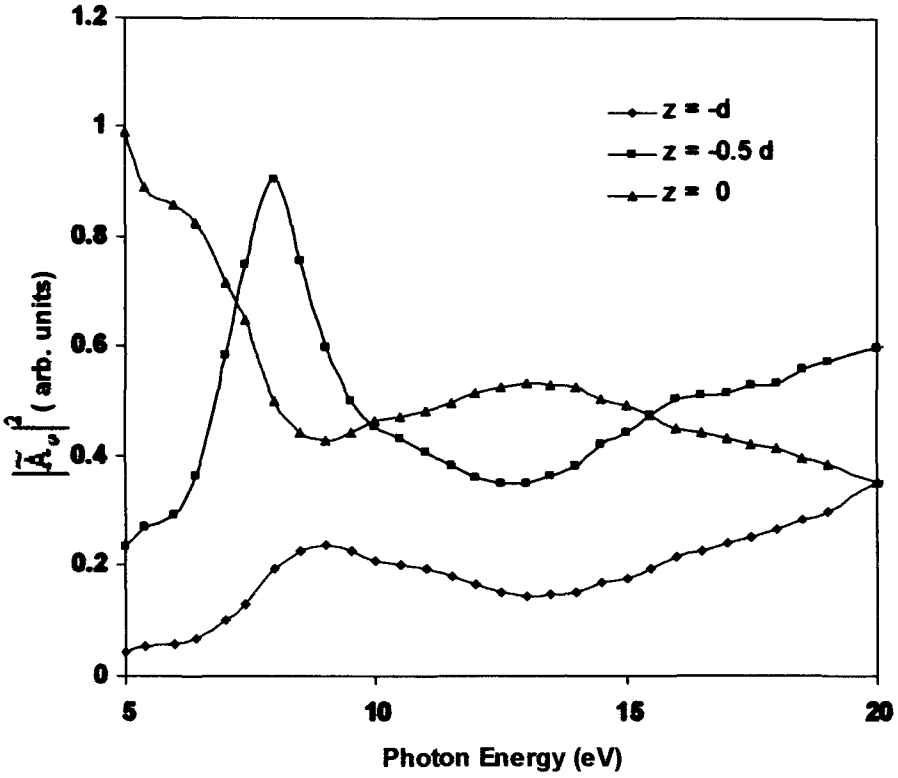

Figure 2. 7: Variation of square of electromagnetic field plotted against photon energy in the case of Cr for location of surface plane at z = -*d* (bulk), z = - 0.5 *d* (surface) and z = 0 (vacuum).

(d) Gallium Arsenide:

Semiconductors, like most metals, also have surface states which had been proved by angle integrated photoemission techniques[47,48]. However, the surface reconstruction which is occurring in most of the semiconductors is, an exception for metals. The calculations of field with respect to parameters like photon energy give us first hand information about the photoemission cross-section, we therefore calculated $\left|\tilde{A}_{\omega}(z)\right|^2$ against the photon energy $\hbar\omega$ in the case of GaAs.

Fig. (2. 8) shows the plot of $\left|\tilde{A}_{\omega}(z)\right|^2$ against the photon energy $\hbar\omega$ for the case of gallium arsenide for the surface planes located at z = - *d* (bulk), z = - 0.5 *d* (surface) and z = 0 (vacuum). The plot of $\left|\tilde{A}_{\omega}(z)\right|^2$ for z = - 0.5 *d* showed a broad peak at photon energy $\hbar\omega$ = 16 eV and with the increase in $\hbar\omega$, it decreases to a minimum at 21 eV (the plasmon energy ($\hbar\omega_p$) for GaAs is 15.8 eV). The behaviour of $\left|\tilde{A}_{\omega}(z)\right|^2$ in the bulk region and vacuum regions showed different patterns. However, the trends obtained from the plot of field $\left|\tilde{A}_{\omega}(z)\right|^2$ against the photon energy $\hbar\omega$ for the surface region shows at least qualitative features as shown by other metals like Ag or Al.

(e) Indium Arsenide:

In Fig. (2. 9) we show also the plot of $\left|\tilde{A}_{\omega}(z)\right|^2$ in the case of another semiconductor InAs. It is seen that in the case of InAs also, for surface region (i.e. z = - 0.5 *d)*, behaviour of $\left|\tilde{A}_{\omega}(z)\right|^2$ is similar to that obtained for GaAs at least

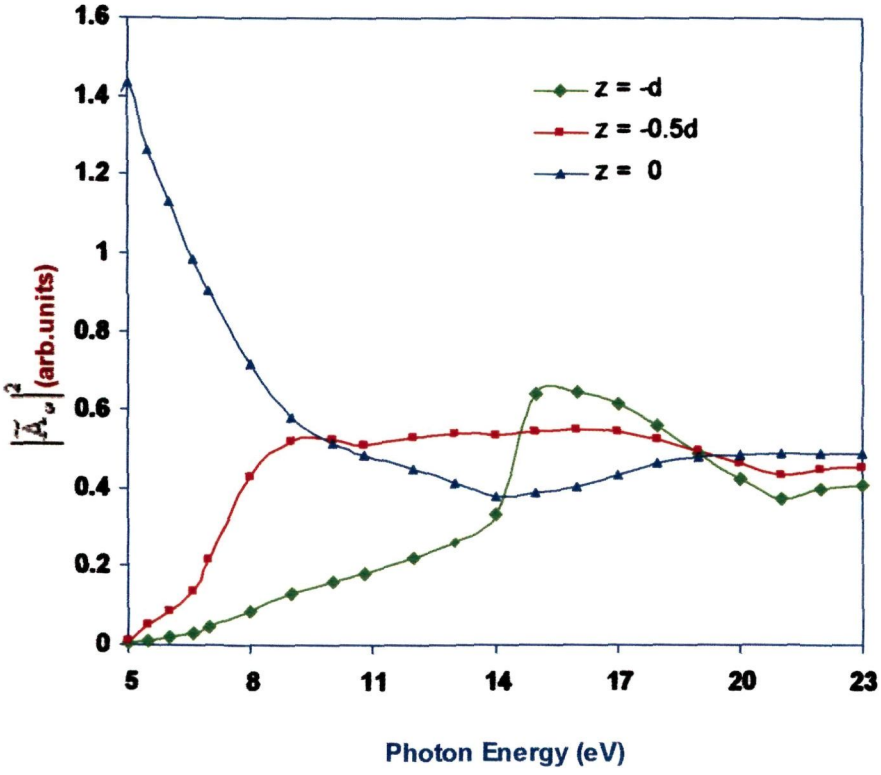

Figure 2. 8: Plot of square of electromagnetic field against photon energy for location of surface planes at $z = -d$ (bulk), $z = -0.5\,d$ (surface) and $z = 0$ (vacuum) in the case of GaAs.

qualitatively. It showed a peak in field square at photon energy $\hbar\omega$ = 11.5 eV and decreases with the increase in photon energy. However the difference with other metals like Ag or Al and semiconductor GaAs is that it showed a constant minimum for values of $\hbar\omega$ = 20 eV to 25 eV. Further, for z = 0(vacuum) also, peak at $\left|\tilde{A}_\omega(z)\right|^2$ was seen at $\hbar\omega$ = 15 eV and showed minimum for values of $\hbar\omega$ extending from 20 eV to 25 eV. Bulk side (z = - d) of semiconductor InAs showed sudden decrease to minimum at $\hbar\omega \sim$ 13 eV.

We find from the variation of z-component of vector potential i.e. $\left|\tilde{A}_\omega(z)\right|^2$ in the case of several metals and semiconductors that almost in all the cases, plot of $\left|\tilde{A}_\omega(z)\right|^2$ against photon energy showed interesting features especially in the surface region (when z = -0.5d). For example, a peak occurred for $\hbar\omega < \hbar\omega_p$ almost in all the cases, and it occurred generally at $\hbar\omega = \hbar\omega_p/\sqrt{2}$. With the further increase in photon energy the values of $\left|\tilde{A}_\omega(z)\right|^2$ decreased and reduced to minimum at $\hbar\omega = \hbar\omega_p$, the plasmon energy of solids. For $\hbar\omega > \hbar\omega_p$ usually a small hump of negligible height in $\left|\tilde{A}_\omega(z)\right|^2$ is obtained. The variation of $\left|\tilde{A}_\omega(z)\right|^2$ plays an important role in normal photoemission which had been elaborately discussed by Bagchi and Kar[23] by considering a simple model for dielectric response function. They considered a classical jellium model to define the dielectric response in the metal side. Two conclusions from their point of view are very important. Firstly, normal component of electric field outside the surface vanishes at $\omega = \omega_p$. Secondly, the

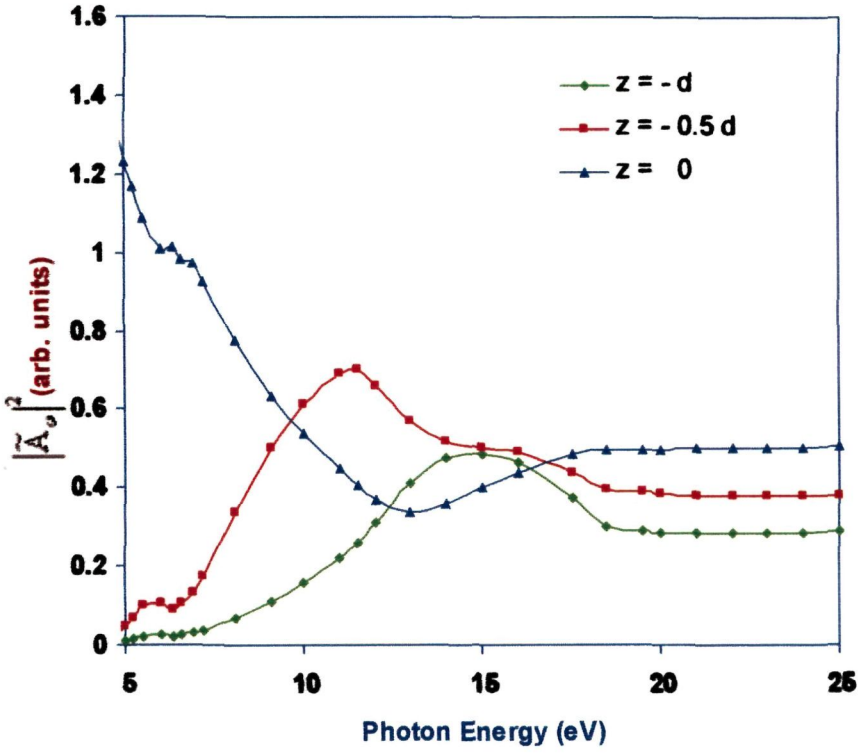

Figure 2. 9: Plot of square of electromagnetic field against photon energy for location of surface planes at z = - *d* (bulk), z = -0.5 *d* (surface) and z = 0 (vacuum) in the case of InAs.

electric field has a sharp peak at $\hbar\omega = \hbar\omega_p . \sqrt{2}$. This however is contradicting the type of results for electromagnetic fields that we have presented. In our results, we have shown that electromagnetic fields in the surface region is maximum at $\hbar\omega_s = \hbar\omega_p / \sqrt{2}$ .For fields outside in the vacuum (z = 0), we find that $\left|\tilde{A}_\omega(z)\right|^2$ showed minimum at $\hbar\omega = \hbar\omega_p$. In our case, peak in $\left|\tilde{A}_\omega(z)\right|^2$ did not occur at $\hbar\omega = \hbar\omega_p . \sqrt{2}$ as shown by Bagchi and Kar[23].

However, we find that the dielectric model used do not seem to be applicable to the case of semiconductors like GaAs and InAs. The reason being that the peaks are not sharp for $\hbar\omega < \hbar\omega_p$ as in the case of metals. Further, a well defined minimum is not obtained at plasmon energies. With this one may conclude that a model suitable to these cases needs to be developed appropriately.

CHAPTER 3

PHOTOCURRENT CALCULATIONS USING MATHIEU POTENTIAL MODEL

In this chapter, we present the calculations of photocurrent from metals and semiconductors by using the Mathieu potential which defines the crystal potential. Mathieu potential is a sinusoidal type of potential which had been used by Davison and Levine[29] for surface band calculations. They have used it to calculate the surface band states by solving the Schrödinger's equation. Pachuau *et.al.*[33] had used this approach of Davison and Levine[29] for deriving the initial state wavefunctions for evaluation of the matrix element $\langle \psi_f | \mathcal{H}' | \psi_i \rangle$ for calculating photocurrent. The calculated photocurrent results as obtained by Pachuau *et.al.*[33] in the case of free electron metals like Al and Be showed satisfactory behaviour especially for photon energy below and above the plasmon energies. They have developed also formulae for initial state wavefunction which is applicable to other metals than free electron metals. This was applied to calculate photocurrent[49] by using Eq. (1. 3) of chapter 1 from d-band metals like W, Mo, Cu and semiconductor Si. The photocurrent data in the ultra-violet photon energy range showed interesting features comparable to experimental results[46] especially in the case of W and Mo.

However, there are two drawbacks in the method of calculation of photoemission as discussed by Pachuau *et.al*[49]. Firstly, for example, the matrix element $\langle \psi_f | \mathcal{H}' | \psi_i \rangle$ involved in scattering cross-section can be expanded as follows:

$$I = \langle \psi_f | \mathcal{H}' | \psi_i \rangle = \int_{-\infty}^{\infty} \psi_f^* \mathcal{H}' \psi_i \, dz = \int_{-\infty}^{\infty} \psi_f^* \left(\tilde{A}_\omega(z) \frac{d}{dz} + \frac{1}{2} \frac{d}{dz} \tilde{A}_\omega(z) \right) \psi_i \, dz$$

$$= \int_{-\infty}^{-d} \psi_f^* \, \tilde{A}_\omega \, \psi_i \, dz + \int_{-d}^{0} \psi_f^* \, \tilde{A}_\omega \frac{d\psi_i}{dz} dz + \frac{1}{2} \int_{-d}^{0} \psi_f^* \frac{d\tilde{A}_\omega}{dz} \psi_i \, dz + \int_{-d}^{0} \psi_f^* \, \tilde{A}_\omega \, \varepsilon(\omega) \frac{d\psi_i}{dz} dz \quad \ldots \quad (3.1)$$

It had been found out by numerical analysis that the first and the last integrands in the above equation do not converge due to choice of values of scattering factor α and μ. It is required that $\alpha<\mu$ for these integrals to converge. Secondly, as discussed above, contributions from the bulk as well as from the vacuum regions to matrix element is considered. This is essentially the case of surface resonance where one considers photoemission to be due to surface and bulk effects. We will discuss here the contribution from the surface region $(-d \le z \le 0)$ only to evaluate matrix element in Eq. (3.1) for calculating photocurrent. For this purpose, the matrix element $\langle \psi_f | \mathcal{H}' | \psi_i \rangle$ will be evaluated by using the initial state wavefunctions as used earlier[49].

3. 1. Formalism used:

Rewriting[49] the wavefunction, the formula for initial state wavefunction in atomic units is given by (in one-dimension):

$$\psi_i(z,q)=\begin{cases}\left(\frac{1}{4\pi k_i}\right)^{\frac{1}{2}}\left(1-\frac{q}{16}+\frac{11}{640}q^2\right)e^{-\mu(z_0'-z)}, & surface\ \ (z\le 0)\\ (2\xi)^{\frac{1}{2}}\,e^{-\xi(z-z_0')}, & vacuum\ \ (z\ge 0)\end{cases} \qquad \ldots \quad (3.2)$$

Here, the various constants (in a.u.) used are as follows:

$$\begin{aligned} &q=1\\ &k_i^2=2E_i\\ &\xi=2\\ &z_0'=\frac{\pi}{a}.z_0\end{aligned} \qquad \ldots. \quad (3.\ 3)$$

where z_0 is the location of the surface state wavefunction and a is the lattice constant which is taken as 6.

We have calculated photocurrent for two locations of the initial state wavefunctions in the surface region, that is, at $z_0 = z_a$ and z_b, where z_a is closer to vacuum-surface interface and z_b is closer to bulk-surface interface. Matrix element in Eq. (3. 1) can now be represented by

$$I = \int_{-d}^{0} \psi_f^* \tilde{A}_\omega(z) . \frac{d\psi_i}{dz} . dz + \frac{1}{2} \int_{-d}^{0} \psi_f^* . \frac{d\tilde{A}_\omega(z)}{dz} . \psi_i . dz \qquad \ldots \qquad (3.4)$$

Eq. (1. 3) had been used to compute photocurrent from metals and semiconductors by using integrals of Eq. (3. 4).

The final state wavefunction $|\Psi_f\rangle$ used is the scattering state of the step potential which is encountered by the electron. Step potential is defined by $V(z) = -V_0\,\theta(z)$ where $\theta(z)$ is unit function such that $\theta(z) = 1$ (0) for $z > 0$ ($z < 0$). In atomic units, final state wavefunction is given by

$$\psi_f(z) = \begin{cases} \left(\frac{1}{2\pi q_f}\right)^{\frac{1}{2}} \frac{2q_f}{q_f + k_f} e^{ik_f z} e^{-\alpha|z|}, & z \le 0 \\ \left(\frac{1}{2\pi q_f}\right)^{\frac{1}{2}} \left(e^{iq_f z} + \frac{q_f - k_f}{q_f + k_f} \right) e^{-iq_f z}, & z \ge 0 \end{cases} \qquad \ldots \qquad (3.5)$$

where $k_f^2 = 2E_f$, $q_f^2 = 2(E_f - V_0)$ and $E_f = E_i + \hbar\omega$. In Eq. (3. 5), the factor $e^{-\alpha|z|}$ is included on the surface and bulk sides to take into account the inelastic scattering of the electrons. Now ψ_f for surface region is given by

$$\psi_f(z)=\left(\frac{1}{2\pi q_f}\right)^{\frac{1}{2}}.\frac{2q_f}{q_f+k_f}.e^{ik_f z}.e^{-\alpha|z|} \qquad \ldots \qquad (3.6)$$

For vector potential $\tilde{A}_\omega(z)$, we have used the formula derived in Eq. (2. 28) of chapter 2. Eq. (1. 3) of chapter 1 had been used to calculate photocurrent from metals Ag, Fe, Ni and Pd and from semiconductors GaAs and PbSe.

The detail expansions of Eq. (3. 4) is shown in APPENDIX-I. As these integrals cannot be calculated analytically, FORTRAN programme were written to evaluate them which is given in APPENDIX-II.

3. 2. Results and Discussions:

We dicuss here the photocurrent results in the case of metals like Ag, Fe, Ni and Pd, and semiconductors GaAs and PbSe. For metals, we use the experimentally measured dielectric constants as given by Weaver [42], whereas for semiconductors, that given by Edward [43]. Choice of parameter like initial state energy (E_i), magnitude of potential (V_0), Fermi level (E_F), were those pertaining to respective metals and semiconductors. However, angle of incidence was $\theta_i = 45^0$ for *p*-polarised light under consideration in all the cases. Photocurrent had been calculated for values of z_0 = -2 a.u. and z_0 = -8 a.u. As the width of the surface is 10 a.u. in all the cases, z_0 = -2 a.u.is near the surface-vacuum interface and z_0 = -8 a.u. is towards the surface-bulk interface. We have shown in all the cases the plot of photocurrent which had been converted to normalized unity. This had been done in order to avoid the large difference in numerical magnitude of the calculated photocurrent data in these two values of z_0.

Metals:

(a) Silver:

In Fig. (3. 1), we show the plot of photocurrent against photon energy in the case of Ag. We have plotted the results in normalised unit for two locations of surface state wavefunctions. For location of ψ_i near the surface-vacuum interface, i.e., in the surface region (z_0 = -2 a.u.), we find that photocurrent showed a peak at $\hbar\omega$ = 10 eV. With the increase in photon energy, it decreases and attained a minimum value at $\hbar\omega$ = 22 eV. Measured value[50] of plasmon energy ($\hbar\omega_p$) of Ag is 25 eV, hence we find that photocurrent decreased to minimum near about the bulk plasmon energy of Ag. For further increase in photon energy beyond $\hbar\omega_p$, photocurrent attained another maxima at $\hbar\omega$ = 35 eV, but of smaller height than at $\hbar\omega$ = 10 eV. However, in the case of z_0 = -8 a.u. in which the surface state wavefunction is located closer towards the bulk, the behaviour of the photocurrent is somewhat different. There is neither a peak nor a minimum in photocurrent as in the case of z_0 = -2 a.u. for values of photon energy below and above $\hbar\omega_p$.

(b) Iron:

Fig. (3. 2) shows the behaviour of photocurrent in the case of Fe where we have shown the plot again for two locations of surface states wavefunctions, that is, at z_0 = -2 a.u. and z_0 = -8 a.u. The observed value[50] of plasmon energy of Fe is 15. 8 eV. In the case of wavefunction located at z_0 = -2 a.u. plot of photocurrent showed a maxima at $\hbar\omega$ = 9 eV and it decreased to a minima at $\hbar\omega$ = 13 eV. A second peak of

small magnitude in height was found at $\hbar\omega$ = 15 eV. The case of z_0 = -8 a.u. shows a different trend which decreases rapidly as the photon energy increases and having a minima also at $\hbar\omega$ = 13 eV. However, there is no proper peak in photocurrent near plasmon energy.

(c) Nickel:

We have also considered another ferromagnetic substance Ni for which the calculated plot of photocurrent against photon energy is shown in Fig. (3. 3). Plasmon energy[50] of Ni is 19.5 eV. Interestingly, for z_0 = -2 a.u., photocurrent showed a maxima at $\hbar\omega$ = 10 eV and decreased as photon energy increased. A minimum in photocurrent was found at $\hbar\omega$ = 20 eV, which is closer to plasmon energy of Ni. For the case of z_0 = -8 a.u., we find that the photocurrent showed a minimum at $\hbar\omega$ = 15 eV, however, a peak was obtained at 18 eV, which is closer to plasmon energy.

(d) Palladium:

Fig. (3. 4) shows the plot of photocurrent in the case of Pd for two locations of the surface state wavefunctions namely, z_0 = -2 a.u. and -8 a.u. respectively. The experimental[50] plasmon energy of Pd is 25.5 eV. For z_0 = -2 a.u. we find the photocurrent increases gradually with the increase of photon energy and is maximum at $\hbar\omega$ = 8 eV. It decreases as usual like in the other metals as photon energy is increased, becomes minimum at $\hbar\omega$ = 21 eV, which is closer to plasmon energy of Ni. In the case of z_0 = -8 a.u., behaviour of photocurrent was different having a minima at $\hbar\omega$ =15 eV.

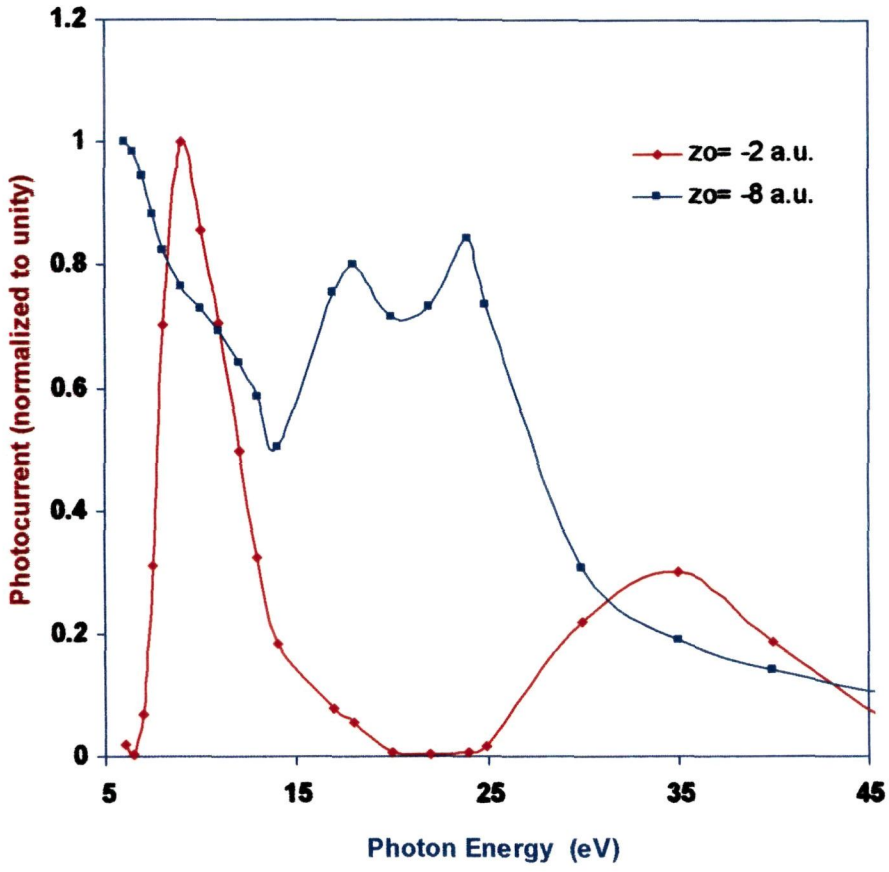

Figure 3. 1: Plot of photocurrent against photon energy with ψ_i defined by Mathieu potential in the case of Ag.

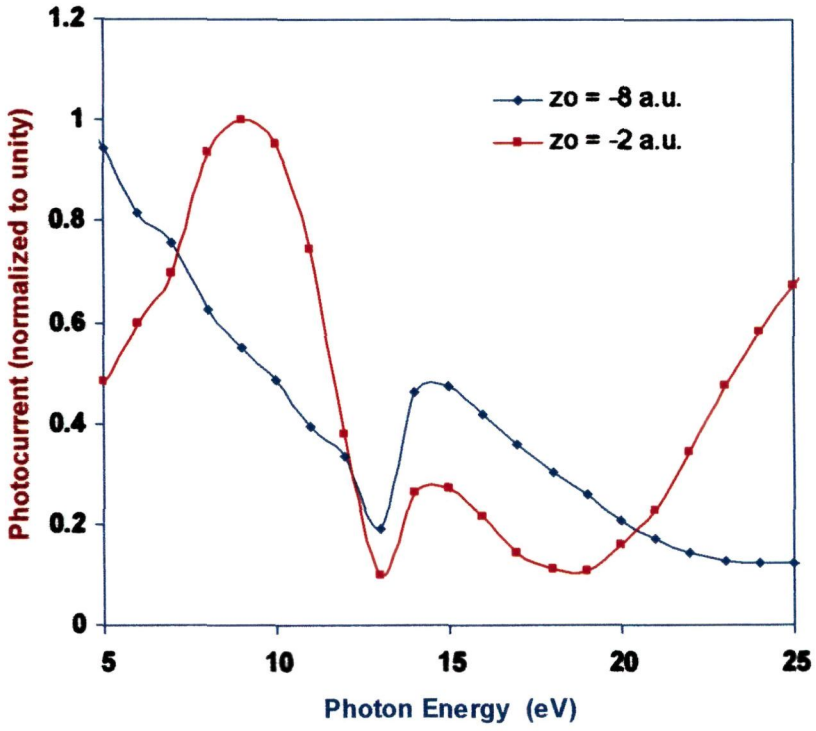

Figure 3. 2: Plot of photocurrent against photon energy with ψ_i defined by Mathieu potential in the case of Fe.

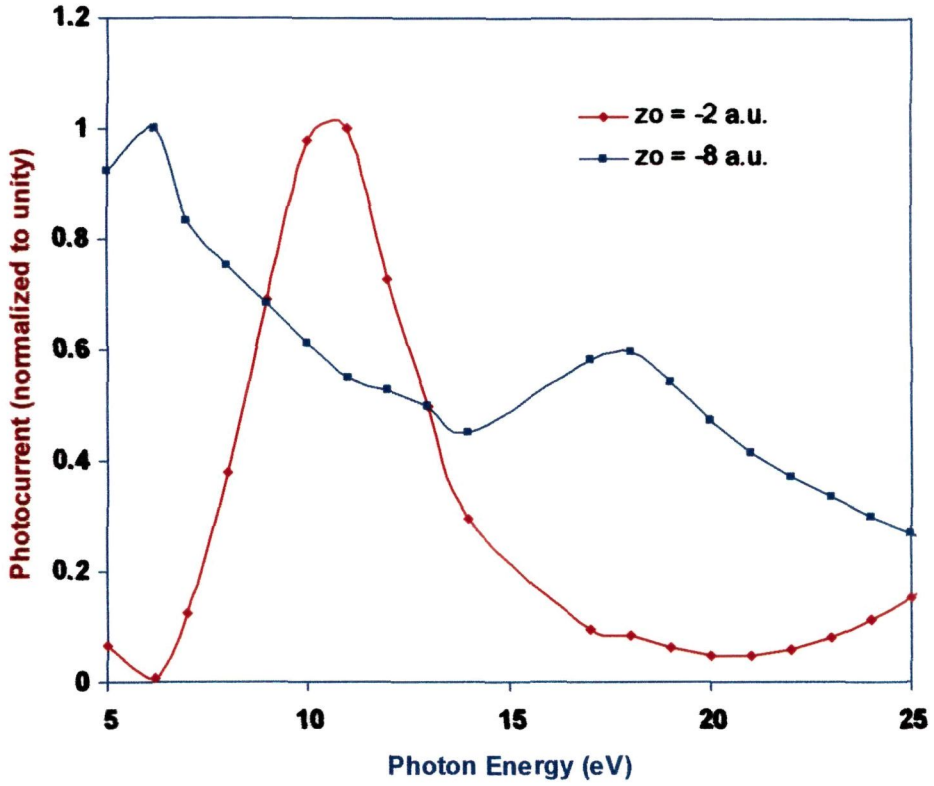

Figure 3.3: Plot of photocurrent against photon energy with ψ_i defined by Mathieu potential in the case of Ni.

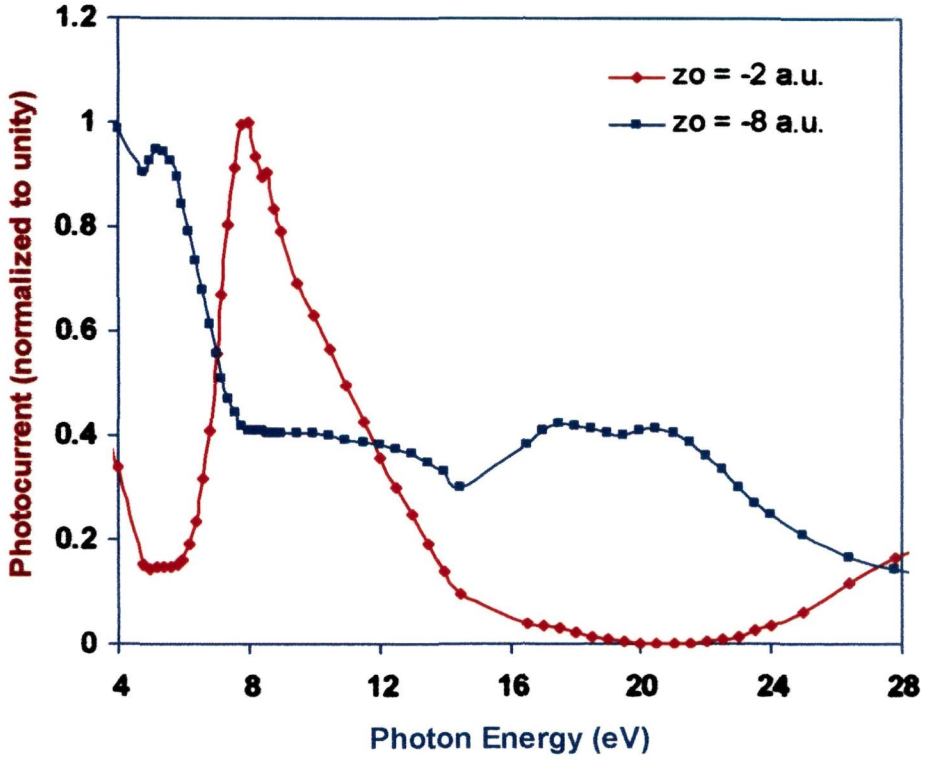

Figure 3. 4: Plot of photocurrent against photon energy with ψ_i defined by Mathieu potential in the case of Pd.

(e) Semiconductors:

We have also considered the application of the formalism developed for calculating photocurrent from semiconductors. Here we are considering only the case of GaAs and PbSe.

(i) Gallium Arsenide:

In the case of GaAs, as shown in Fig. (3. 5), we found that for z_0 = -2 a.u. photocurrent was maximum at $\hbar\omega$ = 7 eV and decreased to a minimum at $\hbar\omega$ = 13 eV. The plasmon[50] energy for GaAs is 14.7 eV where our result is close to this value. Again it showed the occurrence of a second peak at $\hbar\omega$ = 16 eV which is much smaller in height. In the case of z_0 = -8 a.u., the photocurrent decreases from a high value at $\hbar\omega$ = 13 eV to a very low value without any humps.

(ii) Lead Selenide:

In Fig. (3. 6) we show the plot of photocurrent against photon energy in the case of PbSe for z_0 = -2 a.u. and z_0 = -8 a.u. Photocurrent increases with the increase in $\hbar\omega$ for z_0 = -2 a.u. and reaches a maximum at $\hbar\omega$ = 7.5 eV. It decreases with the further increase in $\hbar\omega$ but showed a minimum at $\hbar\omega$ = 10 eV. A small peak in photocurrent is obtained at $\hbar\omega$ = 11 eV and photocurrent decreases with further increase in $\hbar\omega$. For the case of z_0 = -8 a.u., photocurrent goes on decreasing with the increase in $\hbar\omega$ and showed minimum at $\hbar\omega$ = 10 eV. Beyond $\hbar\omega$ = 10 eV, photocurrent showed similar behaviour as shown in the case of case z_0 = -2 a.u.

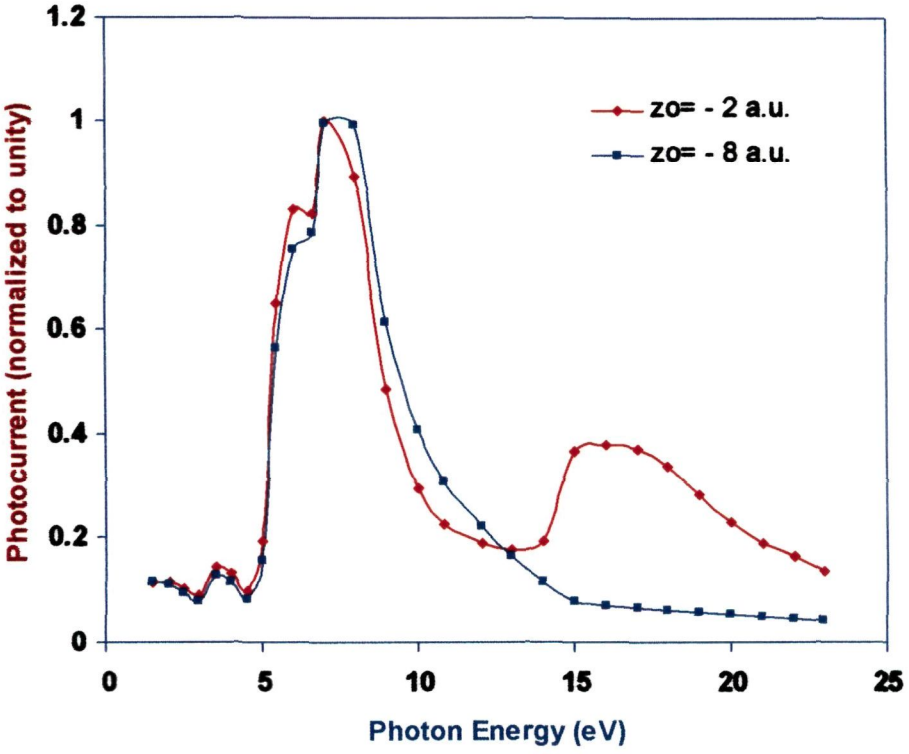

Figure 3. 5: Plot of Photocurrent against Photon Energy with ψ_i defined by Mathieu potential in the case of GaAs.

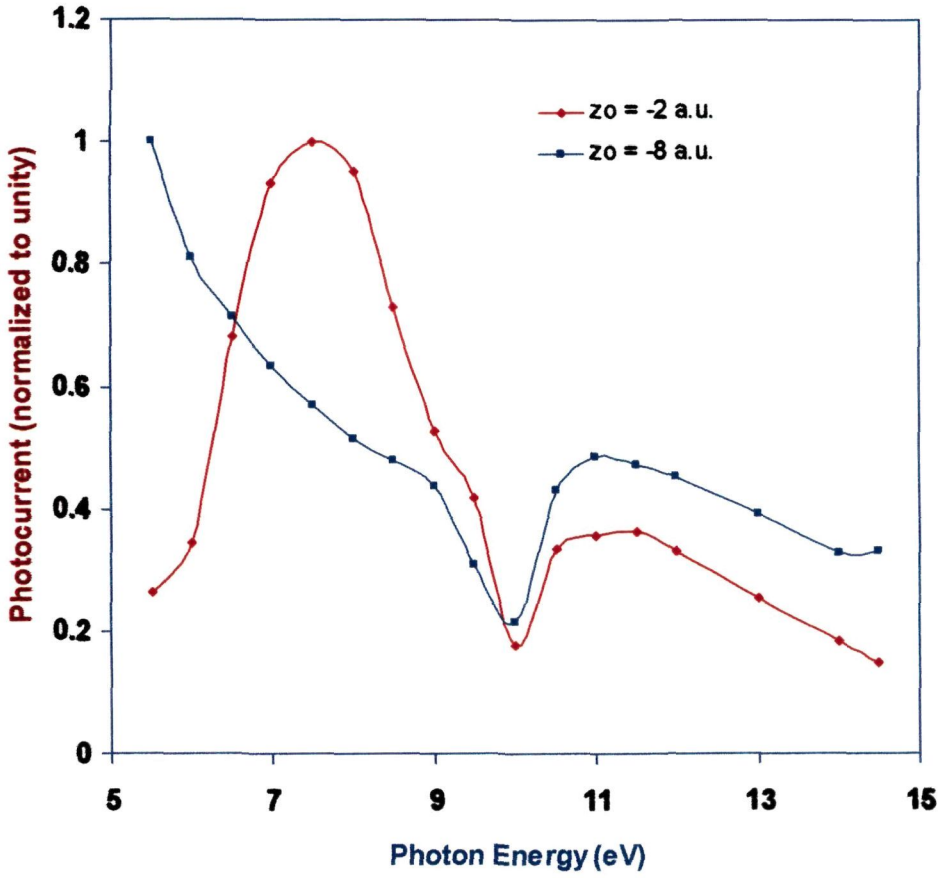

Figure 3. 6: Plot of photocurrent against photon energy with ψ_i defined by Mathieu potential for the case of PbSe.

We find that almost in all the case of metals, photocurrent showed similar trends. For example, as photon energy increased, photocurrent reached a maximum at around the values of photon energy equal to plasmon energy of metals. Beyond the plasmon energy, a second peak in photocurrent was obtained whose height is smaller in magnitude than the first one at $\hbar\omega < \hbar\omega_p$. The reason for the occurrence of peak in photocurrent at $\hbar\omega < \hbar\omega_p$ is due to surface refraction effect where the z-component of electromagnetic field becomes maximum at $\hbar\omega = \hbar\omega_p / \sqrt{2}$. This had been also seen in the experimental[46] results of W and Mo. However, in the case of semiconductors, we do not observe the trends as exhibited by photocurrent in the metals. For example in the case of GaAs, for both the cases of z_0 = -2 a.u. and -8 a.u., we find that it showed similar trends at least below the value of $\hbar\omega$ = 13 eV. For $\hbar\omega$ >13 eV, in the case of z_0 = -2 a.u., a peak of small height in photocurrent occurred, whereas for z_0 = -8 a.u., no such peak was found. However, in the case of PbSe, as well as in the case of PbTe[51], we find that especially in the case of z_0 = -2 a.u., similar trends as shown by metals were obtained.

We therefore conclude that the model used here for photocurrent calculations especially for surface region is applicable to metals and semiconductors. However, in the case of GaAs, we feel that such behaviour is due to abnormal variation of dielectric constants in the surface region. We therefore feel that for semiconductor, dielectric model used is not applicable and a model as suggested by Cappellini and Delsole[52] could be a better choice. The other drawback of the model used here is that the initial state wavefunction used for defining the surface state did not pertain to any

symmetry points. It is known that surface state exists only in a band gap which belongs more or less always pertaining to a particular symmetry points.

However, despite these facts, the photocurrent results showed interesting features. In the next chapter, we will show the inclusion of symmetry of energy band gap taken into consideration for deriving the initial state wavefunction for photoemission calculations.

CHAPTER 4

A THEORETICAL FORMULATION OF INITIAL STATE WAVEFUNCTION FOR PHOTOEMISSION CALCULATIONS BY USING PROJECTION OPERATOR METHOD OF GROUP THEORY.

The interpretation of electron spectroscopy relies on scattering states, because the electron is detected, or emitted, outside the solid. For example in LEED[13], the solid can be seen as a well separated scattering target, and in photoemission the target surrounds the emitting source, the detector being separated from the solid. Furthermore, surface band structure methods based on a supercell geometry, which periodically repeats a volume-vacuum unit cell perpendicular to the surface are bulk-like calculations as well, and do not permit scattering boundary conditions. Thus, the choice of applicable methods is confined to those being able to treat half-space systems. The intrinsic difference between the scattering and bound state boundary conditions makes it more difficult to transfer the remaining methods.

The clarification of the electronic structure of crystalline solids and their surfaces with respect to the ground state and low-lying excited states can be roughly achieved and fitted to experiment by knowing the bound states. Photoemission is a powerful experimental tool suitable to those investigations which, in the framework of simple band mapping, yields a first, however, not very accurate, access to the electronic structure and to many of the derived properties. Quite naturally, most of the theoretical investigators have concentrated on the bound state regime and developed there highly efficient and accurate methods and numerical algorithms distinctly better than now found for scattering states.

However, the scattering states play a prominent role in electron spectroscopies and they must also be known to a high precision, if the actual experimental resolution is to be exploited. *Ab initio* methods, common to bound states are rare because of the need of large computational resources, confined to small and simple systems. Photoemission spectra actually bear a lot of information, which cannot always be

understood through band mapping or more elaborately, by line profile analysis, but must, especially in the case of valence band investigations, be extracted from direct comparison with calculated spectra. Therefore knowledge of scattering states is very essential.

Various approaches and models have been proposed by several workers. For example, Pendry[13] was among the first to present the detailed scattering formalism for band structure calculations of surface and bulk of solids which is now popularly known as Low Energy Electron Diffraction (LEED). This procedure has been also extended to photoemission calculations.[53] Schattke[54] has also done a detailed calculation by including the one-step model of photoemission and applied it to the case of semiconductor like GaAs. Ishii *et.al*[55] have presented the LEED-type calculations using the KKR-scheme. The results for Al (100) and Na (110) were found by them to agree very well with the experiment. A real space angle-resolved photoemission formalism has been proposed by Ernst *et.al.*[56] In this approach, Ernst *et.al.*[56] have used the multiple scattering description within the independent-particle approximation to develop a real-space semi-relativistic angle-resolved photoemission code which has been successfully applied to the case of Cu. This had been also extended[57] to ultra-thin films and interfaces to study electronic and magnetic properties.

Some of the methods discussed above are infact, very interesting, but pose a complex and serious mathematical and computational problem. In this chapter, we will discuss a simple approach to photoemission calculation in which projection operator (P.O.) method of group theory will be employed. We see from Chapter 3, that calculation of photocurrent (given by Eq. 3.1) involves the evaluation of the

matrix element $\langle \psi_f | \mathcal{H}' | \psi_i \rangle$, we will therefore use the P.O. method to derive the initial state wavefunction ψ_i by suitably describing the basis function involved. Photocurrent will be calculated for the case of crystals with empty potential and a periodic potential which is defined by Kronig-Penney δ - type potential.

4.1 Application of Projection Operator method to deduce the basis function:

In this section, application of projection operator method of group theory is presented which is used for deriving the basis functions. These basis functions are used to formulate the initial state wavefunction for use in photoemissions for calculating photocurrent as given by Eq. (3. 1). Atomic and molecular orbital are represented mathematically in terms of basis functions. A group of basis functions used to represent an orbital is called a *basis set*. Basis set can comprise of one or more basis functions. Basis function may be defined therefore in such a way that a set of l-dimensional matrices $\Gamma(T)$ form a representation of a group of operators, and $\phi_1(r), \phi_2(r), \ldots\ldots, \phi_l(r)$ are a set of linearly independent functions, such that a transformation operator $P(T)$ operating on it gives,

$$P(T)\phi_n(r) = \sum_{m=1}^{l} \Gamma(T)_{mn} \phi_m(r), \quad n = 1, 2 \ldots l, \qquad \ldots \quad (4.1)$$

then, the functions $\phi_n(r)$ are said to be partners in a set of basis functions for the representation Γ, the function $\phi_n(r)$ being said to transform as the n-th row of this representation.

Any normalizable function $\phi(r)$ can be decomposed into linear combinations of the irreducible representation of the group of operators G i.e.

$$\phi(r) = \sum_{p} \sum_{n=1}^{l_p} \phi_n^p(r) \qquad \ldots \qquad (4.2)$$

where $\phi_n^p(r)$ is the n-th row of the unitary irreducible representation Γ^p and $\sum_p$ is the sum over all the non-equivalent unitary irreducible representation of $\mathcal{G}$. The decomposition of an arbitrary normalizable function into basis functions can be carried out in a simple way by using projection operator which may be defined as[38]

$$\mathcal{P}_{mn}^p = \frac{l_p}{g} \sum_T \Gamma^p(T)_{mn}^* P(T) \qquad \ldots \qquad (4.3)$$

Here l_p is the dimension of the unitary irreducible representation of the group $\mathcal{G}$, g is order of $\mathcal{G}$ and $\sum_T$ is the summation over all the transformation T of $\mathcal{G}$.

If $\phi_t^q(r)$ transforms as the i-th row of Γ^q then

$$\mathcal{P}_{mn}^p \phi_t^q(r) = \delta_{pq} \delta_{nt} \phi_m^p(r) \qquad \ldots \qquad (4.4)$$

From Eq. (4. 2) and (4. 4), we have

$$\mathcal{P}_{mn}^p \phi(r) = \mathcal{P}_{nn}^p \sum_{p} \sum_{n=1}^{l_p} \phi_n^p(r) = 0 + \ldots + \delta_{pp} \delta_{nn} \phi_n^p(r) + 0 + \ldots\ldots = \phi_n^p(r)$$

$$\therefore \quad \mathcal{P}_{nn}^p \phi(r) = \phi_n^p(r) \qquad \ldots \qquad (4.5)$$

Thus from Eq. (4. 5) we see that $\mathcal{P}_{nn}^p$ projects a function $\phi(r)$ and generates a new function $\phi_n^p(r)$. This function $\phi_n^p(r)$ is called the basis function. This method of derivation of the basis function using projection operator technique has been applied to deduce the initial state wavefunctions for electronic states in various types of metals. Two cases are of special interest to us namely, empty potential[58, 59] and a

periodic potential, for which appropriate basis functions will be developed to derive the initial state wavefunction ψ_i.

4.2. Formulation of initial state wavefunction by using basis functions derived by projection operator method.

(i) Case of empty potential:

The calculation of initial state wavefunction is a complicated problem due to the presence of surface state. However, the crystal states lying in the bulk band gaps which pertain to a particular kind of surface states can be identified, and, the initial state wavefunction ψ_i which represents the electron state can be calculated by using projection operator method. We have assumed an empty lattice potential as shown in Fig. (4. 1). One can write ψ_i as

$$\psi_i(z) = \begin{cases} \phi(z)\left(e^{ik_i z} + \mathrm{R}e^{-ik_i z}\right)e^{\mu z} & \textit{surface \& bulk} \quad z \le 0 \\ T e^{-\chi z} & \textit{vacuum} \quad z \ge 0 \end{cases} \quad \ldots \quad (4.6)$$

where $\phi(z)$ is the atomic orbital which is evaluated by using the projection operator. The reflection (R) and transmission coefficients (T) are evaluated by matching the wavefunctions and its derivatives at $z = 0$, and are given by

$$R = -\frac{(1+k_i) - i(\chi+\mu)}{(1-k_i) - i(\chi+\mu)}.$$
$$T = -\frac{2k_i}{(1-k_i) - i(\chi+\mu)}. \quad \ldots \quad (4.7)$$

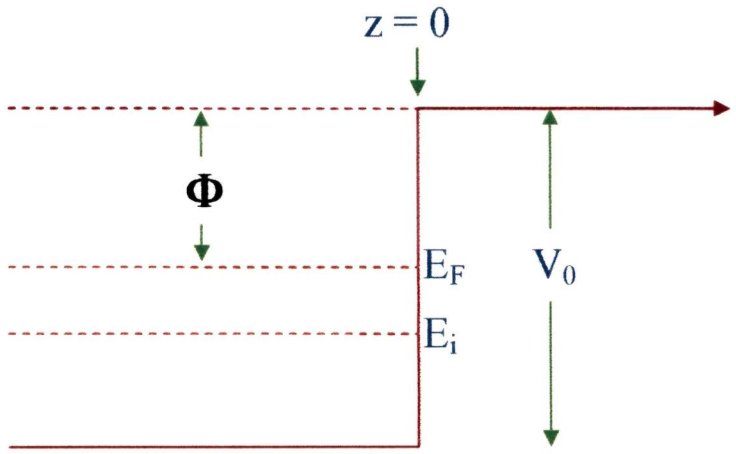

Figure 4.1: Model potential diagram for calculating initial state wavefunction ψ_i for the case of an empty potential.

We have derived the initial state wavefunction ψ_i for Cu (110) surface states. For Cu (110), surface state occurs[37] in $L_{2'} - L_1$ band gap. The linear combination of atomic orbital (LCAO) representation for $L_{2'}$ point is $\frac{1}{\sqrt{3}}(x+y+z)$. We have therefore considered the point $L_{2'}$ for which the point group is C_{2v}, and obtained the basis function for this point group corresponding to Cu (110) surface state by using the projection operator formula[38] given by Eq. (4. 5). The detailed derivation of basis function using projection operator technique and the derivation of ψ_i is given in APPENDIX- III(1). The final form of ψ_i obtained in one dimensional case then can be written as

$$\psi_i(z) = \begin{cases} e^{\iota z}\left(e^{\iota k_i z} + \mathrm{Re}^{-\iota k_i z}\right)e^{\mu z} & \textit{surface \& bulk} \quad z \le 0 \\ T e^{-\chi z} & \textit{vacuum} \quad z \ge 0 \end{cases} \qquad \ldots (4.8)$$

where $k_i^2 = 2E_i$, $\chi^2 = 2(V_0 - E_i)$, $\mu = k_i - \frac{\pi}{a}$ and a is the lattice constant. Initial state wavefunction ψ_i of Eq. (4.8) is used to evaluate photocurrent from Cu (110) surface. Photocurrent had been calculated by using Eq. (1. 3) of Chapter 1. Final state wavefunction ψ_f is as given in Eq. (3. 5) and the photon field $\tilde{A}_\omega(z)$ is the one given by Eq. (2.28). FORTRAN programmes has been written to evaluate photocurrent which is given in detail in APPENDIX- IV.

We have applied the wavefunction ψ_i developed by using P.O. in calculating photocurrent from Cu (110) surface, where surface states have been observed experimentally in photoemission[60,61] and inverse photoemission[62, 63] measurements.

We were mainly interested to see the effect in the behaviour of photocurrent from Cu (110) surface by inclusion of ψ_f in the matrix element. As it is a model calculation, we have assumed empty potential to exist in the bulk. Experimentally determined dielectric constants[42] were used for calculating the photon field vector and the lattice constant for Cu was chosen to be $a = 3.61$ $\overset{0}{\text{A}}$. We have assumed the surface state to be located at 2. 72 eV below the Fermi level of Cu.

The variation of photocurrent against photon energy pertaining to this surface state is shown in Fig. (4. 2). We find that photocurrent is maximum when photon energy($\hbar\omega$) is 12 eV and it decreases to a minimum at $\hbar\omega = 14$ eV. Further increase in photon energy causes it to rise to a second maximum at around $\hbar\omega = 17$ eV, after which the photocurrent decreases towards minimum. This decrease in photocurrent is due to the presence of the term α associated in the wavefunction. We find that by incorporating the dielectric model developed in chapter 2 into the matrix element for photocurrent calculation which involve wavefunction ψ_f deduced by Mathieu potential, gives photocurrent results[58] which showed similar variation as that found in metals like[64, 65] Be, W etc. Furthermore, the photocurrent data in the case of Cu (110) surface state showed better qualitative agreement than that obtained using Mathieu potential[49] model.

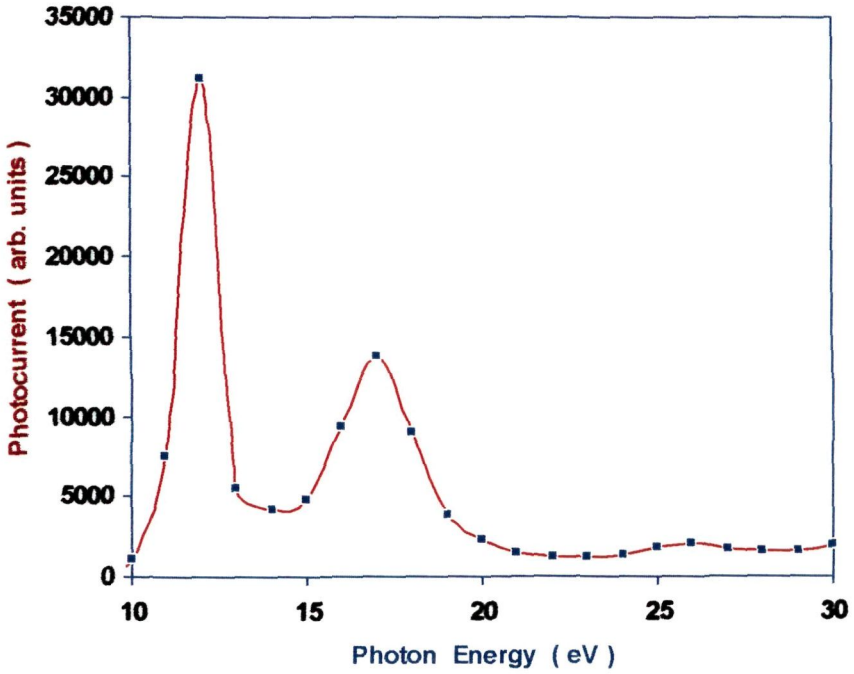

Figure 4.2: Plot of photocurrent as a function of photon energy for Cu for surface state located at 2.72 eV below Fermi level with surface width d= 10 a.u.

(ii) Case of periodic potential:

We have discussed in section 4. 2(i), the model calculation of photoemission by incorporating the basis function obtained by using projection operator technique for an empty potential case. The case of empty potential is not applicable to strongly bonded metals like d-band metals or semiconductors. In such circumstances, we will define the crystal potential by δ - potential which represents the Kronig-Penney potential and is periodic with the periodicity of the lattice as shown in Fig. (4. 3). Schrödinger equation will be solved to obtain the solution in terms of Green function[34].

Kronig-Penney model has been used in connection with surface electronic states by several authors[29, 66-68]. Schaich and Ashcroft[4] have calculated numerically the photoyield by using the modified form of the Kronig-Penney model. Steslicka[69] had performed a detailed calculation of the surface states using the Kronig-Penney model both for the semi-infinite and the finite crystal model. Eldib *et al* [70] has also applied Kronig-Penney model to one dimensional crystal. They had calculated only the electronic energy bands for mono and poly-atomic crystals and compared the data with the one computed using LCAO method.

For one dimensional case, the Schrödinger equation can be written as

$$\left(\nabla^2 + k_t^2\right)\psi(z) = V(z)\psi(z) \qquad \ldots \quad (4.\ 9)$$

where $k_t^2 = 2E_t$. If Green function of a free particle is defined as G(z,y), then the equation for a point source is,

$$\left(\nabla^2 + k_t^2\right)G(z,y) = \delta(z-y) \qquad \ldots \quad (4.\ 10)$$

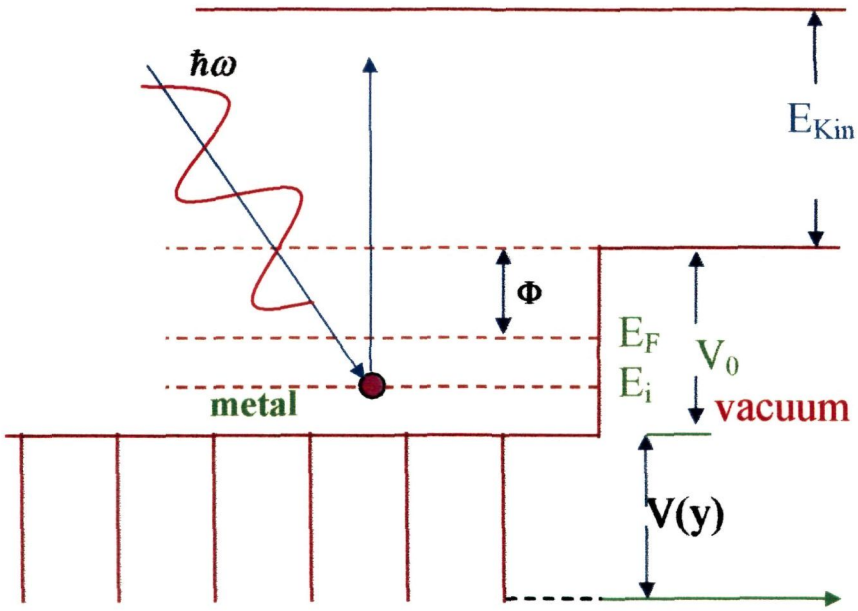

Figure 4. 3: Schematic representation of Kronig-Penney δ -potential model for calculating the initial state wave function by using projection operator method of Group Theory.

In terms of Green function, Schrödinger equation (Eq 4. 9) can now be replaced by the integral equation

$$\psi(z)=\int_{-\infty}^{+\infty}V(y)\psi(y)G(z,y)\,dy \qquad \ldots \quad (4.11)$$

Considering the periodicity of the crystal gives $V(y+na) = V(y)$, and the Bloch-Floquet theorem yields

$$\psi(y+na)=e^{ik_t na}\psi(y). \qquad \ldots \quad (4.12)$$

Eq. (4. 11) can now be written as

$$\psi(z)=\sum_{n=-\infty}^{\infty}e^{ik_t na}\int_0^a V(y)\psi(y)G(z,y+na)\,dy \qquad \ldots \quad (4.13)$$

Putting $s = z-y$ and $t=s-a\left[\frac{s}{a}\right]$

$$\psi(z)=-\frac{1}{2k_t}\int_0^a e^{ika\left[\frac{s}{a}\right]}\frac{e^{ika}\sin k_t t-\sin k_t(t-a)}{\cos k_t a-\cos ka}\psi(y)V(y)\,dy \qquad \ldots \quad (4.14)$$

Let the Kronig-Penney potential be represented by a linear Dirac δ-function i.e

$$V(y)=\left(\frac{2p}{a}\right)\sum_{n=-\infty}^{\infty}\delta(y-na) \qquad \ldots \quad (4.15)$$

where $p=\lim_{\substack{b\to 0\\ V_1\to\infty}}\frac{1}{2}\chi_0^2\,ab$ with $\chi_0^2=2(V_1-E_t)$. Here, p is the strength of the δ-function barrier and it is assumed to be positive. In the first cell of the crystal ($0<y<a$),

$$V(y)=\left(\frac{2p}{a}\right)\delta(y-a) \qquad \ldots \quad (4.16)$$

Substituting Eq. (4. 16) in Eq. (4. 14) we have

$$\psi(z) = -\frac{p}{k_t a}\int_0^a e^{\iota k a\left[\frac{s}{a}\right]}(\cos k_t a - \cos ka)^{-1}\left\{e^{\iota ka}\sin k_t\left(z - a\left[\frac{z}{a}\right]\right) - \sin k_t\left(z - a\left[\frac{z}{a}\right] - a\right)\right\}$$

$$\times \psi(y)\,\delta(y-0)\,dy \qquad \ldots \quad (4.17)$$

Putting $z' = z - a\left[\frac{z}{a}\right]$, we have

$$\psi(z) = \frac{p}{k_t a}\psi(0)e^{\iota k(z-z')}\frac{e^{\iota ka}\sin k_t z' - \sin k_t(z'-a)}{\cos ka - \cos k_t a} \qquad \ldots \quad (4.18)$$

where $\psi(0) = -\int_0^a \psi(y)\delta(y-0)\,dy$ when $y = 0$. Setting $z' = z$ Eq. (4. 21) takes the form

$$\psi(z) = \frac{p}{k_t a}\psi(0)\frac{e^{\iota ka}\sin k_t z - \sin k_t(z-a)}{\cos ka - \cos k_t a} \qquad \ldots \quad (4.19)$$

The direct matching procedure for the solution of Schrödinger equation with Kronig-Penney model potential incorporated gives

$$\psi(z) = 2iC\frac{e^{\iota ka}\sin k_t z - \sin k_t(z-a)}{e^{\iota ka} - e^{-\iota k_t a}} \qquad \ldots \quad (4.20)$$

When $z = 0$, $\quad \psi(0) = 2iC\dfrac{\sin k_t a}{e^{\iota ka} - e^{-\iota k_t a}}$ $\qquad \ldots \quad (4.21)$

From Eqs. (4. 21) and (4. 19), we get

$$\psi(z) = \frac{\tau(0)}{\sin k_t a}\left[e^{\iota ka}\sin k_t z - \sin k_t(z-a)\right] \qquad \ldots \quad (4.22)$$

where $\quad \tau(0) = \dfrac{2Cip\sin^2 k_t a}{k_t a(e^{\iota ka} - e^{-\iota k_t a})(\cos ka - \cos k_t a)}$ $\qquad \ldots \quad (4.23)$

The initial state wavefunction $\psi_i(z)$ can now be written as

$$\psi_i(z)=\begin{cases}\psi(z)+R\psi^*(z) & \textit{bulk \& surface} \quad z\le 0\\ T e^{-\chi z} & \textit{vacuum} \quad z\ge 0\end{cases} \qquad \ldots \quad (4.24)$$

where $\psi^*(z)$ is the complex conjugate of $\psi(z)$, R is the reflection coefficient and T is the transmission coefficient across the boundary plane and $\chi_0^2=2(V_0-E_i)$, and V_0 is the potential at the surface which an electron encounters while transmitting through the boundary surface. Matching the wavefunction and its derivatives at $z = 0$ gives the value of coefficients R and T as

$$R=\frac{k_i e^{ika}-k_i\cos k_i a+\chi\sin k_i a}{k_i\cos k_i a-k_i e^{-ika}-\chi\sin k_i a}$$

$$T=\tau(0)\left[\frac{2ik_i\sin ka}{k_i\cos k_i a-k_i e^{-ika}-\chi\sin k_i a}\right] \qquad \ldots \quad (4.25)$$

Now introducing the atomic orbital $\phi(z)$ which includes the basis function derived by P.O. method as discussed in section (4. 1), the final form of initial state wavefunction can be represented by

$$\psi_i(z)=\begin{cases}\psi_i(0)\phi(z)e^{\mu z}(k_i\cos k_i z-\chi\sin k_i z), & \textit{bulk \& surface} \quad z\le 0\\ \psi_i(0)k_i e^{-\chi z}, & \textit{vacuum} \quad z\ge 0\end{cases} \qquad \ldots \quad (4.26)$$

where $\psi_i(0)=\dfrac{2i\sin ka\ \tau(0)}{k_i\cos k_i a-k_i e^{-ika}-\chi\sin k_i a}$ $\qquad \ldots \quad (4.27)$

The detail derivation of initial state wavefunction ψ_i in Eq. (4. 26) is discussed in APPENDIX- III (2).

The initial state wavefunction given by Eq. (4. 26) had been used in conjunction with final state wavefunction ψ_f as defined in Eq. (3. 5) and vector potential $\tilde{A}_\omega(z)$ of Eq. (2. 28) to calculate photocurrent by using the formula given

in Eq. (1. 3) of chapter 1. The matrix element $I=\langle \psi_f | \mathcal{H}' | \psi_i \rangle$ in Eq. (1. 3) can be written as .

$$I= \int_{-\infty}^{d} \psi_f^* \tilde{A}_\omega \psi_i \, dz + \int_{-d}^{0} \psi_f^* \tilde{A}_\omega \frac{d}{dz} \psi_i \, dz + \frac{1}{2} \int_{-d}^{0} \psi_f^* \frac{d\tilde{A}_\omega}{dz} \psi_i \, dz + \int_{0}^{\infty} \psi_f^* \tilde{A}_\omega \varepsilon(\omega) \frac{d}{dz} \psi_i dz \quad \ldots (4.28)$$

We have used dielectric constants corresponding to different metals which were those given by Weaver[42] and Edwards[43]. The potential strength p is taken as 0.5 and the lattice constant for Cu as a =3.61 $\overset{0}{A}$. The other data used are: the scattering factor α = 0.35, angle of incidence (θ_i) = 45^0. The calculation of photocurrent was done for surface width d= 10 a.u. and the narrow surface width (ie. d= 0 a.u). The detailed FORTRAN programme for numerical evaluation of Eq. (4. 28) is given in APPENDIX-V. A systematic photoemission studies by using the model wavefunction for initial state $\psi_i(z)$ is discussed below for metals like Al, Be, Cu, etc.

(a) Aluminium:

Fig. (4. 4) shows the plot of photocurrent versus photon energy ($\hbar\omega$) for the surface region defined by $-d \le z \le 0$ having the surface width d= 10 a.u and narrow surface width d = 0 a.u. We have chosen the initial state energy E_i for a high lying surface state occurring at 0.41 eV below Fermi level, the location of the Fermi level and the work function[4] ϕ for Al are taken as 11.7 eV and 4.25 eV respectively. The photocurrent profile for d =10 a.u. showed a strong photoemission at photon energy $\hbar\omega$ = 9 eV, which was followed by a decrease in photocurrent and the minimum occurring at $\hbar\omega$ = 15 eV (the plasmon energy of Al is $\hbar\omega_p$= 15.3 eV). There is

another hump in the photocurrent data at $\hbar\omega$ = 20 eV. The behaviour of photocurrent in the case of narrow surface width is quite different. For example, almost a flat peak in a photon energy range 10 eV-14 eV was obtained. Although the minimum in photocurrent was seen at $\hbar\omega \approx$ 15 eV, contribution to photoemission was far less important. However the photoemission results for d = 10 a.u. seems to be in qualitative agreement with the experimental results of Levison *et.al*[15] (see Fig.4. 4 (inset)). For example, the experimental data of Levinson *et.al* [15] showed a maxima in photocurrent at $\hbar\omega$ = 13 eV with occurrence of a minima at the plasmon energy ($\approx$15.3 eV). Also, it showed similar behaviour with the calculated results of Thapa *et.al*[24, 33].

(b) Beryllium

Photocurrent against photon energy ($\hbar\omega$) in the case of Be was calculated for values of surface width d= 10 a.u., and narrow surface width (d= 0) by using the following data: Surface state energy = 0.41 eV below Fermi level, Fermi level E_F = 14.3 eV , work function ϕ = 3.92 eV and V_0 = 18.22 eV. We show in Fig. (4. 5) the plot of photocurrent with the choice of these parameters. As incident photon energy increases, the photocurrent showed a peak in its value at $\hbar\omega$ = 10 eV for d = 10 a.u. The photocurrent gradually decreases and minimum occurred at $\hbar\omega$ = 11 eV. With further increase in photon energy, a second hump in photocurrent is observed at $\hbar\omega$ = 25 eV, whose height is only around 25 % times that of peak at $\hbar\omega$ = 10 eV. The interesting feature in the case of Be is that it could reproduce the earlier data as obtained by Thapa and Kar[71] who had done the calculation but by using a simple free electron model. However, the second hump was not indicated in their calculation. We

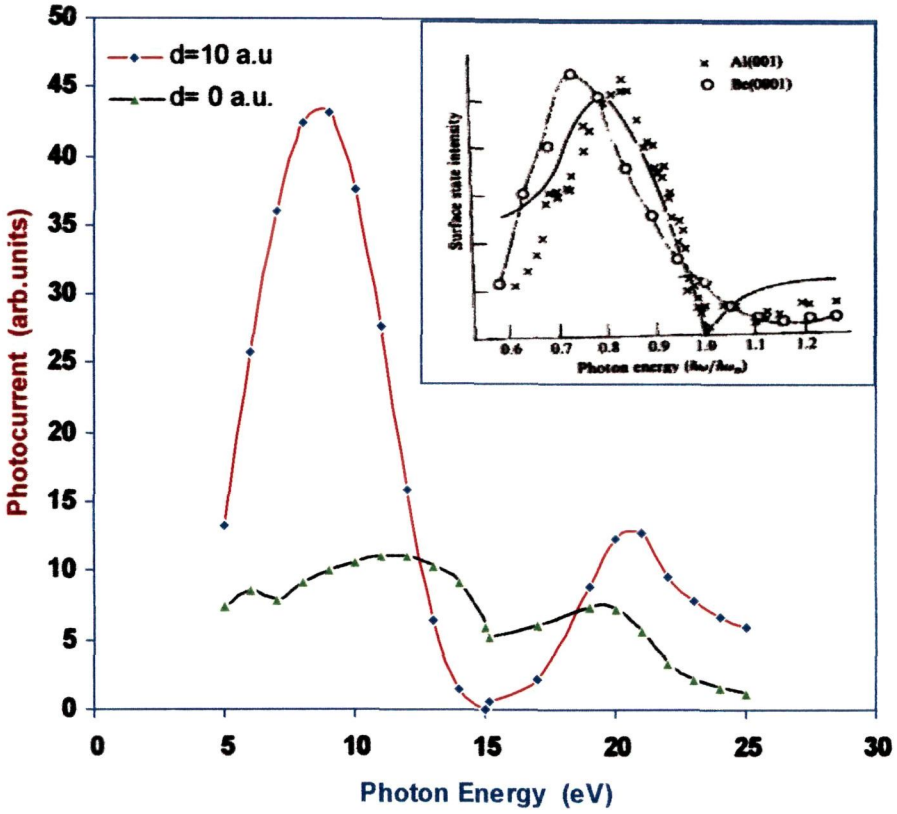

Figure 4. 4: Plot of photocurrent variation against photon energy in the case of Al, for surface width d = 10 a.u. and d = 0 by employing Kronig-Penney δ-potential where ψ_i is derived by projection operator method of Group Theory.

INSET: Experimental results for Al and Be as obtained by Levinson *et.al*[15].

find here that the model calculation also showed a qualitative agreement with the experimental results of Bartynski *et.al*[35].

(c). Copper :

The plot of photocurrent against the photon energy $\hbar\omega$ for Cu is shown in Fig. (4. 6).The photocurrent was calculated for two values of surface widths namely d= 0 and d = 10 a.u. and for the same value of surface state energy (2. 72 eV below Fermi level) and potential barrier height (11. 4 eV). We find that for d = 10 a.u., a maximum in the value of photocurrent occurs at $\hbar\omega$ = 14 eV. With further increase of photon energy, photocurrent decreases to a minimum value at $\hbar\omega$ = 19 eV and the next hump occurs again at $\hbar\omega$ = 23 eV. But for a narrow surface width (d = 0), the behaviour of photocurrent is quite different as shown in Fig. (4. 6). We do not find any peak for values of photon energy below and above 19 eV. The behaviour of photocurrent shows a qualitative agreement with those shown by other metals[72] like W, Si, etc. in which Kronig-Penney potential model was also used.

(d) Tungsten:

In Fig. (4. 7), we have shown the plot of photocurrent against the photon energy ($\hbar\omega$) in the case of tungsten for values of surface width d = 10 a.u. and narrow surface width when d=0. Following Weng *et.al.*[46] we have considered the surface state to lie at 0. 4 eV below the Fermi level, whereas the potential barrier V_0 = 14. 75 eV, Fermi level E_F = 10. 25 eV and work function ϕ = 4. 5 eV. These data are taken from those given by Aschcroft and Mermine[73]. We find that for d= 10 a.u., photocurrent showed a maxima at $\hbar\omega$ = 18 eV, and decreased to minimum at $\hbar\omega$ = 26

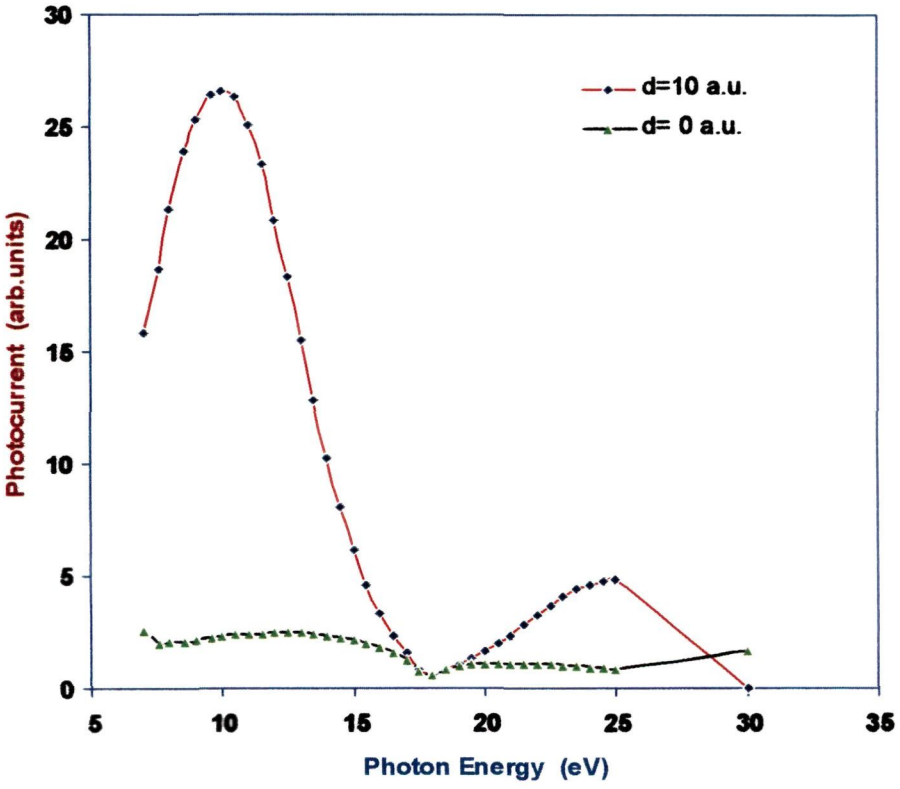

Figure 4. 5: Plot of photocurrent against photon energy for surface widths d= 10 a.u and d= 0 in Be using Kronig-Penney δ - potential where ψ_i is derived by projection operator method of Group Theory.

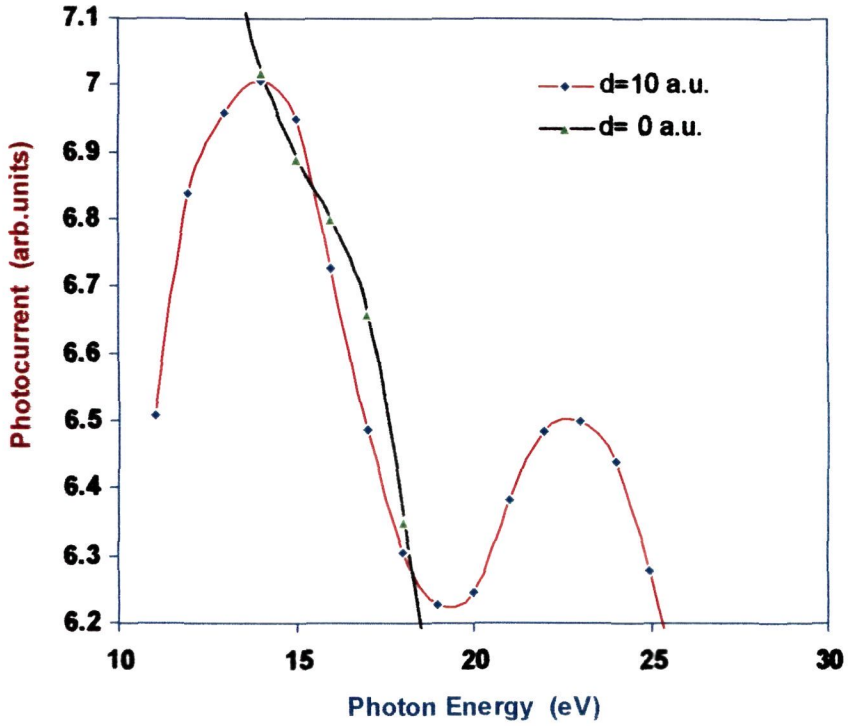

Figure 4. 6: Plot of variation of photocurrent with photon energy for surface widths d= 10 a.u and d= 0 in Cu using Kronig-Penney δ-potential where ψ_i is derived by projection operator method of Group Theory.

eV. With further increase of the incident photon energy, a small peak in the photocurrent data at $\hbar\omega = 130$ eV was observed whose magnitude in height was almost less than 10 % than that at $\hbar\omega = 18$ eV. For narrow surface width case, behaviour of photocurrent is quite different which showed maximum at $\hbar\omega = 22$ eV and did not exhibit minimum at the plasmon energy of tungsten (which is around 25. 3 eV) but instead decreased to minimum at 30 eV. The experimental data of Weng *et. al.*[46] in Fig. 4. 7 (inset) showed minimum at $\hbar\omega = 25$ eV, with a second peak in photocurrent at $\hbar\omega = 29$ eV.

We find that, our model calculations of photocurrent in the case of tungsten could reproduce what Weng *et. al.*[46] had obtained experimentally. The only exception in our calculated data lies in the fact that first maxima in photocurrent occurred at $\hbar\omega = 18$ eV. However, we could see that qualitatively, it agreed quite satisfactorily with the experimental results of Weng *et.al.*[46]

(e) Semiconductors:

The presence of surface states on semiconductor surfaces was verified early by using angle integrated photoemission[47,48]. Moreover, their existence is obvious through the pinning of the Fermi level at the surface. In bulk semiconductors the Fermi level shifts, depending upon the doping level, from the top of the valence band to the bottom of the conduction band. In contrast, early angle integrated photoemission and work function measurement[74] showed that the Fermi level is pinned at the surface, almost independent of the doping level. Even though the existence of surface states on semiconductor was confirmed relatively early, little is

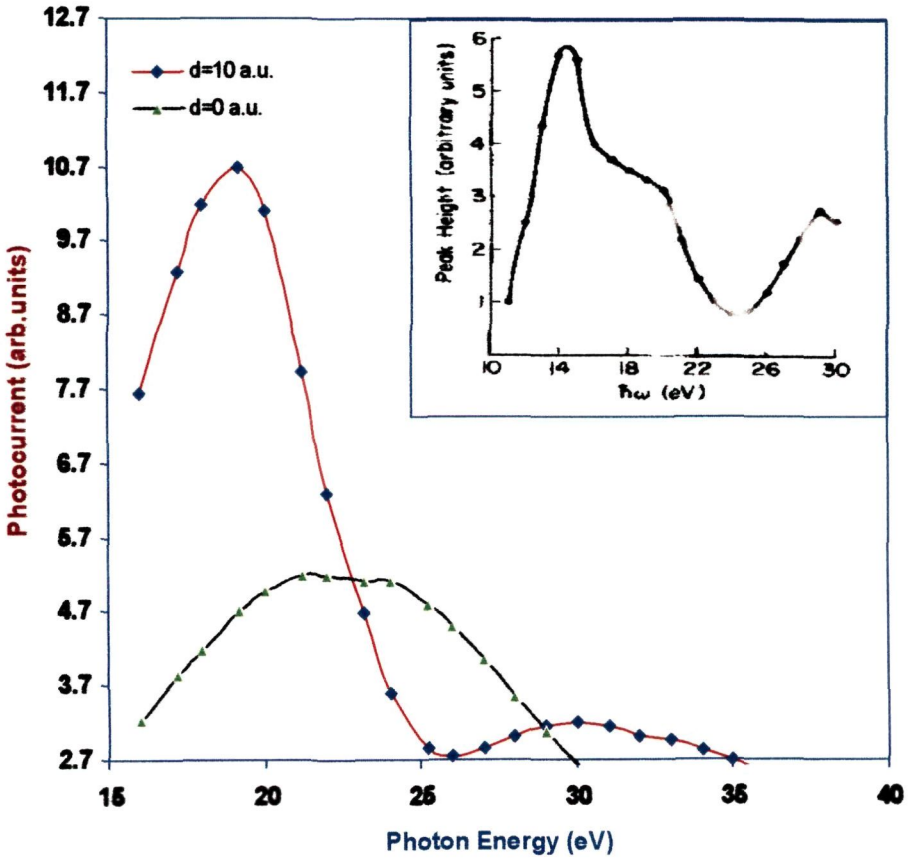

Figure 4. 7: Plot of photocurrent variation with photon energy for two surface widths d= 10 a.u and d= 0 in W using Kronig-Penney δ-potential where ψ_i is derived by projection operator method of Group Theory.

INSET: Experimental results of photoemission intensity for W as obtained by Weng *et.al.*[46] for high lying surface (E_i = 0. 4 eV below Fermi level).

known about these states compared to surface states on metals. Most semiconductor surfaces reconstruct[75,76]. The best known example is the Si (111) surface. A freshly cleaved surface shows a (2×1) super structure. Upon heating to 400^0 C this irreversibly transforms into a 7×7 reconstructed surface.The Si (111) surface is only one example of a variety of reconstructed semiconductor surfaces. Models for these surfaces have been developed, mostly on the basis of dynamical LEED calculations. They clearly show the fundamental difference between a metal and semiconductor surface. Semiconductors with their covalent (Si, Ge, diamond) or heteropolar bonding (GaAs or III-V's or VI's) nearly always exhibit reconstructed surfaces and the perturbation can extend into the second, third, fourth, or deeper layer[77]. We shall discuss below the photoemission calculations from the surface states of some of the semiconductors like GaAs and Si.

(i) Galium arsenide:

The plot of photocurrent against the photon energy ($\hbar\omega$) for a semiconductor GaAs for the case of surface widths at d= 10 a.u and narrow surface width (d =0) is shown in Fig. (4. 8). We have assumed the surface state to occur at 0.38 eV below Fermi level, the potential barrier value was also taken as 15 eV. For the surface width d= 10 a.u. the photocurrent peak occurs at the photon energy $\hbar\omega$ = 8 eV and as the photon energy increases the minimum occurs at $\hbar\omega$ = 15 eV which corresponds to the plasmon energy. This value of plasmon energy obtained agrees qualitatively with that of the result as obtained by Manzke[78]. With the increase in photon energy ($\hbar\omega$) the next peak occurs at $\hbar\omega$ = 18 eV and after which the photocurrent decreases to with further increase in photon energy.

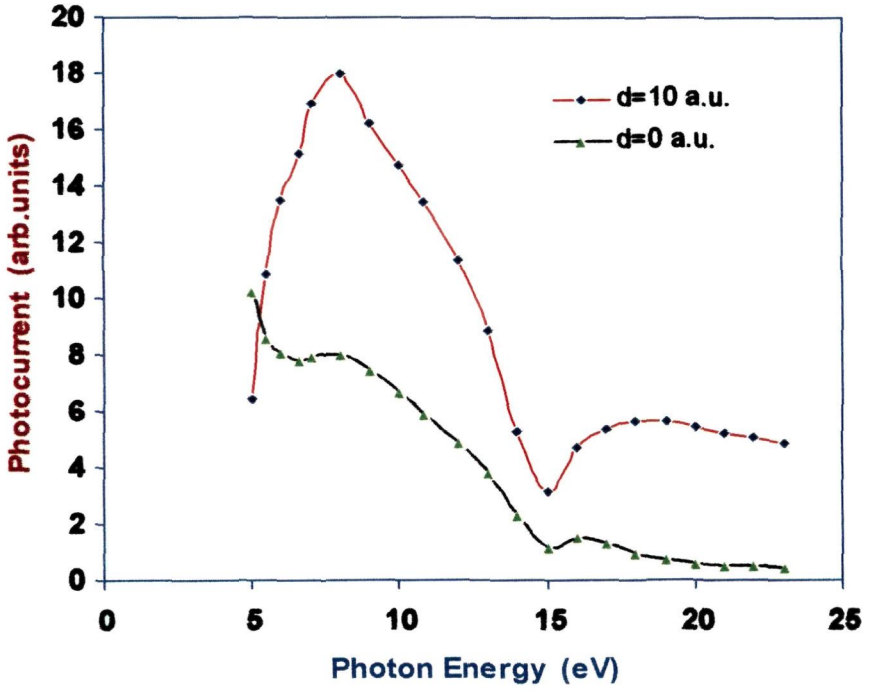

Figure 4. 8: Plot of photocurrent variation with photon energy in GaAs for surface widths d= 10 a.u. and d= 0 using Kronig-Penney δ - potential where ψ_i is derived by projection operator method of Group Theory. Here, surface state is assumed to present at 0.34 eV below Fermi energy and the potential strength V_0 = 15 eV.

The case of narrow surface width shows the same behaviour, but at a much diminished magnitude in photocurrent values.

(ii) Silicon:

Fig. (4. 9) shows the plot of variation of photocurrent with the photon energy for the two surface widths of Si namely for d= 10 a.u. and narrow surface width (d=0). The surface state was taken as 1.2 eV below Fermi level as calculated by Spicer[79] and the potential barrier was taken as 0.662 eV. The photocurrent variation at d = 10 a.u. shows a maximum at photon energy $\hbar\omega$ = 13.5 eV and the minimum which corresponds to plasmon energy is obtained at $\hbar\omega_p$ = 17 eV which agrees well with the results obtained by Aiyama *et.al.*[80] There is another hump again at $\hbar\omega$ = 19 eV after which the photocurrent decreases with increase of photon energy. The reason for this second hump can be traced to the behaviour of $\varepsilon(\omega)$ for silicon[81] which has the resonance in the region of photon energy $\hbar\omega$ =21 eV. The photocurrent calculation with the narrow surface width shows the same trend but the magnitude is greatly diminished.

We have shown in this chapter the calculations of photocurrent by using the initial state wavefunction (ψ_i) deduced by applying the projection operator method of group theory. The wavefunction was deduced for the case of empty potential and a periodic crystal potential which was defined by Kronig -Penney δ - function type. In the case of empty potential, the photocurrent was evaluated from Cu (110) surface due to the existence of band gap at $L_{2'} - L_1$. Photocurrent data showed behaviour which was also indicated by other metals like Al, Be, etc. Similarly, calculations of

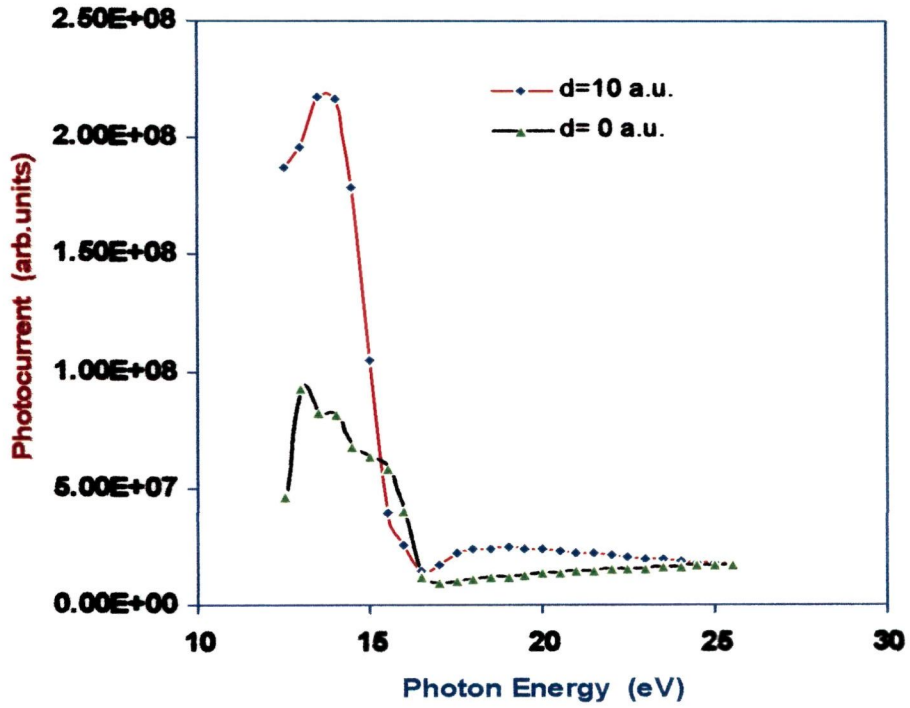

Figure 4. 9: Plot of photocurrent variation with photon energy for surface widths d= 10 a.u and d= 0 in Si. Kronig-Penney δ-potential model is employed and the initial state wavefunction is calculated by using projection operator method of group Theory.

photocurrent was also done by using wave function ψ_i deduced by using the Kronig-Penney δ-type function. Reason for such calculation being to define realistically the potentials of the metals. Photocurrent data showed interesting features conforming to experimentally measured results. For example, in the case of tungsten, the experimentally measured[46] photoemission intensity from the high lying surface state was reproduced by our approach of calculations.

CHAPTER 5

CONCLUSION

In this thesis, we have presented photoemission calculations by using a modified form of dielectric model as given by Bagchi and Kar[23]. At first, we have calculated the variation of vector potential for location of the planes in the bulk, surface and vacuum regions. Calculations of vector potential were done for metals like Ag, Al, Cr and semiconductors GaAs and InAs. In most of the cases, we find that plot of vector potential $\left|\tilde{A}_{\omega}(z)\right|^2$ showed maxima at $\hbar\omega = \frac{\hbar\omega_p}{\sqrt{2}}$, where $\hbar\omega_p$ is the bulk plasmon energy of metals. Interestingly, all metals showed a minimum in the value of vector potential when value of incident photon energy ($\hbar\omega$) was equal to $\hbar\omega_p$.

The calculated results of vector potential in the case of W supported the experimental results as reported by Weng *et.al*[46]. This is evident from the occurrence of maxima at $\hbar\omega$ = 21 eV and a minimum at $\hbar\omega_p$, which is equal to 26 eV in the case of W. Further, the occurrence of maxima below plasmon energy value of incident photon energy had been attributed to the spatial variation of $\tilde{A}_{\omega}(z)$ ie, $\frac{d\tilde{A}_{\omega}}{dz}$ in the surface region of metals. This is evident from plot of $\frac{d\tilde{A}_{\omega}}{dz}$ against distance from the surface in the case of Al. It is therefore seen that the vector potential $\tilde{A}_{\omega}(z)$ deduced in chapter 2 by using the modified from of dielectric model for the surface region of metal can be employed in matrix element for photoemission calculations.

We had used in chapter 3, the Mathieu potential model to describe the lattice potential. A Mathieu potential is a sinusoidal type of potential and it was used to solve the Schrödinger's equation to get appropriate initial state wavefunction (ψ_i) for

evaluation of matrix element $\langle \psi_f | \mathcal{H}' | \psi_i \rangle$ for calculating photocurrent. Two cases are of importance here namely, the empty lattice and a lattice with strong potential. We have dealt with the case of strong lattice potential only in this thesis for which results of photocurrent is plotted against photon energy. We have presented the photocurrent results for Ag, Fe, Ni, Pd and semiconductors GaAs and PbSe. It is seen that the behaviour of photocurrent as a function of photon energy ($\hbar\omega$) for the values of $\hbar\omega$ below the plasmon energy showed peak at $\hbar\omega \approx \frac{\hbar\omega_p}{\sqrt{2}}$ and also a minima at $\hbar\omega \sim \hbar\omega_p$ for all metals. Therefore, it showed a qualitative agreement with the experimental data of Weng *et.al*[46].

We have seen that in chapter 3 photoemission was considered to take place in metals/semiconductors, for location of surface state below the Fermi level. We have derived the initial state wavefunction ψ_i pertaining to a particular surface state for which an energy value was that corresponding to experimental data of the metal. Symmetry state or direction to the existence of surface state in a particular band gap was ignored. Therefore, to include band structure effect, we have applied projection operator method of group theory in chapter 4 to derive initial state wavefunction ψ_i pertaining to a particular band gap. For example, we have taken the case of Cu (110) direction in which surface state exists in the band gap $L_{2'} - L_1$. ψ_i was derived for this symmetry state and photocurrent calculated was for Cu (110) case. Photocurrent was also calculated from other metals like Al, Be, W and semiconductors like GaAs and Si. When calculated results were compared to experimental data and other previous theoretical results, we find that calculated data with this approach of

calculations seemed to agree in a better way. This is quite evident from the photoemission results from W and Al especially for which also experimental results are available.

Although the approach of calculations by using group theoretical method for deducing ψ_i seems to be slightly better than other methods like, Free-electron model of Thapa *et.al* [24, 81], Kronig-Penney potential model of Thapa *et.al* [22, 65, 72,], or Mathieu potential model of Pachuau *et.al* [49], there are still certain drawbacks remaining for further corrections. For example, we have paid attention only to the derivation of initial state wavefunction; the case of final state wavefunction was ignored. Further, we have not considered the nature and type of potentials which defines the bulk and surface regions. This plays equally important role in the definition of dielectric response function too. Also one can define dielectric response function $\varepsilon(\omega, z)$ to include many body effects.

From all the above facts, the model employed in chapter 4 seems to be highly simplified. However, as evidenced from the comparison with other approach of calculations, as well as with experimental results, our method seems to be quite appropriate. Further, we can understand the effect of the choice of a suitable kind of initial state wavefunctions on photoemission, which usually is ignored.

Lastly, with further modification, one can also extend the use of initial state wavefunction deduced by group theoretical method to calculation of photoemission from superconductors like YBCO. The reason for this being that, in cuprate superconductors like $YBa_2Cu_3O_7$, the Cu^+ and O^- ions are in two-dimensional phase and are mainly responsible for superconductivity. Hence if initial state wavefunction ψ_i is derived for this system, photoemission intensity can also be calculated.

Presently, work with this approach is also in progress. Further, the projection operator technique had been also applied to calculations of photofield emissions by Thapa and others[82, 83].

APPENDIX I

SURFACE STATE PHOTOEMISSION CALCULATIONS BY USING MATHIEU POTENTIAL MODEL (THE CASE OF STRONG POTENTIAL).

Rewriting photocurrent density formula from Eq. (1. 3), we have

$$\frac{d\,j(E)}{d\,\Omega}=\frac{2\pi}{\hbar}\sum_{f}\left|\langle\psi_f\left|\mathcal{H}'\right|\psi_i\rangle\right|^2\,\delta(E-E_f)\delta(E_f-E_i-\hbar\omega)\,f_o(E-\hbar\omega)[1-f_o(E)] \qquad \ldots \quad (I.\,1)$$

The initial state wavefunction[49] is given by (in one-dimension):

$$\psi_i(z,q)=\begin{cases}\left(\dfrac{1}{4\pi k_i}\right)^{\frac{1}{2}}\left(1-\dfrac{q}{16}+\dfrac{11}{640}q^2\right)e^{-\mu(z_0'-z)}, & surface\,(z\le 0)\\ (2\xi)^{\frac{1}{2}}\,e^{-\xi(z-z_0')}, & vacuum\,(z\ge 0)\end{cases} \qquad \ldots \quad (I.\,2)$$

Here, the various constants (in a.u.) used are as follows:

$$\begin{aligned} &q=1\\ &k_i^2=2E_i\\ &\xi=2\\ &z_0'=\frac{\pi}{a}.z_0\end{aligned} \qquad \ldots. \quad (I.\,3)$$

z_0 is the location of the surface state wavefunction and a is the lattice constant which is taken as 6.

The final state wavefunction ψ_f for surface region can be written as:

$$\psi_f(z)=\left(\frac{1}{2\pi q_f}\right)^{\frac{1}{2}}.\frac{2q_f}{q_f+k_f}.e^{ik_fz}.e^{-\alpha|z|} \qquad \ldots \quad (I.\,4)$$

and perturbation term $\mathcal{H}'$ in one-dimension is

$$\mathcal{H}' = \frac{e}{mc}\left[\tilde{A}_\omega(z)\frac{d}{dz} + \frac{1}{2}\frac{d\tilde{A}_\omega(z)}{dz}\right] \qquad \ldots \quad (I.\ 5)$$

The vector potential $\tilde{A}_\omega(z)$ from Eq. (2.28) can be written as

$$\tilde{A}_\omega(z) = \begin{cases} -\dfrac{\varepsilon(\omega).\sin 2\theta_i}{\left[\varepsilon(\omega)-\sin^2\theta_i\right]^{\frac{1}{2}}+\varepsilon(\omega).\cos\theta_i} & z \geq 0 \\ -\dfrac{\sin 2\theta_i}{\left[\varepsilon(\omega)-\sin^2\theta_i\right]^{\frac{1}{2}}+\varepsilon(\omega).\cos\theta_i}\,\dfrac{\varepsilon(\omega).d}{d+[1-\varepsilon(\omega)]z}, & -d \leq z \leq 0 \\ -\dfrac{\sin 2\theta_i}{\left[\varepsilon(\omega)-\sin^2\theta_i\right]^{\frac{1}{2}}+\varepsilon(\omega).\cos\theta_i}, & z \leq -d \end{cases} \quad \ldots . (I.\ 6)$$

From the matrix element $\langle\psi_f|\mathcal{H}'|\psi_i\rangle$ of Eq. (I. 1) , the surface state contribution to photocurrent calculations can be expressed as

$$I = \langle\psi_f|\,\mathcal{H}'\,|\psi_i\rangle$$

$$= \int_{-d}^{0}\psi_f^*\tilde{A}_\omega(z).\frac{d\psi_i}{dz}.dz + \frac{1}{2}\int_{-d}^{0}\psi_f^*.\frac{d\tilde{A}_\omega(z)}{dz}.\psi_i.dz$$

$$= I_1 + I_2 \qquad \ldots \quad (I.\ 7)$$

The integrals in Eq. (I. 7) can be expanded as :

$$I_1 = \int_{-d}^{0}\psi_f^*\,\tilde{A}_\omega\frac{d\psi_i}{dz}dz$$

$$= \frac{1}{\pi}\left(\frac{1}{2q_fk_i}\right)^{\frac{1}{2}}.\frac{2q_f}{q_f+k_f}.A_1.\mu\left(1-\frac{q}{16}+\frac{11}{640}q^2\right).\varepsilon(\omega).d$$

$$\times\int_{-d}^{0}\left[\cos k_f z - i\sin k_f z\right]e^{-\alpha z}.e^{-\mu(z_0'-z)}\frac{1}{[1-\varepsilon(\omega)]z+d}.dz \qquad \ldots . \quad (I.\ 8)$$

where $A_1 = -\dfrac{\sin 2\theta_t}{\left[\varepsilon(\omega) - \sin^2\theta_t\right]^{\frac{1}{2}} + \varepsilon(\omega).\cos\theta_t}$

$$I_2 = \int_{-d}^{0} \psi_f^* \, \tilde{A}_\omega \frac{d\psi_i}{dz} dz$$

$$= \frac{1}{2\pi}\left(\frac{1}{2q_f k_i}\right)^{\frac{1}{2}} \cdot \frac{2q_f}{q_f + k_f} . A_1 . \left(1 - \frac{q}{16} + \frac{11}{640} q^2\right) . \varepsilon(\omega) . d$$

$$\times \int_{-d}^{0} \left[\cos k_f z - i \sin k_f z\right] e^{-\alpha z} . e^{-\mu(z_0' - z)} \frac{\left[1 - \varepsilon(\omega)\right]}{\left[(1 - \varepsilon(\omega))z + d\right]^2} . dz \qquad \ldots \qquad (I.9)$$

Photocurrent is calculated by evaluating the integrals I_1 and I_2 by writing FORTRAN programmes, details of which is given in APPENDIX- II.

APPENDIX II

FORTRAN PROGRAMME FOR SURFACE STATE PHOTOEMISSION CALCULATIONS BY USING MATHIEU POTENTIAL MODEL (STRONG POTENTIAL CASE).

```
C       NAME OF PROGRAM: RKMATH1.FOR
C       SURFACE STATE CALCULATIONS, Z EXTENDS FROM -D TO 0.
C       WRITTEN BY DR.R.K.THAPA, CMT, 18-05-2004
C       PROGRAM TO CALCULATE PHOTOCURRENT BY USING
C       MATHIEU POTENTIAL MODEL
C       REFER: PHYS. LETTS. A294 (2002)52-57.
C=============================================================
C       ALAMB3 = (XI+MU)*0.295, Q <---> AQQ
C       ALAMB3 = 1.275,     MU <---> AMU
C       MU=0.5, ZO'<--->XO
C       XI=2.0,XO -->IS THE LOCATION OFTHE SURFACE STATE WAVEFUNCTION.
C       M=3.
C       QM=1.
C       Q=1,
C       ZO'= (PI/A)*ZO
C       A=6.
C=============================================================
        COMPLEX A1,CI,T2,T3,EPS,CMPLX,AQF,EX,TTF,TTX,TTY
        COMMON AKI, AKF, AQF, CI, D, AMU, AQQ, ALPHA, XO
        CI=CMPLX (0. 1.)
        PI=22. /7.
        OPEN (UNIT=1, FILE="RKMATH1_INAS.IN")
        OPEN (UNIT=6, FILE="RKMATH1_INAS.OUT")
        READ (1,*) NP, NINT
        READ(1,*)  EI,THETA,D,VZ,ALPHA,AMU,AQQ,XO,NE
C       READ (1,*) EI, THETA, D, A, MU, XI, VZ, ALPHA, NE
C       WRITE (NP,2) EI,THETA,D,A,MU,XI,VZ,ALPHA,NE
        AKI=SQRT (2.*EI)
        DO 90 IE=1, NE
        READ (1,*) W, EPS1, EPS2
        WEV=W*27.2
        AKF=SQRT (2.*(EI+W))
```

```
       EX=EI+W-VZ
      AQF=SQRT (2.*EX)
      TTX=AQF-AKF
      TTY=AQF+AKF
      TTF=TTX/TTY
      EPS=CMPLX (EPS1, EPS2)
      CALL REFRAC (W, WP, THETA, EPS, A1)
      CALL TERM2 (A1, EPS, T2, NINT)
      CALL TERM3 (A1, EPS, T3, NINT)
      XINT=CABS (T2+T3)
      XCUR=XINT*XINT
      CUR= (XCUR*AKF*AKF)/W
      CUR=CUR/1.83E+03
      WRITE (NP, 3) WEV, EPS1, EPS2, CUR
   3  FORMAT (2X, F8.4, 2X, 2(F15.6, 2X), 2X, E20.6, 2X)
C 5   FORMAT (2X,'W=', F7.4, 2X,'EPS=',2(F15.6,1X),'CUR='E15.6)
  90  CONTINUE
      STOP
      END
C     SUBROUTINE TERM2 (A1, EPS, T2, NINT)
      COMPLEX EPS, A1, T2, R1, CI, F1, Q, AQF
      DIMENSION F1 (700),F2(700)
      COMMON AKI, AKF, AQF, CI, D, AMU, AQQ, ALPHA, XO
      CI=CMPLX (0., 1.)
      Q1= (1.-(AQQ/16.)+ (11./640.)*AQQ**2.)
      Q=A1*D*EPS*Q1*AMU
      Q=Q*SQRT (1./(2.*AQF*AKI))*(AQF/(AQF+AKF))
      AG=-D
      AH=0.
      DD= (AH-AG)/ (NINT-1)
      DO 10 I=1, NINT
      X=AG+ (I-1)*DD
      AMX=AMU*(XO-X)
      F1 (I)= (COS(AKF*X)-CI*SIN(AKF*X))*EXP(-AMX)
  10  F1(I)=F1(I)*EXP(-ALPHA*X)/((1.-EPS)*X+D)
      CALL SINT (AG, AH, F1, NINT, R1)
      T2=R1*Q/3.1416
      RETURN
      END
```

```
CCCCCCCCCCCCCCCCCCCCCCCCCCCCCCCCCCCCCCCCCCCCCCCCC
      SUBROUTINE TERM3 (A1, EPS, T3, NINT)
      COMPLEX EPS, A1, T3, R1, CI, F1, CMPLX, Q, AQF
      DIMENSION F1(700),F2(700)
      COMMON AKI, AKF, AQF, CI, D, AQQ, AMU, ALPHA, XO
      CI=CMPLX (0., 1.)
      Q1= (1.-(AQQ/16.)+ (11./640.)*AQQ**2.)
      Q=A1*D*EPS*Q1
      Q=Q*SQRT (1./(2.*AQF*AKI))*(AQF/(AQF+AKF))
      AG=-D
      AH=0.
      DD=(AH-AG)/(NINT-1)
      DO 10 I=1, NINT
      X=AG+(I-1)*DD
      AMX=AMU*(XO-X)
      F1(I)=(COS(AQF*X)-CI*SIN(AQF*X))*EXP(-AMX)
   10 F1(I)=F1(I)*EXP(-ALPHA*X)/((1.-EPS)*X+D)**2.
      CALL SINT(AG,AH,F1,NINT,R1)
      T3=R1*Q/(2.*3.1416)
      RETURN
      END
CCCCCCCCCCCCCCCCCCCCCCCCCCCCCCCCCCCCCCCCCCCCCCCCCC
C     THIS SUBROUTINE CALCULATES THE PORTION A1 OF THE FIELD.
CCCCCCCCCCCCCCCCCCCCCCCCCCCCCCCCCCCCCCCCCCCCCCCCCC
      SUBROUTINE REFRAC (W, WP, THETA, EPS, A1)
      COMPLEX A1, CX, CSQRT, EPS, CI, CMPLX, CY
      S2=SIN (2.*THETA)
      S1=SIN (THETA)
      C1=COS (THETA)
C     B1=1.-EPS
C     B1=1. / (B1*X+D)
      CY=EPS-S1*S1
      CX=CSQRT (CY)
      A1=-S2/(CX+EPS*C1)
      RETURN
      END
CCCCCCCCCCCCCCCCCCCCCCCCCCCCCCCCCCCCCCCCCCCCCCCCCC
C     THIS SUBROUTINE PERFORMS INTEGRATION OF TERM1 AND TERM2
```


```
C       BY USING SIMPSON'S ONE THIRD RULE
CCCCCCCCCCCCCCCCCCCCCCCCCCCCCCCCCCCCCCCCCCCCCCCCCCCCCCCC
        SUBROUTINE SINT (A, B, F, N, R)
        COMPLEX F, R, S
        DIMENSION F(N)
        H=(B-A)/(N-1)
        S=0.0
        S=S+F(1)+F(N)
        M=N-1
        DO 10 I=2,M,2
   10   S=S+4.*F(I)+2.*F(I+1)
        R=H*S/3.
        RETURN
        END
```

APPENDIX- III

DERIVATION OF BASIS FUNCTION BY USING PROJECTION OPERATOR METHOD OF GROUP THEORY FOR DEVELOPMENT OF INITIAL STATE WAVEFUNCTION FOR PHOTOEMISSION CALCULATIONS.

We shall show here the derivation of the basis function for the surface state existing in Cu by using projection operator technique of group theory as described in chapter 4. Surface state in Cu (110) is found in the energy band gap ($L_{2'} - L_1$). We shall try to obtain the symmetrised basis function for this band gap taking the band $L_{2'}$ where the point group is C_{2v} and the linear combination of atomic orbital (LCAO) representation for $L_{2'}$ is $(x+y+z)/\sqrt{3}$. For a point group C_{2v} the transformation operations are $E, C_2, \sigma_v(xz)$ and $\sigma'_v(yz)$.

The group C_{2v} has four one-dimensional irreducible representations and the characters of these four irreducible representations can be obtained as below:

C_{2v}	E	C_2	$\sigma_{v(xy)}$	$\sigma'_{v(yz)}$	
Γ^1	1	1	1	1	
Γ^2	1	1	-1	-1	
Γ^3	1	-1	1	-1	
Γ^4	1	-1	-1	1	... (III. 1)

The matrices representing the transformations effected on C_{2v} point group is given as:

$$\text{E:}\begin{bmatrix}1&0&0\\0&1&0\\0&0&1\end{bmatrix},\qquad \text{C}_2\text{:}\begin{bmatrix}-1&0&0\\0&-1&0\\0&0&1\end{bmatrix},\qquad \sigma_v:\begin{bmatrix}1&0&0\\0&-1&0\\0&0&1\end{bmatrix}\text{ and }\ \sigma_v':\begin{bmatrix}-1&0&0\\0&1&0\\0&0&1\end{bmatrix}$$

... (III. 2)

Projection operator formula was obtained as $\mathrm{P}^{p}_{mn}=\frac{l_p}{g}\sum_T \Gamma^p(T)^*_{mn}P(T)$ ... (III. 3)

For a transformation T of a point group it can also be shown that

$$\mathrm{P}(T)\phi(r)=\phi\{R(T)^{-1}r\}=\phi\{\tilde{R}(T)r\} \qquad \text{... (III. 4)}$$

where $\tilde{R}$ is the transpose conjugate of R.

The transpose conjugate for each of the representation can be written as

$$\tilde{R}(E)r=\begin{bmatrix}1&0&0\\0&1&0\\0&0&1\end{bmatrix}\begin{bmatrix}x\\y\\z\end{bmatrix}=\begin{bmatrix}x\\y\\z\end{bmatrix}$$

$$\tilde{R}(C_2)r=\begin{bmatrix}-1&0&0\\0&-1&0\\0&0&1\end{bmatrix}\begin{bmatrix}x\\y\\z\end{bmatrix}=\begin{bmatrix}-x\\-y\\z\end{bmatrix}$$

$$\tilde{R}(\sigma_v)r=\begin{bmatrix}1&0&0\\0&-1&0\\0&0&1\end{bmatrix}\begin{bmatrix}x\\y\\z\end{bmatrix}=\begin{bmatrix}x\\-y\\z\end{bmatrix}\quad\text{and}$$

$$\tilde{R}(\sigma_v')r=\begin{bmatrix}-1&0&0\\0&1&0\\0&0&1\end{bmatrix}\begin{bmatrix}x\\y\\z\end{bmatrix}=\begin{bmatrix}-x\\y\\z\end{bmatrix} \qquad \text{... (III. 5)}$$

Now we have the LCAO function $\Phi(r) = \frac{1}{\sqrt{3}}(x+y+z)$. Therefore, the transformation of the representations for this function is carried out as

$$P(E)\Phi(r) = \Phi\{\tilde{R}(E)\} = \frac{1}{\sqrt{3}}(x+y+z)$$

$$P(C_2)\Phi(r) = \Phi\{\tilde{R}(C_2)\} = \frac{1}{\sqrt{3}}(-x-y+z)$$

$$P(\sigma_v)\Phi(r) = \Phi\{\tilde{R}(\sigma_v)r\} = \frac{1}{\sqrt{3}}(x-y+z)$$

$$P(\sigma_v')\Phi(r) = \Phi\{\tilde{R}(\sigma_v')r\} = \frac{1}{\sqrt{3}}(-x+y+z) \qquad \ldots \text{(III. 6)}$$

For the case of 1 dimensional Γ^1 operation matrix, p=1,and take m=n=1, $l_p = l_1 = 1$.

g=4, $\Gamma^1(E)^*_{11} = 1$, $\Gamma^1(C_2)^*_{11} = 1$, $\Gamma^1(\sigma_v)^*_{11} = 1$ and $\Gamma^1(\sigma_v')^*_{11} = 1$

Thus for the Projection Operator P^1_{11} we have

$$P^1_{11}\Phi(r) = \frac{1}{4\sqrt{3}}[1(x+y+z)+1(-x-y+z)+1(x-y+z)+1(-x+y+z)]$$

$$= \frac{1}{4\sqrt{3}} \times 4z = \frac{1}{\sqrt{3}}z$$

For Γ^2 matrix, p=1, m=n=1, $l_p = l_1 = 1$. g=4, $\Gamma^2(E)^*_{11} = 1$, $\Gamma^2(C_2)^*_{11} = 1$, $\Gamma^2(\sigma_v)^*_{11} = -1$ and $\Gamma^2(\sigma_v')^*_{11} = -1$

And the Projection Operator P^2_{11} operating on $\Phi(r)$ gives

$$P^2_{11}\Phi(r) = \frac{1}{4\sqrt{3}}[1(x+y+z)+1(-x-y+z)-1(x-y+z)-1(-x+y+z)]$$

$$= 0$$

Similarly, we have

$$P_{11}^{3}\,\Phi(r) = \frac{1}{4\sqrt{3}}\left[1(x+y+z) - 1(-x-y+z) + 1(x-y+z) - 1(-x+y+z)\right]$$

$$= \frac{1}{4\sqrt{3}} \times 4x = \frac{1}{\sqrt{3}}x \quad \text{and}$$

$$P_{11}^{4}\,\Phi(r) = \frac{1}{4\sqrt{3}}\left[1(x+y+z) - 1(-x-y+z) - 1(x-y+z) + 1(-x+y+z)\right]$$

$$= \frac{1}{4\sqrt{3}} \times 4y = \frac{1}{\sqrt{3}}y$$

Thus a set of basis function can be obtained as = $\frac{1}{\sqrt{3}}x + \frac{1}{\sqrt{3}}y + \frac{1}{\sqrt{3}}z$. ... (III. 7)

This means that the projection Operators P_{11}^{1}, P_{11}^{2}, P_{11}^{3} and P_{11}^{4} projected the function $\Phi(r) = \frac{1}{\sqrt{3}}(x+y+z)$ to a symmetrised basis function in different direction each equal to $\frac{1}{\sqrt{3}}x$, $\frac{1}{\sqrt{3}}y$ and $\frac{1}{\sqrt{3}}z$ respectively.

Considering photoemission to take place along the z-axis which is normal to the surface, then the basis function obtained from the atomic orbital $\Phi(r) = \frac{1}{\sqrt{3}}(x+y+z)$ will be $\frac{1}{\sqrt{3}}z$. We take the one dimensional case of initial wave function and this basis function in the sinusoidal form can be written as $\phi(z)=e^{iz}$ which is incorporated in the initial state wave functions obtained for respective cases of empty potential and periodic potential.

APPLICATIONS:

1. Case of empty potential:

Rewriting the initial state wavefunction obtained by considering the case of an empty potential in Eq. (4.6), we have

$$\psi_i(z) = \begin{cases} \phi(z)e^{\mu z}\left[e^{\iota k_i z} + \mathrm{Re}^{-\iota k_i z}\right], & \textit{surface \& bulk} \quad z \geq 0 \\ Te^{-\kappa z}, & \textit{vacuum} \quad z \leq 0 \end{cases},$$

Now incorporating the value of basis function,

$$\psi_i(z) = \begin{cases} e^{\iota z}\, e^{\mu z}\left[e^{\iota k_i z} + \mathrm{Re}^{-\iota k_i z}\right], & \textit{surface \& bulk} \quad z \geq 0 \\ Te^{-\kappa z}, & \textit{vacuum} \quad z \leq 0 \end{cases}, \qquad \ldots \text{(III. 8)}$$

Here,

$$R = -\frac{(1+k_i) - i(\chi+\mu)}{(1-k_i) - i(\chi+\mu)}.$$
$$T = -\frac{2k_i}{(1-k_i) - i(\chi+\mu)}. \qquad \ldots \text{(III. 9)}$$

With reference to APPENDIX-I, using Eqs. (I. 10), (I. 11) and (III. 8), photocurrent is calculated by using Eq. (I. 9). The matrix element $\langle \psi_f | \mathcal{H}' | \psi_i \rangle$ can be expanded as follows:

$$\mathrm{I} = \int_{-\infty}^{d} \psi_f^* \tilde{A}_\omega \psi_i \, dz + \int_d^0 \psi_f^* \tilde{A}_\omega \frac{d}{dz}\psi_i \, dz + \frac{1}{2}\int_d^0 \psi_f^* \frac{d\tilde{A}_\omega}{dz}\psi_i \, dz + \int_0^\infty \psi_f^* \tilde{A}_\omega \varepsilon(\omega)\frac{d}{dz}\psi_i dz$$

Or $\mathrm{I} = \mathrm{I}_1 + \mathrm{I}_2 + \mathrm{I}_3 + \mathrm{I}_4$ ... (III. 10)

where each of the integrals can be written as

$$I_1 = \int_{-\infty}^{d} \psi_f^* \, \tilde{A}_\omega \, \psi_i \, dz$$

$$= A_1 \int_{-\infty}^{-d} \left(\frac{1}{2\pi q_f} \right)^{\frac{1}{2}} \frac{2q_f}{q_f + k_f} e^{-ik_f z} e^{\alpha z} \frac{d}{dz} \left\{ e^{(i+\mu)z} \left[e^{ik_i z} + \mathrm{Re}^{-ik_i z} \right] \right\} dz$$

$$= \frac{\sqrt{2}}{(\pi q)^{\frac{1}{2}}} \frac{q_f}{q_f + k_f} A_1 e^{-(\alpha+\mu)} (\cos d - i \sin d) \left[\frac{(\mu + i + ik_i)}{(\alpha+\mu) + i(1 + k_i - k_f)} e^{-(k_i - k_f)d} \right.$$

$$\left. + \frac{R(\mu + i - ik_i)}{(\alpha+\mu) + i(1 - k_i - k_f)} e^{i(k_i + k_f)d} \right] \qquad \ldots \text{(III. 11)}$$

$$I_2 = \int_{-d}^{0} \psi_f^* \, \tilde{A}_\omega \frac{d\psi_i}{dz} dz$$

$$= \int_{-d}^{0} \left(\frac{1}{2\pi q_f} \right)^{\frac{1}{2}} \frac{2q_f}{q_f + k_f} e^{-ik_f z} e^{\alpha z} \frac{A_1 \varepsilon(\omega) d}{[1 - \varepsilon(\omega)]z + d} \frac{d}{dz} \left\{ e^{(i+\mu)z} \left[e^{ik_i z} + \mathrm{Re}^{-ik_i z} \right] \right\} dz$$

$$= \frac{\sqrt{2}}{(\pi q_f)^{\frac{1}{2}}} \frac{q_f}{q_f + k_f} A_1 d \, \varepsilon(\omega) \int_{-d}^{0} \left\{ \frac{(i + \mu + ik_i)}{[1 - \varepsilon(\omega)]z + d} e^{(\alpha+\mu)z} e^{i(1 + k_i - k_f)z} \right.$$

$$\left. + \frac{R(i + \mu - ik_i)}{[1 - \varepsilon(\omega)]z + d} e^{(\alpha+\mu)z} e^{i(1 - k_i - k_f)z} \right\} dz \qquad \ldots \text{(III. 12)}$$

$$I_3 = \frac{1}{2} \int_{-d}^{0} \psi_f^* \frac{d \, \tilde{A}_\omega}{dz} \psi_i \, dz$$

$$= \int_{-d}^{0} \left(\frac{1}{2\pi q_f} \right)^{\frac{1}{2}} \frac{q_f}{q_f + k_f} e^{-ik_f z} e^{\alpha z} \frac{d}{dz} \left\{ \frac{A_1 \varepsilon(\omega) d}{[1 - \varepsilon(\omega)]z + d} \right\} \left\{ e^{(i+\mu)z} \left[e^{ik_i z} + \mathrm{Re}^{-ik_i z} \right] \right\} dz$$

$$= -0.5 \frac{\sqrt{2}}{(\pi q_f)^{\frac{1}{2}}} \frac{q_f}{q_f + k_f} A_1 \varepsilon(\omega) d [1 - \varepsilon(\omega)] \int_{-d}^{0} \left[\frac{e^{\alpha+\mu} \, e^{iz} e^{i(k_i - k_f)z}}{\{[1 - \varepsilon(\omega)]z + d\}^2} \right.$$

$$\left. + R \frac{e^{(\alpha+\mu)} e^{iz} \, e^{-i(k_i + k_f)z}}{\{[1 - \varepsilon(\omega)]z + d\}^2} \right] dz \qquad \ldots \text{(III. 13)}$$

$$I_4 = \int_0^\infty \psi_f^* \tilde{A}_\omega \varepsilon(\omega) \frac{d\psi_i}{dz} dz$$

$$= \left(\frac{1}{2q_f k_i}\right)^{\frac{1}{2}} A_1 \varepsilon(\omega) \int_0^\infty \left[e^{-iq_f z} + \frac{q_f - k_f}{q_f + k_f} e^{iq_f z} \right] \frac{d}{dz}\left(T e^{-\chi z}\right) dz$$

$$= -\left(\frac{1}{2q_f k_i}\right)^{\frac{1}{2}} A_1 \varepsilon(\omega) T\chi \left[\frac{1}{\chi + iq_f} + \frac{q_f - k_f}{q_f + k_f} \frac{1}{\chi - iq_f} \right] \quad \ldots \text{(III. 14)}$$

Photocurrent was calculated by evaluating above integrals for which FORTRAN programme was written and is given in detail in APPENDIX - IV.

2. Case of periodic crystal defined by Kronig-Penney δ - potential :

The final form of initial state wavefunction derived by using periodic Kronig-Penney δ-potential whose solution was obtained in terms of Green function was given in Eq. (4. 26) . Incorporating the basis function in this formula gives,

$$\psi_i(z) = \begin{cases} \psi_i(0) e^{iz} e^{\mu z} (k_i \cos k_i z - \chi \sin k_i z), & \textit{bulk \& surface} \quad z \le 0 \\ \psi_i(0) k_i e^{-\chi z}, & \textit{vacuum} \quad z \ge 0 \end{cases}$$

where $\psi_i(0) = \dfrac{2i \sin ka \; \tau(0)}{k_i \cos k_i a - k_i e^{-ika} - \chi \sin k_i a}$ and

$$\tau(0) = \frac{2Cip \sin^2 k_i a}{k_i a (e^{ika} - e^{-ik_i a})(\cos ka - \cos k_i a)} \quad \ldots \text{(III. 15)}$$

Following the procedure as in the case empty potential by taking the same value of ψ_f and $\mathcal{H}'$, we can calculate the photocurrent by solving Eq. (III.10). The integrals involved in the matrix element can be expanded as:

$$I_1 = \int_{-\infty}^{d} \psi_f^* \tilde{A}_\omega \psi_i \, dz$$

$$= A_1 \int_{-\infty}^{-d} \left(\frac{1}{2\pi q_f} \right)^{\frac{1}{2}} \frac{2q_f}{q_f + k_f} e^{-ik_f z} e^{\alpha z} \frac{d}{dz} \left\{ \psi_i(0) e^{(i-\mu)z} \left(k_i \cos k_i z - \chi \sin k_i z \right) \right\} dz$$

$$= A_1 \psi_i(0) \frac{\sqrt{2}}{(\pi q_f)^{\frac{1}{2}}} \frac{q_f}{q_f + k_f} \int_{-\infty}^{-d} e^{(\alpha-\mu)z} e^{i(1-k_f)z} \left[k_i (i-\mu) \cos k_i z - k_i^2 \sin k_i z \right.$$

$$\left. - \chi (i-\mu) \sin k_i z - \chi k_i \cos k_i z \right] dz \qquad \ldots \text{(III. 16)}$$

$$I_2 = \int_{-d}^{0} \psi_f^* \tilde{A}_\omega \frac{d\psi_i}{dz} dz$$

$$= \int_{-d}^{0} \left(\frac{1}{2\pi q_f} \right)^{\frac{1}{2}} \frac{2q_f}{q_f + k_f} e^{-ik_f z} e^{\alpha z} \frac{A_1 \varepsilon(\omega) d}{[1 - \varepsilon(\omega)] z + d} \frac{d}{dz} \left\{ \psi_i(0) e^{(i-\mu)z} \left(k_i \cos k_i z - \chi \sin k_i z \right) \right\} dz$$

$$= A_1 \psi_i(0) \frac{\sqrt{2}}{(\pi q_f)^{\frac{1}{2}}} \frac{q_f}{q_f + k_f} \varepsilon(\omega) d \int_{-\infty}^{-d} \frac{e^{(\alpha-\mu)z} e^{i(1-k_f)z}}{[1 - \varepsilon(\omega)] z + d} \left[k_i (i-\mu) \cos k_i z - k_i^2 \sin k_i z \right.$$

$$\left. - \chi (i-\mu) \sin k_i z - \chi k_i \cos k_i z \right] dz \qquad \ldots \text{(III. 17)}$$

$$I_3 = \frac{1}{2} \int_{-d}^{0} \psi_f^* \frac{d\tilde{A}_\omega}{dz} \psi_i \, dz$$

$$= \int_{-d}^{0} \left(\frac{1}{2\pi q_f} \right)^{\frac{1}{2}} \frac{q_f}{q_f + k_f} e^{-ik_f z} e^{\alpha z} \frac{d}{dz} \left\{ \frac{A_1 \varepsilon(\omega) d}{[1 - \varepsilon(\omega)] z + d} \right\}$$

$$\times \left\{ \psi_i(0) e^{(i-\mu)z} \left(k_i \cos k_i z - \chi \sin k_i z \right) \right\} dz$$

$$= -0.5\frac{\sqrt{2}}{(\pi q_f)^{\frac{1}{2}}}\frac{q_f}{q_f + k_f}\psi_i(0)A_1\varepsilon(\omega)d[1-\varepsilon(\omega)]\int_{-d}^{0}\frac{e^{(\alpha-\mu)z}e^{i(1+k_f)z}}{\{[1-\varepsilon(\omega)]z+d\}^2}$$

$$\times(k_i\cos k_i z - \chi\sin k_i z)dz \qquad \ldots \text{(III. 18)}$$

$$I_4 = \int_0^\infty \psi_f^* \tilde{A}_\omega \varepsilon(\omega)\frac{d\psi_i}{dz}dz$$

$$= \left(\frac{1}{2\pi q_f}\right)^{\frac{1}{2}} A_1\varepsilon(\omega)\int_0^\infty\left[e^{-iq_f z} + \frac{q_f - k_f}{q_f + k_f}e^{iq_f z}\right]\frac{d}{dz}(\psi_i(0)k_i e^{-\chi z})dz$$

$$= -\left(\frac{1}{2q_f k_i}\right)^{\frac{1}{2}} A_1\varepsilon(\omega)\psi_i(0)k_i\chi\left[\frac{1}{\chi + iq_f} + \frac{q_f - k_f}{q_f + k_f}\frac{1}{\chi - iq_f}\right] \qquad \ldots \text{(III. 19)}$$

Substituting integrals I_1, I_2, I_3 and I_4 in Eq. (III. 10), the photocurrent were calculated by the numerical method by writing FORTRAN programmes which is given in APPENDIX-V.

APPENDIX IV

FORTRAN PROGRAMME FOR CALCULATION OF PHOTOCURRENT BY USING PROJECTION OPERATOR TECHNIQUE APPLIED TO AN EMPTY POTENTIAL CASE.

```
C       NAME OF PROGRAM : IJMPB.FOR
C       BY DR. R.K.THAPA, CONDENSED MATTER THEORY RESEARCH GROUP,
C       P.U.COLLEGE, AIZAWL, MIZORAM,INDIA.
C       PROGRAM TO CALCULATE PHOTOCURRENT USING PROJECTION OPERATOR
C       THIS IS THE CASE OF AN EMPTY POTENTIAL.
        COMPLEX A1,CI,T1,T2,T3,T4,EPS,CMPLX,AQF,EX,AMA,
        COMPLEX BMA,R,T,AKP,XINT
        COMMON AKI,AKF,AQF,CI,A,AKP,AMA,AMB,BMA,B1,MU,D,X,R,T,PI
        CI=CMPLX(0.,1.)
        PI=3.1415
        OPEN (UNIT=1,FILE='ALIJMPB.IN')
        READ (1,*) NINT
        OPEN (UNIT=1,FILE='ALIJMPB.IN')
        READ(1,*)  EI,THETA,A,ALPHA,VZ,NE
C       READ (1,*) EI,THETA,A,VZ,NE
C       WRITE (NP,2) EI,THETA,D,A,MU,XI,VZ,ALPHA,NE
        AKI=SQRT(2.*EI)
        MU=(AKI-PI*0.5293/3.61)
        AMA=MU+CI*(1.+AKI)
        AMA=CABS(AMA)
        AMB=(ALPHA+MU)
        BMA=MU+CI*(1.-AKI)
        BMA=CABS(BMA)
        DO 90 IE=1,NE
        OPEN (UNIT=1,FILE='ALIJMPB.IN')
        READ (1,*) W,EPS1,EPS2
        WEV=W*27.2
        AKF=SQRT(2.*(EI+W))
        EX=EI+W-VZ
        AQF=SQRT(2.*EX)
        AKP=SQRT(2.*(VZ-EI))
C=================================================================
```

```
C       TRANSMISSION COEFF=T, REFLECTION COEFF=R
C=================================================================
        T=-2.*AKI/((1.-AKI)-CI*(AKP+MU))
        T=CABS(T)
        R=-((1.+AKI)-CI*(AKP+MU))/((1.-AKI)-CI*(AKP+MU))
        R=CABS(R)
        EPS=CMPLX(EPS1,EPS2)
        CALL REFRAC (W,WP,THETA,EPS,A1)
        CALL TERM1 (A1,EPS,T1,NINT)
        CALL TERM2 (A1,EPS,T2,NINT)
        CALL TERM3 (A1,EPS,T3,NINT)
        CALL TERM4 (A1,EPS,T4,NINT)
        OPEN (UNIT=6,FILE='ALIJMPB1.OUT')
C       WRITE (6,3) W,AQF,T1,T2,T3,T4
        XINT=CABS(T1+T2+T3+T4)
        XCUR=XINT*XINT
        CUR=(XCUR*AKF*AKF)/W
        OPEN (UNIT=6,FILE='ALIJMPB1.OUT')
        WRITE (6,5) WEV,EPS1,EPS2,CUR
  3     FORMAT(2X,2F8.4,2X,8(F15.6,1X))
C   5   FORMAT (2X,'W=',F7.4,2X,'EPS=',2(F15.6,2X),'CUR='E20.6)
    5   FORMAT (2X,F7.4,2X,2(F15.6,2X),E20.6)
   90   CONTINUE
        STOP
        END
C
        SUBROUTINE TERM1 (A1,EPS,T1,NINT)
        COMPLEX EPS,A1,T1,T11,T1A,T1B,CI,Q,AQF,AMA,AMB,BMA,CMPLX
C       DIMENSION F1(700),F2(700)
        COMMON AKI,AKF,AQF,CI,A,AKP,AMA,AMB,BMA,B1,MU,D,X,R,T,PI
        CI=CMPLX(0.,1.)
        Q=A1*(AQF/(AQF+AKF))
        Q=Q*SQRT(2./(AQF*PI))
        Q=Q*EXP(-AMB*A)
        T1A=(COS(AKI-AKF)*A-CI*SIN(AKI-AKF)*A)*AMA
        T1A=T1A/(AMB+CI*(1.+AKI-AKF))
        T1B=(COS(AKI+AKF)*A+CI*SIN(AKI+AKF)*A)*BMA
        T1B=T1B/(AMB+CI*(1.-AKI-AKF))
        T11=(T1A+T1B*R)*(COS(A)-CI*SIN(A))
```

```
      T1=Q*T11
      RETURN
      END
C
      SUBROUTINE TERM2 (A1,EPS,T2,NINT)
      COMPLEX EPS,A1,T2,T22,R1,R2,BX,CI,CMPLX,F1,F2,Q,AQF
      DIMENSION F1(700),F2(700)
      COMMON AKI,AKF,AQF,CI,A,AKP,AMA,AMB,BMA,B1,MU,D,X,R,T,PI
      CI=CMPLX(0.,1.)
      Q=A1*A*EPS
      Q=Q*SQRT(2./(AQF*PI))*(AQF/(AQF+AKF))
      AG=-A
      AH=0.
      DD=(AH-AG)/(NINT-1)
      DO 10 I=1, NINT
      X=AG+(I-1)*DD
      B1=1.-EPS
      BX=1./(B1*X+A)
      F1(I)=(EXP(AMB)*X)*(COS(X)+CI*SIN(X))
      F1(I)=F1(I)*(COS(AKI-AKF)*X+CI*SIN(AKI-AKF)*X)/BX
      F2(I)=(EXP(AMB)*X)*(COS(X)+CI*SIN(X))
10    F2(I)=F2(I)*(COS(AKI+AKF)*X-CI*SIN(AKI+AKF)*X)/BX
      CALL SINT(AG,AH,F1,NINT,R1)
      CALL SINT(AG,AH,F2,NINT,R2)
      T22=R1*AMA+R2*R*BMA
      T2=T22*Q
      RETURN
      END
C
      SUBROUTINE TERM3 (A1,EPS,T3,NINT)
      COMPLEX EPS,A1,T3,T33,R1,R2,BX,CI,C1,C2,F1,F2,B1
      COMPLEX CMPLX,Q,AQF,CX,R
      DIMENSION F1(700),F2(700)
      COMMON AKI,AKF,AQF,CI,A,AKP,AMA,AMB,BMA,B1,MU,D,X,R,T,PI
      CI=CMPLX(0.,1.)
      Q=-0.5*A1*A*EPS*(1-EPS)
      Q=Q*SQRT(2./(AQF*PI))*AQF/(AQF+AKF)
      AG=-A
      AH=0.
```

```
      DD=(AH-AG)/(NINT-1)
      DO 10 I=1,NINT
      X=AG+(I-1)*DD
      B1=1.-EPS
      BX=1./(B1*X+A)
      F1(I)=(EXP(AMB)*X)*(COS(X)+CI*SIN(X))/BX**2
      F1(I)=F1(I)*((COS(AKI-AKF)*X+CI*SIN(AKI-AKF)*X))
      F2(I)=(EXP(AMB)*X)*(COS(X)+CI*SIN(X))/BX**2
10    F2(I)=F2(I)*((COS(AKI+AKF)*X-CI*SIN(AKI+AKF)*X))
      CALL SINT(AG,AH,F1,NINT,R1)
      CALL SINT(AG,AH,F2,NINT,R2)
      T33=R1+R2*R
      T3=T33*Q
      RETURN
      END
C
      SUBROUTINE TERM4 (A1,EPS,T4,NINT)
      COMPLEX EPS,A1,T4,R1,CI,Q,CMPLX,AQF,T,T4A,T4B
C     DIMENSION F1(700),F2(700)
      COMMON AKI,AKF,AQF,CI,A,AKP,AMA,AMB,BMA,B1,MU,D,X,R,T,PI
      CI=CMPLX(0.,1.)
      Q=-SQRT(1./(2.*AQF*PI))
      Q=T*A1*EPS*AKP*Q
      T4A=1./(AKP+CI*AQF)
      T4B=((AQF-AKF)/(AQF+AKF))*(1./(AKP-CI*AQF))
      T4=Q*(T4A+T4B)
      RETURN
      END
C
      SUBROUTINE REFRAC (W,WP,THETA,EPS,A1)
      COMPLEX A1,CX,CSQRT,EPS,CI,CMPLX,CY
      S2=SIN(2.*THETA)
      S1=SIN(THETA)
      C1=COS(THETA)
C     B1=1.-EPS
C     B1=1./(B1*X+A)
      CY=EPS-S1*S1
      CX=CSQRT(CY)
      A1=-S2/(CX+EPS*C1)
```

```
      RETURN
      END
C
      SUBROUTINE SINT (A,B,F,N,R)
C     INTEGRATION BY SIMPSON'S ONE-THIRD RULE
      COMPLEX F,R,S
      DIMENSION F(N)
      H=(B-A)/(N-1)
      S=0.0
      S=S+F(1)+F(N)
      M=N-1
      DO 10 I=2,M,2
   10 S=S+4.*F(I)+2.*F(I+1)
      R=H*S/3.
      RETURN
      END
```

APPENDIX V

FORTRAN PROGRAMME TO CALCULATE PHOTOCURRENT BY USING PROJECTION OPERATOR TECHNIQUE APPLIED TO CRYSTAL DEFINED BY KRONIG-PENNEY DELTA POTENTIAL

```
C       NAME OF PROGRAM: BZPROJ3.FOR WRITTEN ON 19.07.2003.
C       WRITTEN BY B.ZOLIANA GOVT.ZIRTIRI RESIDENTIAL SCIENCE
C       COLLEGE.AIZAWL.MIZORAM,INDIA.
C       PROGRAM TO CALCULATE PHOTOCURRENT USING PROJECTION OPERATOR
        COMPLEX A1,CI,T1,T2,T3,T4,EPS,CMPLX,AQF,EX,BNUM,DEN,PSI
        COMMON AKF,AQF,CI,A,AKI,AKP,ALPHA,POT,BNUM,DEN,PSI
        CI=CMPLX (0.,1.)
        PI=3.1415
C       ALPHA=0.35
        OPEN (UNIT=1, FILE='W.IN')
        READ (1,*) NINT
        OPEN (UNIT=1, FILE='W.IN')
C       READ (1,*) EI, THETA, A, ALPHA, MU, VZ, NE
        READ (1,*) EI, THETA, A, ALPHA, POT, VZ, NE
C       WRITE (NP, 2) EI, THETA, D, A, MU, XI, VZ, ALPHA, NE
        AKI=SQRT (2.*EI)
        AMU=AKI-PI*0.5293/3.61
        DO 90 IE=1, NE
        OPEN (UNIT=1, FILE='W.IN')
        READ (1,*) W, EPS1, EPS2
        WEV=W*27.2
        AKF=SQRT (2.*(EI+W))
        EX=EI+W-VZ
        AQF=SQRT (2.*EX)
        AKP=SQRT (2.*(VZ-EI))
        EPS=CMPLX (EPS1, EPS2)
        CALL REFRAC (W, WP, THETA, EPS, A1)
        CALL TERM1 (A1, EPS, T1, NINT)
        CALL TERM2 (A1, EPS, T2, NINT)
        CALL TERM3 (A1, EPS, T3, NINT)
        CALL TERM4 (A1, EPS, T4, NINT)
```

```
C       WRITE (NP, 3) W, AQF, T1, T2, T3, T4
        XINT=CABS (T1+T2+T3+T4)
        XCUR=XINT*XINT
        CUR= (XCUR*AKF*AKF)/W
C       CUR=ALOG (CUR)
        OPEN (UNIT=6, FILE='WBZPROJ4.OUT')
        WRITE (6, 5) WEV, EPS1, EPS2, CUR
C 3     FORMAT (2X, 2F8.4, 2X, 4(F15.6, 1X))
C   5   FORMAT (2X,'W=', F7.4, 2X,'EPS=', 2(F15.6, 2X),'CUR='E20.6)
    5   FORMAT (2X, F7.4, 2X, 2(F15.6, 2X), E20.6)
   90   CONTINUE
        STOP
        END
C
        SUBROUTINE TERM1 (A1, EPS, T1, NINT)
        COMPLEX EPS,A1,T1,T11,F1,R1,CI,C1,C2,C3,Q,AQF,BNUM,DEN,PSI
        DIMENSION F1 (700), F2 (700)
        COMMON AKF,AQF,CI,A,AKI,AKP,ALPHA,POT,BNUM,DEN,PSI
        CI=CMPLX (0., 1.)
        PI=3.1415
C       ALPHA=0.35
        AMU=AKI-PI*0.5293/3.61
        BNUM=-4.*PI*POT*SIN (AKI*A)*SIN (AKI*A)
        DEN=A*AKI*(AKI*COS (AKI*A) +AKI-AKP*SIN (AKI*A))
        DEN=DEN*SQRT (2.*PI*AKI)*(1. +COS (AKI*A))
        DEN=DEN*(1. +COS (AKI*A)-CI*SIN (AKI*A))
        PSI=BNUM/DEN
        Q=A1*(AQF/ (AQF+AKF))
        Q=Q*SQRT (2. / (AQF*PI))
        AG=-10.*A
        AH=-A
        DD= (AH-AG)/ (NINT-1)
        DO 10 I=1, NINT
        X=AG+ (I-1)*DD
        C1=(CI-AMU)*COS(AKI*X)-AKI*SIN(AKI*X)
        C2=-AKP*(CI-AMU)*SIN (AKI*X)-AKP*AKI*COS (AKI*X)
        C3=C1+C2
        F1 (I) =C3*EXP ((ALPHA-AMU)*X)
   10   F1 (I) =F1 (I)*EXP (CI*(1.-AKF)*X)
```

```
      CALL SINT (AG, AH, F1, NINT, R1)
      T11=R1
      T1=T11*Q*PSI
      RETURN
      END
C
      SUBROUTINE TERM2 (A1, EPS, T2, NINT)
      COMPLEX EPS, A1, T2, T22, R1, BZ
      COMPLEX CI,CMPLX,F1,Q,AQF,C1,C2,C3,BNUM,DEN,PSI
      DIMENSION F1 (700), F2 (700)
      COMMON AKF,AQF,CI,A,AKI,AKP,ALPHA,POT,BNUM,DEN,PSI
      CI=CMPLX (0., 1.)
      PI=3.1415
C     ALPHA=0.35
      AMU=AKI-PI*0.5293/3.61
      BNUM=-4.*PI*POT*SIN (AKI*A)*SIN (AKI*A)
      DEN=A*AKI*(AKI*COS (AKI*A) +AKI-AKP*SIN (AKI*A))
      DEN=DEN*SQRT (2.*PI*AKI)*(1. +COS (AKI*A))
      DEN=DEN*(1. +COS (AKI*A)-CI*SIN (AKI*A))
      PSI=BNUM/DEN
      Q=A1*A*EPS
      Q=Q*SQRT (2. / (AQF*PI))*(AQF/ (AQF+AKF))
      AG=-A
      AH=0.
      DD= (AH-AG)/ (NINT-1)
      DO 10 I=1, NINT
      X=AG+(I-1)*DD
      BZ=(1.-EPS)*X+A
      C1=(CI-AMU)*COS(AKI*X)-AKI*SIN(AKI*X)
      C2=-AKP*(CI-AMU)*SIN(AKI*X)-AKP*AKI*COS(AKI*X)
      C3= C1+C2
      F1(I)=C3*EXP((ALPHA-AMU)*X)/BZ
10    F1(I)=F1(I)*EXP(CI*(1.-AKF)*X)
      CALL SINT(AG,AH,F1,NINT,R1)
      T22=R1
      T2=T22*Q*PSI
      RETURN
      END
C
```

```
      SUBROUTINE TERM3 (A1,EPS,T3,NINT)
      COMPLEX EPS,A1,T3,T33,R1,BZ,CI,C1,F1
      COMPLEX CMPLX,Q,AQF,BNUM,DEN,PSI
      DIMENSION F1(700),F2(700)
      COMMON AKF,AQF,CI,A,AKI,AKP,ALPHA,POT,BNUM,DEN,PSI
      CI=CMPLX(0.,1.)
      PI=3.1415
C     ALPHA=0.35
      AMU=AKI-PI*0.5293/3.61
      BNUM=-4.*PI*POT*SIN(AKI*A)*SIN(AKI*A)
      DEN=A*AKI*(AKI*COS(AKI*A)+AKI-AKP*SIN(AKI*A))
      DEN=DEN*SQRT(2.*PI*AKI)*(1.+COS(AKI*A))
      DEN=DEN*(1.+COS(AKI*A)-CI*SIN(AKI*A))
      PSI=BNUM/DEN
      Q=-0.5*A1*A*EPS*(1.-EPS)
      Q=Q*SQRT(2./(AQF*PI))*AQF/(AQF+AKF)
      AG=-A
      AH=0.
      DD=(AH-AG)/(NINT-1)
      DO 10 I=1,NINT
      X=AG+(I-1)*DD
      BZ=(1.-EPS)*X+A
      C1=COS(AKI*X)-(AKP*SIN(AKI*X))
      F1(I)=C1*EXP((ALPHA-AMU)*X)/(BZ*BZ)
   10 F1(I)=F1(I)*EXP(CI*(1.+AKF)*X)
      CALL SINT(AG,AH,F1,NINT,R1)
      T33=R1
      T3=T33*Q*PSI
      RETURN
      END
C
      SUBROUTINE TERM4 (A1,EPS,T4,NINT)
      COMPLEX EPS,A1,T4,R1,R2,C1,CI,Q,CMPLX,AQF,C2,BNUM,DEN,PSI
C     DIMENSION F1(700),F2(700)
      COMMON AKF,AQF,CI,A,AKI,AKP,ALPHA,POT,BNUM,DEN,PSI
      CI=CMPLX(0.,1.)
      PI=3.1415
C     ALPHA=0.35
      AMU=AKI-PI*0.5293/3.61
```

```
      BNUM=-4.*PI*POT*SIN(AKI*A)*SIN(AKI*A)
      DEN=A*AKI*(AKI*COS(AKI*A)+AKI-AKP*SIN(AKI*A))
      DEN=DEN*SQRT(2.*PI*AKI)*(1.+COS(AKI*A))
      DEN=DEN*(1.+COS(AKI*A)-CI*SIN(AKI*A))
      PSI=BNUM/DEN
      Q=-A1*EPS*SQRT(1./(2.*AQF*PI))*AKP*AKI
      C1=1./(AKP+CI*AQF)
      C2=(AQF-AKF)/(AQF+AKF)
      C2=C2/(AKP-CI*AQF)
      T4=Q*PSI*(C1+C2)
      RETURN
      END
C
      SUBROUTINE REFRAC (W,WP,THETA,EPS,A1)
      COMPLEX A1,CX,CSQRT,EPS,CI,CMPLX,CY
      S2=SIN(2.*THETA)
      S1=SIN(THETA)
      C1=COS(THETA)
C     B1=1.-EPS
C     B1=1./(B1*X+D)
      CY=EPS-S1*S1
      CX=CSQRT(CY)
      A1=-S2/(CX+EPS*C1)
      RETURN
      END
C
      SUBROUTINE SINT (A,B,F,N,R)
C     INTEGRATION BY SIMPSON'S ONE-THIRD RULE
      COMPLEX F,R,S
      DIMENSION F(N)
      H=(B-A)/(N-1)
      S=0.0
      S=S+F(1)+F(N)
      M=N-1
      DO 10 I=2,M,2
   10 S=S+4.*F(I)+2.*F(I+1)
      R=H*S/3.
      RETURN
      END
```

REFERENCES:

1. J. A. Appelbaum and D.R.Hamann, *Phys. Rev.* **B6**, 2166 (1972)
2. G. P. Alldrege and L .Klienman, *Phys. Rev.*, **B10**, 559 (1974)
3. K. Mitchell, *Proc. Roy. Soc.*, **A146**, 442 (1934).
4. W. L. Schaich and N. W. Ashcroft, *Phys. Rev.*, **B3**, 2453 (1971).
5. G. D. Mahan, *Phys. Rev. Lett.*, **24,** 1068 (1970).
6. T. Maniv and H. Metiu, *Phys. Rev.*, **B22**, 4731 (1980).
7. D. R. Penn, *Phys. Rev. Lett.*, **28**, 1041 (1972).
8. J. G. Endriz, *Phys. Rev.*, **B7,** 3464(1973)
9. H. Petersen and S. B. M. Hagstorm, *Phys.Rev.Lett.*, 41, 1314(1978)
10. I. Adawi, *Phys. Rev.*, **134A**, 788 (1964).
11. A. Liebsch, *Phys. Rev. Lett.*, **32**, 1203 (1973).
12. J. B. Pendry, *Surf. Sci.*, **57**, 679 (1976).
13. J. B. Pendry, *Low Energy Electron Diffraction* (*Academic Press*, London, 1974).
14. P. J. Feibelman, *Phys. Rev.*, **B12**, 1319 (1975); *Phys. Rev. Lett.*, **34**, 1092 (1975).
15. H. J. Levinson, E. W. Plummer and P. J. Feibelman, *Phys. Rev.Lett.*, **43**, 952 (1979).
16. G. Mukhopadhyay and S. Lundqvist, *Physica Scripta*, **17**, 69 (1978).
17. A. Bagchi, *Phys. Rev.*, **B15**, 3060 (1977).
18. K. L. Kliewer, *Phys. Rev.*, **B14**, 1412 (1976).
19. F. Forstman and H. Stenschke, *Phys. Rev. Lett.*, **38**, 1365 (1977).

20. K. Kempa and F. Forstman, *Surf. Sci.*, **129**,516 (1983).

21. N. Barberan and J. E. Inglesfield, *J. Phys.*, **C14**, 3114 (1981).

22. R. K. Thapa, *A Theoretical Study of Photon fields near Surfaces With Application to Photoemission*, Ph.D. thesis, North Bengal University (1994).

23. A. Bagchi and N. Kar, *Phys. Rev.*, **B18**, 5240 (1978).

24. P. Das, R. K. Thapa and N. Kar, *Mod. Phys. Lett.*, **B5**, 65 (1991); R. K. Thapa, P. Das and N. Kar, *Mod. Phys. Lett.*, **B8**, 36 (1994).

25. R. K. Thapa and N. Kar, *Indian J.Pure and Appl. Phys.*, **26**, 620 (1988).

26. R. de L. Kronig and W. G. Penney, *Proc. Roy. Soc.*, **A130**, 499 (1931).

27. H. Statz, *Z.Naturforch*, **5A**, 534 (1950).

28. J. D. Levine, *Phys. Rev.* **171**, 701 (1968).

29. S. G. Davison and J. D.Levine, *Solid State Physics*, **25**, 1 (1970).

30. J. C. Slater and G. K. Koster, *Phys. Rev.*, **94**, 1498 (1954).

31. T. R. Carver, *Am .J. Phys.*, **39**, 1225 (1971).

32. Z. Pachuau, *Theoretical Study of Photoemission from Metals and Semiconductors*, Ph.D. thesis, NEHU (2001)

33. Z. Pachuau, B. Zoliana, D. T. Khathing, P. K. Patra and R. K. Thapa, *Phys. Lett.*, **A275**, 459 (2000).

34. S. G. Davison and M. Steslicka, *Basic Theory of Surface States* (Clarendon, Oxford, 1992).

35. R. A. Bartynski, E. Jensen, T. Gustafson and E. W. Plummer, *Phys. Rev.*, **B32**, 952 (1985).

36. M. Tinkham, *Group Theory and Quantum Mechanics* (McGraw-Hill, 1964).

37. E. Bertel, *Phys. Rev.* **B50**, 4925 (1994).

38. J. F. Cornwell, *Group Theory and Electronic Energy Band in Solids* (North-Holland, 1969), p.54.

39. N. E. Christensen and B. Feuerbacher, *Phys. Rev.*, **B10**, 2349 (1974)
B. Feuerbacher and N. E. Christensen, *Phys. Rev.*, **B10**, 4932 (1974)
P. J. Feibelman and D. E. Eastman, *Phys. Rev.*, **185**, 882 (1969).

40. G. Mukhopadhyay and S. Lundqvist, *Solid State. Comm.*, **25**, 881 (1978).

41. L. D. Landau and E. M. Lifshitz, *Electrodynamics of Continuous Media* (Pergamon Press, 1984), p. 304.

42. J. H. Weaver, *Handbook of Chemistry and Physics* (CRC Press, Boca Raton, FL, 1987) p. E377.

43. Edwards D. Pallick (ed.), *Handbook of Optical Constants of Solids* (Academic Press, 1991) p. 429.

44. J. A. Appelbaum, *Surface Physics of Materials,* (ed.), J. H. Blakely Vol. I (Academic Press, New York, 1975) p. 77.

45. B. Zoliana and R. K. Thapa, *Electronic field calculation using s- and p-polarised light.* (unpublished data).

46. S. L. Weng, T. Gustaffson and E. W. Plummer, *Phys. Rev.* **B18**, 1718 (1978).

47. L. F. Wagner and W. E. Spicer, *Phys.Rev.Lett.*, **28**, 1381 (1972).

48. D. E. Eastman and W. D. Grobman, *Phys. Rev. Lett.*, **28**, 1378 (1972).

49. Zaithanzauva Pachuau, B. Zoliana, P. K. Patra, D. T. Khathing and R. K. Thapa, *Phys. Letts.*, **A 294**, 52 (2002).

50. Maurice Glicksman, *Solid State Physics,* **26**, 338 (1971)

51. B. Zoliana and R. K. Thapa, *Photoemission calculations using Mathieu potential from surface state of metals and semiconductors* (unpublished data).

52. G. Cappelli and R. Del Sole, *Phys. Rev.* **B 15**, 9892 (1993).

53. P. Das and N. Kar, *Mod.Phys. Letts.*, **B8**, 36 (1994).

54. W. Schattke, *Phys. Stat.Sol.* , **54**, 211 (1997).

55. A. Ishi and T. Aissąka, *Surf. Sci.* **242**, 250 (1991).

56. A. Ernst, W. M. Temmerman, Z. Szotek, M. Wood and P. J. Durhan, *Phil. Mag.*, **B 78,** 503 (1998).

57. J. Henk and A. Ernst, *J. Electron Spect. Related Phenom.*, **125**, 107 (2002), A. Ernst, J.Henk, P.Bruno and R.K.Thapa, *J. Phys: Condens. Matter.* (communicated).

58. B. Zoliana, Z. Pachuau, Lalthakimi Zadeng, R. K. Thapa, D.T. Khating and P. K. Patra, *3rd Regional Conference on Physics Reseach in N. E. India,* Dibrugarh Univ., 9th Nov. 2002.

59. B. Zoliana, Z. Pachuau, Lalthakimi Zadeng, D. T. Khathing and R. K. Thapa, *Int. J. Mod. Phys.*, **B 17**, 2897 (2003).

60. P. Heimann, J. Hermann, H. Miosqa and Neddermeyer, *Surf. Sci.*, **85**, 263 (1979).

61. S. D. Kevan, *Phys. Rev.* **B 28**, 4822 (1983).

62. P. Sandl and E. Bertel, *Surf. Sci. Lett.* **302,** L325 (1994).

63. W. Jacob, V. Dose, U. Kolac, Th. Fauster and A. Goldmann, *Z. Phys.*, **B63,** 459 (1986).

64. R. K. Thapa, N. Kar, *Phys. Rev.*, **B51**, 17980 (1995).

65. R. K. Thapa, *Phys. Stat. Sol.* **B 179**, 391 (1993).

66. Ig. Tamm, *Phys. Z. Souvjet*, **1**, 717 (1935).

67. A. W. Mane, *Z.Physik*, **94,** 717 (1935).

68. W. Shockley, *Phys. Rev.*, **56**, 317 (1939).

69. M. Steslicka, *Prog. Surf. Sci.*, **5**, 157, (1974).

70. A. M. Eldib, H. F. Hasson and M. A. Mohmad, *J. Phys.*, **C 20**, 3011 (1987).

71. R. K. Thapa and N. Kar, *Phys. Rev.* **B49**, 17980 (1995).

72. R .K. Thapa, N. Kar, *Mod.Phys. Letts.*, **B8**, 361 (1994).

73. N. W. Aschcroft and N. D. Mermine, *Solid State Physics* (CBS Publishing, Japan,1976) p. 146.

74. F. G. Allen and G. W. Gobeli, *Phys. Rev.*, **127**, 150 (1962).

75. B. Feubacher, B. Fitton, R. F. Willis, *Photoemission and Electronic Properties of Surfaces* (Wiley, New York, 1978).

76. A. Zangwill, *Physics at Surfaces* (Cambridge University Press, 1989).

77. T. D. Poppendieck, T. C. Ngoc and M. B. Webb, *Surf. Sci.*, **74**,34 (1978).

78. R. Manzke, *J. Phys.* **C 13**, 911 (1980).

79. W. E. Spicer, *Chemistry and Physics of Solids Surfaces* (CRC Press Inc. Cleveland, Ohio, 1977) p. 235-254.

80. T. Aiyama and K. Yada, *J. Phys. Soc. Jpn.*, **36**, 1554 (1974).

81. R. K. Thapa and N. Kar, *Indian J .Phys.* **64A**, 321(1990).

82. R. K. Thapa and Gunakar Das, *Intl. Jour. Mod. Phys.* (Accepted).

83. R. K. Thapa, Gunakar Das, S.Gurung, Lalthakimi Zadeng and R. Bhattacharjee, *Indian Jour. Phys.* (To be published).

BIODATA

Name	:	B.Zoliana
Father's Name	:	B.Lalchheuva
Date of Birth	:	03.04.1968.
Institutional Address	:	Govt. Zirtiri Residential Science College. Aizawl-796 001. Mizoram.
Residential Address	:	T-15, Bungkawn, Aizawl-796 001, Mizoram.
E-mail Address	:	bzoliana@ sancharnet.in bzoliana@ yahoo.com
Designation	:	Senior Lecturer (Physics)
Teaching Experience	:	10 years
Research Experience	:	6 years
Academic Qualifications	:	

Sl.No.	Exami-nation	Division	% of marks	Subject(s)	Year	Board/ University	Distinction achieved
1	HSLC	Distinction	81	Miz, Eng, Sc. Maths,S.S., Addl.Maths	1984	MBSE	1st Position in Board
2	P.U. (Sc)	First	65.7	Eng,Maths, Phys.,Bio, Chem	1986	NEHU	
3.	B.Sc.	First	60.9	Eng,F.C, Maths, Electronics, Phys. (Hons.)	1990	NEHU	10th Position in University
4	M.Sc.	First	63.6	Physics	1992	NEHU	4th Position in University
5	Dip. in Radiol-ogical Phys.	First	62.6	Radn.Phys, Radn. Dosimetry, Radn. Safety,etc.	1996	Bombay University. (course conducted by BARC)	

Computational Experience : Exposed to the programmes and languages like FORTRAN 77, FORTRAN 90 & 95, Lotus Smart suite, MS office, Adope Pagemaker,MS-DOS, Internet explorer, Netscape Navigator, etc. Also a computational knowledge in Treatment Planning System (Rad. plan) for cancer treatment.

Research Publications:

1) *Application of Mathieu potential to photoemission from metals,* Z.Pachuau, B.Zoliana, D.T.Khathing, P.K.Patra and R.K.Thapa, *Phys.Lett.* **A, 275**, 459-462 (2000).

2) *A simple study of photoemission from metals,* B.Zoliana, Z.Pachuau, S.Srivastav, R.C.Tewari, P.K.Patra and R.K.Thapa, *Indian Jour. Phys.*, **76A,[2],** 201-209 (Mar2002).

3) *Application of Mathieu potential to photoemission calculations: the case of a strong potential,* Zaithanzauva Pachuau, B.Zoliana, P.K.Patra, D.T.Khathing and R.K.Thapa, *Phys. Letts* **A 294**, 52-57 (2002).

4) *A model photoemission calculations using the Projection Operator Method,* B.Zoliana, Zaithanzauva Pachuau, Lalthakimi Zadeng, R.K.Thapa. P.K.Patra and D.T.Khathing, *International Jour. Mod. Phys.*, **B17 [17],** 2897-2902 (July 2003).

5) *Photoemission calculations from Fe and Ni by using the Mathieu potential model,* B.Zoliana, Z.Pachuau, Lalthakimi Zadeng, P.K.Patra, D.T.Khathing and R.K.Thapa. *Indian Jour. Phys.* **A77, [4],** 393-396 (July 2003).

6) *Photoemission calculations from transition metals Ni, Fe,* R.K.Thapa, Lalthakimi Zadeng, S.Srivastava, B.Zoliana, Z.Pachuau, P.K.Patra. (*Accepted for publication in Indian Jour. Pure and Appld. Physics*).

7) Photoemission calculations by using Projection Operator method for periodic potential. B.Zoliana and R.K.Thapa (*To be communicated to Physics Letter A, North Holland*).

Conference Papers

1. *Application of Projection Operator method of Group Theory to Photoemission calculations,* B.Zoliana, Zaithanzauva Pachuau, P.K.Patra, D.T.Khathing and R.K.Thapa, *Third Regional Conference on Physics Research in North-East,* Dibrugarh University, Dibrugarh, 9th November 2002.

2. *Application of Mathieu potential to Photoemission calculations,* Zaithanzauva Pachuau,B.Zoliana,P.K.Patra and R.K.Thapa,*Third Regional Conference on Physics Research in North-East,* Dibrugarh University, Dibrugarh, 9th November 2002.

3. *Application of Kronig-Penney model to photoemission calculation from Fe and Ni,* Lalthakimi Zadeng, S.Srivastava, R.K.Thapa,P.K.Patra,B.Zoliana and Z.Pachuau, *Third Regional Conference on Physics Research in North-East,* Dibrugarh University, Dibrugarh, 9th November 2002.

4. *Application of projection operator method of group theory in forming basis functions to define the initial state wavefunctions and its use in photoemission calculations,* B.Zoliana, P. K. Patra and R. K.Thapa, submitted to *Condense Matter Days* Conference, North Eastern Hill University, Shillong, August, 2004.

5. *A model photoemission calculation by using projection operator method of group theory*, B. Zoliana and R. K. Thapa , submitted to *Young Physicist Colloqium,* Kolkata. September, 2004.

ELSEVIER

Physics Letters A 10168 (2000) xxx

PHYSICS LETTERS A

www.elsevier.nl/locate/pla

Application of mathieu potential to photoemission from metals

Zaithanzauva Pachuau [a], B. Zoliana [a], D.T. Khating [b], P.K. Patra [c], R.K. Thapa [c,*]

[a] *Department of Physics, Government Zirtiri Residential Science College, Aizawl 796 001, Mizoram, India*
[b] *Department of Physics, North-Eastern Hill University, Shillong 793 022, India*
[c] *Department of Physics, Pachhunga University College, North-Eastern Hill University, Aizawl 796 001, Mizoram, India*

Received 30 June 2000; accepted 30 August 2000
Communicated by J. Flouquet

Abstract

The Mathieu potential is used to define the crystal potential from which the initial state wavefunction for the surface state is derived. The wavefunction is used for photoemission calculations in the case of free electron metals like Al and Be.

PACS: 73.20; 79.60
Keywords: Photoemission; Photocurrent; Wavefunction; Surface; Dielectric function

Over the last few decades interests in the detailed understanding of the physical properties of condensed materials and their surfaces have grown enormously. Further the miniaturization in microelectronics have reached a point where surface properties have become very much dominant. Sufficient progress has been made in the production of two-dimensional structures like multilayers or thin films, which have new and fascinating features. For investigating the electronic properties of clean and adsorbate covered surfaces and thin films, angle-resolved ultraviolet photoemission spectroscopy (ARUPS) has become one of the important tools as it allows measuring the dispersion of the bands for both occupied and unoccupied bands and therefore reveals the structure around the Fermi level with a high level of accuracy [1–4]. In order to interpret the experimental spectra, it is useful to have a quantitative comparison between the theoretical and experimental photoemission data. This demand has led to the developments of various approaches for calculating the photocurrent which ranges from sophisticated but tractable many-body theories [5] to one-electron formulations. Experimental data from ARUPS have been extensively useful in surface physics, and to analyze the data, methods for photoemission calculations have been developed where the wavefunctions for the semi-infinite solid are constructed accurately. However the spatial variations of the electromagnetic fields is generally neglected in such type of calculations. The reason for this being that it is a complex problem and *ab initio* calculations are available only for jellium [6–9]. On the other hand, empirical calcu-

* Corresponding author. Fax: 0091 - 389 - 323491; Tel.: 0091 - 389 - 328044.
E-mail address: rkt@dte.vsnl.net.in (R.K. Thapa).

0375-9601/00/$ - see front matter
PII: S0375-9601(00)00602-2

lations of the fields near surfaces with the local dielectric functions have been used to interpret the qualitative features in photoemission data from metals and semiconductors. Free electron [10] and Kronig–Penney [11,12] models have been used in such cases for developing the initial state wavefunctions which were then employed to calculate the matrix elements for evaluating the photocurrent.

We report here a simple formalism developed for photoemission calculations in which the free-electron states are derived by using the Mathieu potential [13,14]. The Mathieu potential has been at first used by Statz [15] for surface state calculations. Levine [16] had also used the Mathieu potential for calculating the condition for arbitrary surface terminations. We have used in this formalism the model as described by Davison and Steslicka [13,14] for describing the crystal potential which was then used for deriving the initial state wavefunctions.

The photocurrent density formula [17] from the golden rule approximation can be written as

$$\frac{\mathrm{d}j(E)}{\mathrm{d}\Omega} = \frac{2\pi}{\hbar}\sum|\langle\psi_f|\Delta|\psi_i\rangle|^2\delta(E-E_f) \times\delta(E_f-E_i-\hbar\omega)[1-f_0(E)], \quad (1)$$

where ψ_i (ψ_f) refers to the initial (final) state wavefunction and $\Delta = (e/2m_e c)(\boldsymbol{A}\cdot\boldsymbol{p}+\boldsymbol{p}\cdot\boldsymbol{A})$ where m_e is the mass of the electron, $\boldsymbol{p}$ the one-electron momentum operator and $\boldsymbol{A}$ is the vector potential of the incident photon field. To compute the photon field, we have used the simple model of Bagchi and Kar [17] which has been used earlier also [10–12]. With simple modification the photon field used in our calculation can be written as

$$\tilde{A}_\omega(x) = \begin{cases} A_1, & x < -d \\ \dfrac{A_1\varepsilon(\omega)d}{[1-\varepsilon(\omega)]x+d} & -d \leqslant x \leqslant 0 \\ A_1\varepsilon(\omega), & x > 0 \end{cases} \quad (2)$$

where A_1 is a constant depending on the dielectric function $\varepsilon(\omega)$, photon energy $\hbar\omega$ and the angle of incidence θ_i. To determine $\psi_i(x)$ in Eq. (1) we have included a surface of width d in the crystal potential as shown in Fig. 1. We have considered a nearly

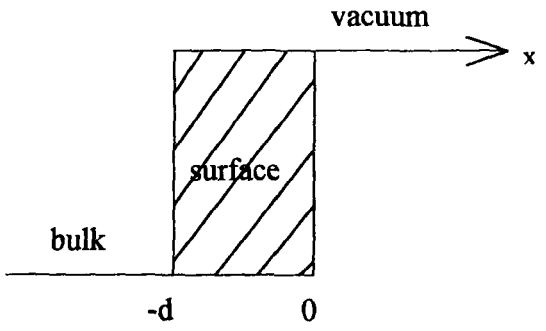

Fig. 1. Model potential used for calculating the initial state wavefunction ψ_i and the photon field.

empty lattice with a finite step potential [13,14]. The initial state wavefunction is given by (in au)

$$\psi_i(x,q) = \begin{cases} \left(\dfrac{1}{4\pi k_i}\right)^{1/2}\phi(x_0,q)\mathrm{e}^{-\eta(x_0-x)}, & (\text{for } \eta>0)\ x\leqslant 0 \\ (2\zeta)^{1/2}\mathrm{e}^{-\zeta(x-x_0)}, & (\text{for } \zeta>0)\ x>0 \end{cases} \quad (3)$$

where x_0 is the crystal surface location. For a nearly empty lattice with a height of the step potential as ζ, we have since $q\sim 0$, a hybridization parameter $\lambda \cong \tan m'(x_0-\zeta^{-1})$. Also $\phi(x_0,q) \cong \lambda\cos m'x - \sin m'x$ such that $m' = ma/\pi$ where m is the band index and a is the period of the potential. We have chosen the following data both for the case of Al and Be: $x_0 = a/2$, $\zeta = 12/a$ and $m = 1$. The matrix element in Eq. (1) for calculating the photocurrent now reduces to the following:

$$I = \int_{-\infty}^{-d}\psi_f^*\tilde{A}_\omega(x)\frac{\mathrm{d}\psi_i}{\mathrm{d}x}\mathrm{d}x + \int_{-d}^{0}\psi_f^*(x)\tilde{A}_\omega(x)\frac{\mathrm{d}\psi_i}{\mathrm{d}x}\mathrm{d}x + \frac{1}{2}\int_{-d}^{0}\psi_f^*\frac{\mathrm{d}\tilde{A}_\omega(x)}{\mathrm{d}x}\psi_i\,\mathrm{d}x + \int_0^\infty\psi_f^*\tilde{A}_\omega(x)\frac{\mathrm{d}\psi_i}{\mathrm{d}x}\mathrm{d}x. \quad (4)$$

The photocurrent was calculated as a function of photon energy ($\hbar\omega$) by evaluating the integrals in Eq. (4). The formalism was then applied to the case

of metals Al and Be as they are free electron type of metals. For these metals we have used the experimentally determined dielectric function [18] for calculating the photon fields through a subroutine of the main FORTRAN programme.

The plot of the photocurrent as a function of $(\hbar\omega)$ for normal photoemission is shown in Fig. 2. We have shown here the photoemission for a constant initial state for which the energy was located at the Fermi level. As it is a model calculation, we have chosen the location of the Fermi level for both Al and Be to be at 0.43 Hartrees. The photocurrent profile for Al showed a strong photoemission at photon energy $\hbar\omega = 10$ eV. This was followed by a suppressed photoemission and therefore the photocurrent was minimum at $\hbar\omega = 15$ eV (the plasmon energy of Al is $\hbar\omega_p = 15.3$ eV). There is another hump in photocurrent data at $\hbar\omega = 18$ eV. We find that there is a qualitative agreement between the experimental data [19] and the previously calculated results [10]. The experimental data of Levinson et al. [19] showed a maxima in photocurrent at $\hbar\omega = 13$ eV with the occurrence of a minima at the plasmon energy. However in the case of Be the behaviour of the photocurrent is similar to that of Al.

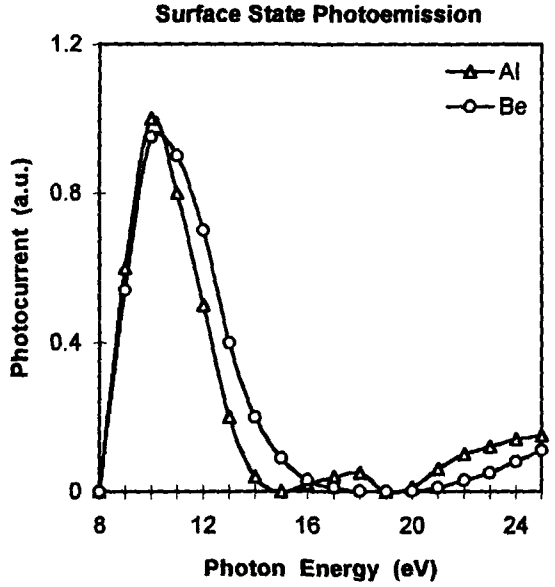

Fig. 2. Plot of photocurrent (normalized to unity) against the photon energy (−eV) for Al and Be.

For example it showed a maximum at $\hbar\omega = 10$ eV followed by a minimum but not occurring at $\hbar\omega = \hbar\omega_p$ (the plasmon energy of Be is 19.5 eV) like in the previously calculated results [20]. It showed a minimum in the photocurrent within the photon energy range of 18 eV to 20 eV. There was an enhancement in the photocurrent value for $\hbar\omega > \hbar\omega_p$. We see from the variation of the photocurrent data that even in the case of Be, it showed a qualitative behaviour as seen earlier in the theoretical [20] and experimental data [21].

The features seen in the behaviour of the photocurrent in Al and Be can be attributed to the fact that in the free electron metals the change in bulk potential is too weak to impart sufficient momentum for photoexcitation. The surface photo-effect is due to the rapid variation of photon fields in the surface region. This is evident from the matrix element in Eq. (1) where $\mathrm{d}\tilde{A}_\omega/\mathrm{d}x$ is directly dependent on photocurrent as the photon energy passes through the threshold for photoexcitation. Moreover we have considered a low photon energy photoemission, hence the incident radiation is too weak to photoexcite electrons from the bulk bands. The origin of the peak in the photocurrent data in the case of Be for $\hbar\omega < \hbar\omega_p$ has been explained by Karlsson et al. [22] from the band picture. He attributed this to the existence of the surface state at $\bar{\Gamma}$ with energy 2.8 eV in the bulk energy band gap $\Gamma_3^+ - \Gamma_4^-$.

Though the model presented in this report is very simple, however, the inclusion of the initial state wavefunction (derived by using the Mathieu potential) into the matrix element appears to reproduce the qualitative features as observed earlier in photocurrent data of Al and Be. There are however shortcomings in the formalism developed. For example, we have used the same ψ_i both for the surface and the bulk regions of the solids. Further it is the spatial variation of the photon fields which is monitoring the change in the photocurrent. However it is a simple type of calculations which enables one to see the effect of inclusion of the Mathieu potential also in the photoemission calculations. It would be still appropriate and realistic if one can extend such type of calculations to other metals like d-band or transition type by appropriately incorporating the sine and cosine elliptic functions to the initial state wavefunc-

tions [13,14]. One should also take into consideration the band structure to widen the scope of such studies to electronic structure calculations.

Acknowledgements

Z.P. acknowledges gratefully a research grant from the University Grants Commission, Guwahati, India. Thanks are also due to Dr. C. Thanthianga, Principal, Pachhunga University College, Aizawl (India) for extending the necessary facilities. R.K.T. acknowledges the literature received from Mrs. P. Davison, University of Waterloo, Canada.

References

[1] B. Feurbacher, B. Fitton, R.F. Willis, Photoemission and Electronic Properties of Surfaces, Wiley, New York, 1978.
[2] J.E. Inglesfield, Rep. Prog. Phys. 45 (1982) 223.
[3] J.B. Pendry, Surf. Sci. 57 (1976) 679.
[4] A. Ishii, T. Aissaka, Surf. Sci. 242 (1991) 250.
[5] J. Braun, Rep. Prog. Phys. 59 (1996) 1267.
[6] P.J. Feibelman, Phys. Rev. Lett. 34 (1975) 1092.
[7] P.J. Feibelman, Phys. Rev. 12 (1975) 1319.
[8] H.J. Levinson, E.W. Plummer, J. Vac. Sci. Technol. 17 (1980) 216.
[9] A. Kiejna, Prog. Surf. Sci. 61 (1999) 85.
[10] P. Das, R.K. Thapa, N. Kar, Mod. Phys. Lett. B 5 (1991) 65.
[11] R.K. Thapa, Phys. Stat. Sol. B 179 (1993) 391.
[12] R.K. Thapa, N. Kar, Surf. Sci. 338 (1995) 138.
[13] S.G. Davison, M. Steslicka, Basic Theory of Surface State, Clarendon, Oxford, 1992.
[14] S.G. Davison, J.D. Levine, Solid State Phys. 25 (1970) 2.
[15] H. Statz, Z. Naturforsch 5A (1950) 534.
[16] J.D. Levine, Phys. Rev. 171 (1968) 701.
[17] A. Bagchi, N. Kar, Phys. Rev. B 18 (1978) 5240.
[18] J. Weaver, in: E.D. Pallik (Ed.), Handbook of Chemistry and Physics, CRC Press, Boca Raton, Ohio, 1987 for optical data of Al; Handbook of Optical Constants of Solids, Academic, 1991, p. 429 for optical data of Be.
[19] H.J. Levinson, E.W. Plummer, P.J. Feibelman, Phys. Rev. Lett. 43 (1979) 952.
[20] R.K. Thapa, N. Kar, Phys. Rev. B 51 (1995) 17980.
[21] R.A. Bartynski, E. Jensen, T. Gustaffson, E.W. Plummer, Phys. Rev. B 32 (1985) 1921.
[22] U.O. Karlsson, S.A. Flodstrom, R. Engelhardt, W. Gadeka, E.E. Koch, Solid State Comm. 49 (1984) 711.

Indian J. Phys. **76A** (2), 207-209 (2002)

NOTE

IJP A

— an international journal

A simple study of photoemission from metals

B Zoliana[a], Z Pachuau[a], P K Patra, S Srivastava, R C Tewari[b] and R K Thapa*

Department of Physics, Pachhunga University College, Aizawl 796 001, Mizoram

[a] Department of Physics, Government Zirtiri Residential Science College, Aizawl 796 001, Mizoram

[b] Department of Physics, Government Serchip College, Serchip-796181 Mizoram

E-mail ramkumar_thapa@yahoo.com

Received 28 May 2001, accepted 30 October 2001

Abstract We have applied the Kronig-Penney model potential to calculate photocurrent from metals Mo and Cu. Spatially dependent vector potential had been used to evaluate the relevant matrix elements

Keywords Photoemission, photocurrent, kronig-penny model potential

PACS No. 79 60 Bm

In this note, a simple study of the behavior of photocurrent data is presented for molybdenum and copper metals in the low photon energy range. Photocurrent is calculated by using the golden rule formula [1]

$$\frac{dj}{d\omega} = \frac{2\pi}{\hbar}\sum \left| < \psi_f \left| H' \right| \psi_i > \right|^2 \delta(E - E_f)\delta(E_f - E_{ii} - \hbar\omega) \times f_0(E - \hbar\omega)[1 - f_0(E)], \quad (1)$$

where H' is the perturbation responsible for photoemission due to incident radiation of frequency ω. $|\psi_i>(|\psi_f>)$ refers to the initial (final) state wavefunctions, $E_i(E_f)$ are initial (final) state energy, $f_0(E)$ denotes the Fermi occupation function. We are considering the photoemission to take place along $z-$ axis which is normal to the surface. H' can be written as

$$H' = \frac{e}{mc}\left[\tilde{A}_\omega(z)\frac{d}{dz} + \frac{1}{2}\frac{d}{dz}\tilde{A}_\omega(z)\right], \quad (2)$$

where $\tilde{A}_\omega(z) = \frac{A^z_\omega(z)}{A_0}$, with $A^z_\omega(z)$ as the component of vector potential along z-axis, A_0 is the amplitude of the incident beam. We assume the z-direction to be perpendicular to the surface which is chosen as $z = 0$. The metal is assumed [2] to occupy all space to the left of the $z = 0$ plane. The response of the electromagnetic field is bulk-like every where except in the surface region defined by $-a \le z \le 0$. In this region, the model dielectric function is chosen to be a local one which interpolates linearly between the bulk value inside the metal and the vacuum value (unity) outside. The model frequency-dependent dielectric function used for calculating $\tilde{A}_\omega(z)$ is given by

$$\varepsilon(\omega) \equiv \varepsilon_1(\omega) + i\varepsilon_2(\omega) \quad \text{for} \quad z < -a,$$

$$\varepsilon(\omega, z) = 1 + [1 - \varepsilon(\omega)]\cdot\frac{z}{a} \quad \text{for} \quad -a \le z \le 0,$$

$$= 1 \quad \text{for} \quad z > 0. \quad (3)$$

We consider [2] a p-polarised light to be incident on the surface plane making an angle θ_i with the z-axis. The vector potential of interest $\tilde{A}_\omega(z)$ in the long wavelength $(\omega a/c) \to 0$ is given by

$$\tilde{A}_\omega(z) = -\frac{\sin 2\theta_i}{\left[\varepsilon(\omega) - \sin^2\theta_i\right]^{\frac{1}{2}} + \varepsilon(\omega)\cos\theta_i} \quad \text{for} \quad z < -a,$$

$$= -\frac{\sin 2\theta_i}{\left[\varepsilon(\omega) - \sin^2\theta_i\right]^{\frac{1}{2}} + \varepsilon(\omega)\cos\theta_i}\cdot\frac{a\varepsilon(\omega)}{[1 - \varepsilon(\omega)]z + a}$$

$$\text{for} \quad -a \le z \le 0,$$

* Corresponding Author

$$\frac{\varepsilon(\omega)\sin 2\theta_i}{\left[\varepsilon(\omega)-\sin^2\theta_i\right]^{\frac{1}{2}}+\varepsilon(\omega)\cos\theta_i} \quad \text{for } z>0 \qquad (4)$$

This initial state wavefunction ψ_i used in eq (1) is the one deduced by Thapa and Kar [3] by employing Kronig – Penney potential model and had been applied to various cases [4-7] Experimentally measured values of dielectric constants [8] were used for calculating the photon fields Photocurrent was calculated form these metals for two values of the surface widths, namely $a = 0$ (narrow surface width) and $a = 10$ a u for the same values of surface state energy (10 24 eV) potential barrier height (14 99 eV) and $\theta_i = 45°$ Figure 1 shows the plot of photocurrent as a function of photon energy ($\hbar\omega$) in the case of Mo We find that for $a = 10$ a u a maximum in the value of photocurrent occurs at $\hbar\omega$ 10 eV With the further increase of photon energy photocurrent decreases to a minimum value at $\hbar\omega = 12$ eV and shows a small hump at $\hbar\omega = 14$ meV But for a narrow surface width ($a = 0$) the behavior of photocurrent is quite different as shown in Figure 1 We do not find any peak for values of photon energy below and above 12 eV

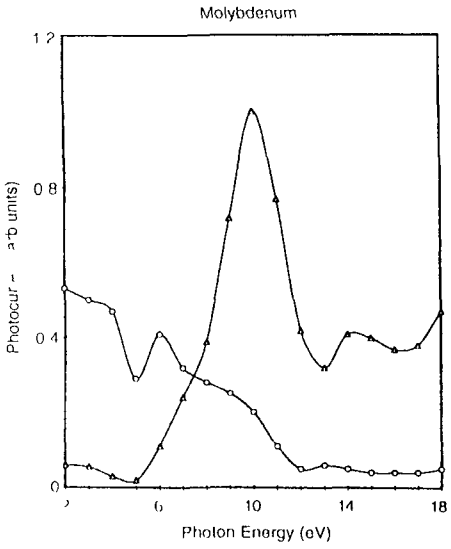

Figure 1 Plot of photocurrent from Mo as a function of photon energy (eV) for narrow surface width ($a = 0$) (open circles) and surface width $a = 10$ a u (triangle)

Figure 2 shows the plot of variation of photocurrent as a function of photon energy in the case of Cu For the surface width $a = 10$ a u the peak in the value of photocurrent occurs at $\hbar\omega = 20$ eV and decreases to a minimum at 26 eV photon energy A second peak is also seen in the case of Cu at $\hbar\omega = 30$ eV Copper shows totally different behavior for the narrow surface width ($a = 0$) which is evident from Figure 2

We find that both the metals Mo and Cu have shown atleast a qualitative agreement with the behavior of photocurrent as

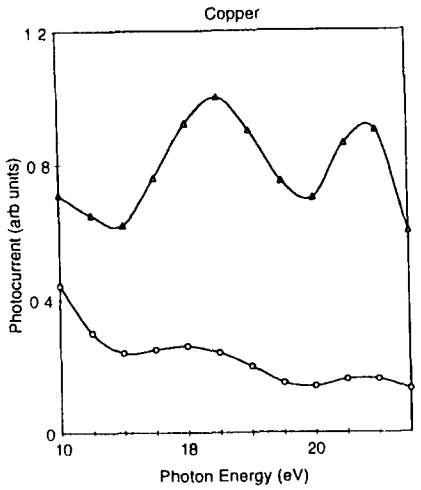

Figure 2 Plot of photocurrent from Cu as a function of photon energy (eV) for narrow surface width ($a = 0$) (open circles) and surface width $a = 10$ a u (triangle)

indicated also by other metals like Pd[4], W[5], Si[5] *etc* in which we have also used the Kronig-Penney potential model However, we see that the model employed do not exactly reproduce the earlier reported results For example, in the case of Mo, Weng *et al* [9] have shown that in the case of high lying surface state case photoemission intensity which is maximum at a photon energy of 15 eV, tends towards a minimum at 25 eV photon energy followed by a hump at $\hbar\omega = 30$ eV It does show a minimum in photocurrent at plasmon energy of Mo *i e* 24 4 eV The reasons for not exactly conforming to other models and the experimentally measured data [10] may be attributed to the fact that our model is a rather approximate one For example, it does not consider the details of the band structure effects Also the matrix element is mainly dependent on the variation of the vector potential as evidenced in previous cases [4,5] In fact, it is the variation of the vector potential which mainly modulates the matrix element thereby bringing in the changes in photocurrent This fact had been also argued by Weng *et al* [9] that the occurrence of a peak in photoemission intensity in the case of Mo is caused by the excitation of electrons by the A_z component of the vector potential He further pointed out that the initial states with Δ_1 symmetry can only be photoexcited by the A_z component of the incident photon field Though the model used here is simple, it gives first-hand information with regard to the effect of changes in surface width, as well as the location of initial state energy on photocurrent data

Acknowledgments

B Z and Z P acknowledge fellowship grants from Higher and Technical Education, Government of Mizoram Aizawl RKT and

PKP acknowledge a research grant from the University Grants Commission New Delhi

References

[1] D R Penn *Phys. Rev. Lett.* **28** 1041 (1972)

[2] R K Thapa and S G Davison *Indian J. Pure Appl. Phys.* **34** 118 (1996)

[3] R K Thapa and N Kar *Indian J. Pure Appl. Phys.* **26** 620 (1988)

[4] R K Thapa *Phys. Stat. Sol.* **B179** 391 (1993)

[5] R K Thapa and N Kar *Mod. Phys. Lett.* **B8** 361 (1994)

[6] R K Thapa and N Kar *Surf. Sci.* **338** 138 (1995)

[7] Z Pachuau S Gurung R K Thapa D T Khating and N Kar *Indian J. Phys.* **73A** 237 (1999)

[8] J H Weaver *Handbook of Chemistry and Physics* (Ohio CRC Press) 68th edn p E 377 (1987 88)

[9] S L Weng E W Plummer and T Gustafsson *Phys. Rev.* **B48** 1718 (1978)

[10] B J Wacklawski and E W Plummer *Phys. Rev.* **29** 783 (1972)

NH

VIER

11 February 2002

Physics Letters A 291 (2002) 52–57

PHYSICS LETTERS A

www.elsevier.com/locate/pla

Application of Mathieu potential to photoemission calculations: the case of a strong potential

Zaithanzauva Pachuau [a], B Zoliana [a], P K Patra [c], D T. Khating [b], R.K. Thapa [c,*]

[a] *Department of Physics, Government Zotlei Residential Science College, Aizawl 796 001, Mizoram, India*

[b] *Department of Physics, North Eastern Hill University, Shillong 793 022, India*

[c] *Condensed Matter Theory Research Group, Department of Physics, Pachhunga University College, Mizoram University, Aizawl 796 001, Mizoram, India*

Received 29 August 2001, accepted 18 December 2001

Communicated by J. Flouquet

Abstract

We have applied the Mathieu potential model to photoemission calculations from metals. The case of a strong potential is considered to describe the wavefunctions which is used for the evaluation of photocurrent from tungsten, molybdenum, copper and silicon. © 2002 Published by Elsevier Science B.V.

PACS: 73.20; 79.60

Keywords: Photoemission; Photocurrent; Wavefunction; Surface; Dielectric function

1. Introduction

We report here a simple formalism developed for photoemission studies by using the Mathieu potential to describe the bulk and the surface regions of metals. This case had been already reported [1] but in the case of aluminium and beryllium. Though the photocurrent data in these metals showed good behaviour conforming to some extent to the theoretical and experimental results published earlier, however, the nearly empty potential model ($q \sim 0$) had its own limitations. For example it could be applied only to the free electron type of metals. In order that the model could be extended to the case of metals which has strong potentials ($q > 0$), one can therefore make use of Mathieu potential model to strong and finite type of potentials to deduce the wavefunctions for the bulk and surface regions. Wavefunctions so deduced can be then used to calculate the photocurrent by evaluating the matrix element as a function of photon energy and surface width.

Mathieu potential has been used at first by Statz [2] for surface state calculations. Levine [3] had also used the Mathieu potential for calculating the conditions for arbitrary surface terminations. We have used in this formalism the model as described by Davison and Steslicka [4], as shown in Fig. 1. The simplest way to represent a periodic potential in a one-dimensional

* Corresponding author.
E-mail address: ramkumar_thapa@yahoo.com (R.K. Thapa).

0375-9601/02/$ – see front matter
PII: S0375-9601(01)00856-5

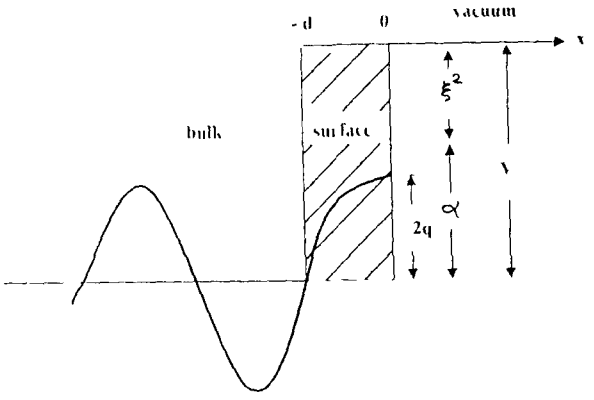

Fig. 1. Mathieu potential model used for calculating the initial state wavefunction ψ_i.

crystal is by a sinusoidal wave. For such type of potential Schrodinger equation reduces to well-known Mathieu equation. The amplitude V_a of the sinusoidal wave is a measure of the crystal potential strength. If V_a is small (large), the Mathieu potential model approaches the nearly free electron (tight binding approximation) limit and hence this model acts as a bridge between these two extreme cases. Two cases arises due to the effects of empty lattice and strong periodic lattice potential on the electronic states for deriving the electron wavefunctions. The case of empty lattice ($q \sim 0$) had been already reported [1], hence in this Letter we will focus our attention to the case of strong periodic lattice potential ($q > 0$).

2. Formalism

The photocurrent density formula from golden rule approximation can be written as

$$\frac{d_f(I)}{d\Omega} = \frac{2\pi}{\hbar}\sum\left|\langle\psi_f|H'|\psi_i\rangle\right|^2 \times \delta(L - E_f)\delta(E_f - E_i - \hbar\omega) \times f_0(E - \hbar\omega)\left[1 - f_0(E)\right], \quad (1)$$

where ψ_i (ψ_f) refer to the initial (final) state wavefunctions and perturbation H' can be written as

$$H = \left(\frac{e}{2m_e c}\right)(A\ \ p + p\ \ A)$$

where m_e is the mass of the electron, p is the one-electron momentum operator and A is the vector potential of the incident photon field. To compute the photon field we have used the simple dielectric model of Bagchi and Kar [5] which has been used earlier also [6,7]. With simple modifications the photon field used in our calculations for three regions can be written as

$$\tilde{A}_\omega(\omega, x) = \begin{cases} A_1, & x < -d, \\ \frac{A_1\varepsilon(\omega)d}{[1-\varepsilon(\omega)]x+d}, & -d \leqslant x \leqslant 0, \\ A_1\varepsilon(\omega), & x > 0, \end{cases} \quad (2)$$

where A_1 is a constant depending on the dielectric function $\varepsilon(\omega)$, photon energy $\hbar\omega$ and angle of incidence θ_i.

Considering one dimensional crystal its potential is represented by $V(x) = V_a\cos(2\pi x/a)$, where a is the period of the potential and maximum (repulsive) value is V_a at $x = 0$. The one-dimensional Schrodinger's equation can now be written as

$$\psi''(z) + (a - 2q\cos 2z)\psi(z) = 0, \quad (3)$$

where $2q = V_a/a$, $z = \pi x/a$, $T = (\pi/a)^2$, $a = E/T$. Here q is the magnitude of the potential which measures its strength. Eq. (3) can be solved for obtaining initial state wavefunction $\psi_i(x)$ for the bulk and surface regions ($x \leqslant 0$), and also for the vacuum regions ($x > 0$). These wavefunctions as derived are given as follows (in atomic units)

$$\psi_i(x, q) = \begin{cases} \left(\frac{1}{4\pi k_i}\right)^{1/2}\phi(x_0', q)e^{-\mu(x_0' - x)} \\ \quad (\text{for } \mu > 0), \quad x < 0, \\ (2\zeta)^{1/2}e^{-\zeta(x - x_0)} \\ \quad (\text{for } \zeta > 0), \quad x > 0, \end{cases} \quad (4)$$

where $x_0' = \pi/a\,x_0$, and x_0 is the location of the crystal surface plane. The other constants like μ, ζ, etc. have been already described earlier [1]. It is, therefore, necessary to find an explicit form of atomic orbitals $\phi(x_0', q)$ to derive the initial state wavefunction $\psi_i(x)$. The most general form is a linear combination of all the bulk standing states $se_m(x_0', q)$ and $ce_m(x_0', q)$ for all the Fermi energy gap m. Thus the surface states will be largely a hybrid of sine and cosine elliptic functions which is given by the expression

$$\phi(x_0', q) = \lambda_m ce_m(x_0', q) - se_m(x_0', q), \quad (5)$$

where λ_m is the hybridization parameter which can be written as

$$\lambda_m = \frac{se_m(x_0', q) - (\xi + \mu)^{-1}se_m'(x_0', q)}{ce_m(x_0', q) - (\xi + \mu)^{-1}ce_m'(x_0', q)} \quad (6)$$

The sine and cosine elliptic functions in Eq. (5) in expanded form can be written as

$$\begin{aligned} se_m(v_0', q) &= \sin m v_0' \\ &\quad - \frac{q}{4}\left[\frac{\sin(m+2)v_0'}{m+1} - \frac{\sin(m-2)v_0'}{m-1}\right] \\ &\quad + \frac{q}{3}\left[\frac{\sin(m+4)v_0'}{(m+1)(m+2)} + \frac{\sin(m-4)v_0'}{(m-1)(m-2)}\right] \\ &\quad + \end{aligned} \tag{7}$$

and

$$\begin{aligned} ce_m(v_0', q) &= \cos m v_0' \\ &\quad - \frac{q}{4}\left[\frac{\cos(m+2)v_0'}{m+1} - \frac{\cos(m-2)v_0'}{m-1}\right] \\ &\quad + \frac{q}{3}\left[\frac{\cos(m+4)v_0'}{(m+1)(m+2)} + \frac{\cos(m-4)v_0'}{(m-1)(m-2)}\right] \\ &\quad + \end{aligned} \tag{8}$$

For finite surface potential, surface state existence condition implies that

$$v_0 = \frac{a}{2}, \qquad \xi = \frac{12}{a}, \qquad \lambda > 0, \quad \text{and}$$
$$m = 3, 5 \tag{9}$$

We are considering surface state occurring for $m = 3$ and hence from Eqs. (7) and (8) we can write

$$\begin{aligned} &ce_3(v_0', q) = 0, \\ &ce_3'(v_0', q) = 3\left(1 + \frac{q}{16} - \frac{q^2}{640}\right), \\ &se_3(v_0', q) = -1 + \frac{q}{16} - \frac{11}{640}q^2, \\ &se_3'(v_0', q) = 0 \end{aligned} \tag{10}$$

The hybridization constant λ_3 now reduces to

$$\lambda_3 = \frac{(\xi+\mu)\left[1 - \frac{q}{16} + \frac{11}{640}q^2\right]}{3\left(1 + \frac{q}{16} - \frac{q^2}{640}\right)}. \tag{11}$$

Since Eq. (9) is the condition for the surface state existence, with the help of Eqs. (10) and (11), therefore the initial state wavefunctions corresponding to electronic states in the surface and bulk, and vacuum regions can be written as

$$\psi_i(x, q) = \begin{cases} \left(\frac{1}{4\pi k_i}\right)^{1/2}\left(1 - \frac{q}{16} + \frac{11}{640}q^2\right) \\ \quad \times e^{-\mu(v_0' - v)}, \quad x \leqslant x_0', \\ (2\zeta)^{1/2} e^{-\xi(v - v_0')}, \quad x > x_0'. \end{cases} \tag{12}$$

The derivation of $\psi_i(x, q)$ is discussed in detail by Pachuau [8].

The final state wavefunction ψ_f used is the scattering state [9] of the step potential which is encountered by the electron. Step potential is defined by $V(x) = -V_0\theta(x)$, where $\theta(x)$ is unit function such that $\theta(x) = 1$ (0) for $x > 0$ ($x < 0$). The final state wavefunction which is the solution of the step potential is given by (in atomic units)

$$\psi_f(z) = \begin{cases} \left(\frac{1}{2\pi q_f}\right)^{1/2} \frac{2q_f}{q_f + k_f} e^{ik_f z} e^{-a|z|}, \\ \quad z < 0 \quad \text{(bulk and surface)}, \\ \left(\frac{1}{2\pi q_f}\right)^{1/2}\left[e^{iq_f z} + \left(\frac{q_f - k_f}{q_f + k_f}\right)e^{-iq_f z}\right], \\ \quad z > 0 \quad \text{(vacuum)}, \end{cases} \tag{13}$$

where $k_f^2 = 2E_f$, $q_f^2 = 2(E_f - V_0)$ and $E_f = E_i + \hbar\omega$. In Eq. (13), the factor $e^{-a|z|}$ is included on the surface and bulk side to take into account the inelastic scattering of the electrons.

Photocurrent was calculated as a function of photon energy ($\hbar\omega$) in the case of d-band metals like molybdenum, tungsten, copper and semiconductor silicon. For each of these metals, the experimentally determined dielectric function [10,11] were used for calculating the photon fields but the same surface parameters were used for all of these solids as it is a model calculation.

3. Results and discussion

3.1. Tungsten and molybdenum

The plot of photocurrent as a function of photon energy ($\hbar\omega$) for W and Mo is shown in Figs. 2 and 3 both for surface width $d = 10$ a.u. and narrow surface width ($d = 0$). We have considered the case of high lying surface state as was done by Weng et al. [12]. The high lying surface state lies at -0.4 (-0.3 eV) for W (Mo). The peak in photocurrent occurred at $\hbar\omega = 15$ eV in the case of both W and Mo. But as the value of photon energy increased, the photocurrent decreased and

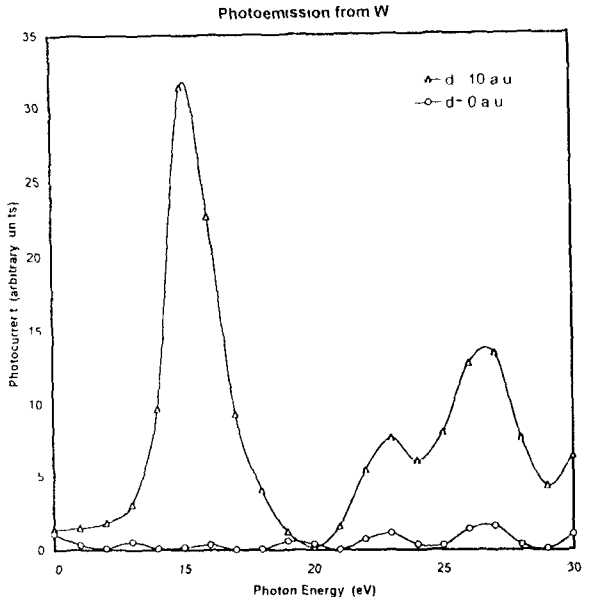

Fig. 2. Plot of photocurrent (in arbitrary units) against the photon energy (eV) for W for the surface width $d = 10$ a.u. and narrow surface width $d = 0$.

showed minimum at the photon energies 20 (21 eV) in the case of W (Mo). The plasmon energies of W and Mo are respectively 25.3 and 24.4 eV. Both of these metals showed a shoulder in photocurrent again at $\hbar\omega = 23$ eV followed by a peak of smaller height at $\hbar\omega = 27$ eV. The ratio between the two peaks in photocurrent at photon energies 15 and 23 eV is approximately 13% (49%) in the case of W (Mo). However, the case of narrow surface width did not exhibit such behaviour in photocurrent for both the metals W and Mo.

The experimental data of Weng et al. [12] showed that the ratio between the two peaks in photocurrent in the case of W and Mo are approximately 45% and 54%. This is a close approximation to our calculated data. Also the occurrence of second peak in photocurrent in our calculated data in both W and Mo is closely related to the experimental data of Weng et al. [12]. However the minimum in photocurrent for W (Mo) did not occur at the plasmon energies which was clearly displayed by the experimental data. We thus find that the Mathieu potential model used in this calculation for defining the initial state wavefunction is a useful model as the data calculated showed at least the qualitative behaviour with the experimental results.

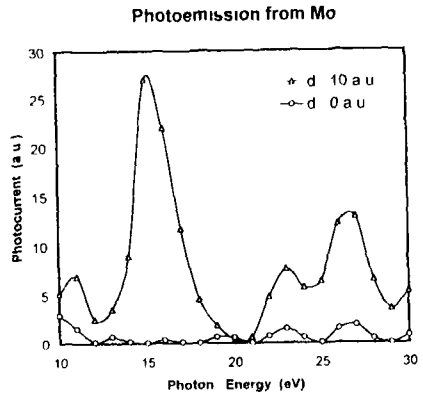

Fig. 3. Plot of photocurrent (in arbitrary units) against the photon energy (eV) for Mo for the surface width $d = 10$ a.u. and narrow surface width $d = 0$.

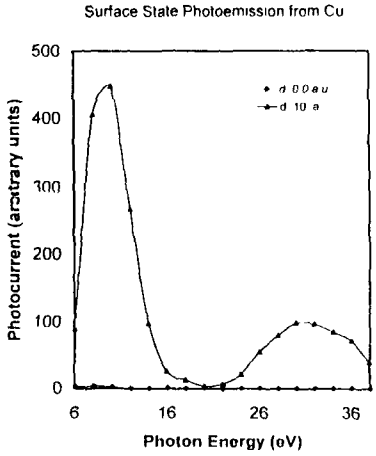

Fig. 4. Plot of photocurrent (in arbitrary units) against the photon energy (eV) for Cu for the surface width $d = 10$ a.u. and narrow surface width $d = 0$.

3.2. Copper

We have plotted the behaviour of photocurrent as a function of photon energy both for surface width $d = 10$ a.u. and narrow surface width for Cu (Fig. 4). For the surface width $d = 0$ a.u., the photocurrent showed a maximum at $\hbar\omega = 10$ eV and decreased to minimum at 20 eV, the plasmon energy of Cu. At photon energy $\hbar\omega = 30$ eV, it showed a second peak in current but of lower height than at $\hbar\omega = 10$ eV.

It has been reported by Himpsel and Ortega [13] that for Cu(100), Fermi level photoemission intensity when plotted as a function of photon energy, the data showed maxima at $\hbar\omega = 10.5$ eV. Similar reports were

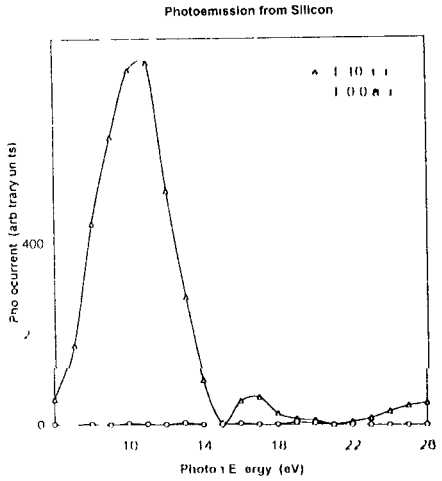

Fig. 5. Plot of photocurrent (in ubitrary units) against the photon energy (eV) for Si for the surface width $d = 10$ a.u. and narrow surface width $d \sim 0$.

also given by Eastman et al. [14] but with maximum intensity occurring at $\hbar\omega = 10.6$ eV. In our case our model calculations has shown peak in photocurrent at $\hbar\omega = 10$ eV. The occurrence of such peak in photocurrent in the band structure had been attributed to transition in energy between the lower and upper s–p bands either at the Fermi level or near it and has Δ_5 symmetry. The case of photocurrent for narrow surface width just produced a linear line of very negligible magnitude in photocurrent. We find that Cu has shown at least the qualitative feature with the behaviour of photocurrent as indicated also by other metals like W [5], Pd [6], Si [4], etc. which were calculated earlier.

3.3. Silicon

We have also used this model for calculating photocurrent from semiconductor Si which is shown in Fig. 5 for surface width $d = 10$ a.u. we find that photocurrent showed a maximum height at $\hbar\omega = 10$ eV followed by a minimum at $\hbar\omega = 15$ eV. A second peak of small magnitude was found at $\hbar\omega = 17$ eV and decreased again to minimum at 21 eV with further increase in photon energy. This can be attributed to the behaviour of $\varepsilon(\omega)$ for silicon [15] which has a resonance at 21 eV. In the case of Si also for the case of narrow surface width the magnitude of photocurrent is negligible for all the values of photon energy.

We also have calculated the wavefunction given in Eq. (12) to see whether this can reproduce the results calculated earlier in the case of empty potential ($q \sim 0$) and for surface state condition $m = 1$. When this was applied to the case of aluminium (Al) and beryllium (Be), respectively, it was seen that the photocurrent data matched exactly the earlier reported data [11] both for Al and Be. Further, the origin of the occurrence of the peak in photocurrent for the values of photon energies below the plasmon energies of metals has been attributable to the spatial variation of the photon fields in the surface region. This has been indicated [6] by the plot of $d\tilde{A}_0/dx$ against x for values of photon energy at which peak in photocurrent occurred.

A study of these cases show that one can also make use of Mathieu type of potential in photoemission calculations. Though the model used is very simple, however the inclusion of initial state wavefunction into the matrix element appears to produce the qualitative features as observed earlier in the experimentally measured data of photocurrent. The main drawback of the model used is that the same initial state wavefunction ψ_i is used to describe both the surface and bulk regions of the solids under study. We have used the constant initial state energy for all the cases and also kept constant other parameters as it is a model calculation. However, it is interesting to note that the wavefunctions formulated for strong periodic potential easily reproduces the wavefunctions for empty potential (free electron) cases. It was also found that bulk potential had very little effect on photoemission. This fact had been explained by Levinson and others [16,17] as seen in the case of aluminium. Further the large drop in the value of photocurrent as photon energy approached the plasmon energy is due to the decrease in the value of $d\tilde{A}_0/dx$.

Acknowledgements

R.K.T. and his research group is grateful to Prof. A.K. Sharma, Vice-Chancellor, Mizoram University, Aizawl for his inspiration and encouragement. Dr. C. Thanthianga, Principal, Pachhunga University College, Aizawl and Dr. D.K. Baikakati, Head, Physics Department, Pachhunga University College, Aizawl has given all the help and support. Dr. S.G. Davison and Mrs. Prue Davison, University of Waterloo

Ontario, Canada, have provided the relevant literature connected to the works reported here. Z.P. and B.Z. thanks UGC (Guwahati) for the sanction of a research grant. This work was funded by University Grants Commission, New Delhi.

References

[1] Z. Pachuau, B. Zohlana, D.T. Khating, P.K. Patra, R.K. Thapa, Phys. Lett. A 275 (2000) 459.
[2] H. Stutz, Z. Naturforsch. 5A (1950) 534.
[3] J.D. Levine, Phys. Rev. 17 (1950) 701.
[4] S.G. Davison, M. Steslicka, Basic Theory of Surface States, Clarendon, Oxford, 1992.
S.G. Davison, J.D. Levine, Solid State Phys. 25 (1970) 2.
[5] A. Bagchi, N. Kar, Phys. Rev. B 18 (1978) 5240.
[6] R.K. Thapa, Phys. Stat. Sol. B 179 (1993) 391.
[7] R.K. Thapa, N. Kar, Phys. Rev. B 51 (1995) 17980.
[8] Z. Pachuau, Ph.D. thesis submitted to North Eastern Hill University, Shillong, India (2001).
[9] L.D. Landau, E.M. Lifshitz, Quantum Mechanics, Addison-Wesley, Reading, MA, 1958, p. 60.
[10] J. Weaver, Handbook of Chemistry and Physics, CRC Press, Boca Raton, FL, 1987.
[11] E.D. Pallik (Ed.), Handbook of Optical Constants of Solids, Academic Press, 1991, p. 429.
[12] S.L. Weng, T. Gustaffson, E.W. Plummer, Phys. Rev. B 18 (1978) 1718.
[13] F.J. Himpsel, J.E. Ortega, Phys. Rev. B 46 (1992) 9719.
[14] D.E. Eastman, J.A. Knapp, F.J. Himpsel, Phys. Rev. Lett. 41 (1978) 825.
[15] R.K. Thapa, Ph.D. thesis, North Bengal University, Darjeeling, India (1993).
[16] H.J. Levinson, E.W. Plummer, P.J. Feibelman, Phys. Rev. Lett. 43 (1979) 952.
[17] R.K. Thapa, N. Kar, Mod. Phys. Lett. B 8 (1994) 361.

International Journal of Modern Physics B
Vol 17, No 15 (2003) 2897 2902

World Scientific
www worldscientific com

A MODEL PHOTOEMISSION CALCULATIONS USING PROJECTION OPERATOR METHOD

B ZOLIANA[‡], ZAITHANZAUVA PACHUAU[‡], LALTHAKIMI ZADENG[†], R K THAPA[*,†], P. K. PATRA[§] and D T KHATHING[¶]

[†]*Condensed Matter Theory Research Group, Department of Physics, Pachhunga University College, Mizoram University, Aizawl, Mizoram 796001 India*
[‡]*Department of Physics, Govt. Zirtiri Residential Science College, Aizawl, Mizoram 796001 India*
[§]*Science Education Centre, North-Eastern Hill University, Shillong 793003 India*
[¶]*Department of Physics, North-Eastern Hill University, Shillong 793022 India*
[*]*rktt@sancharnet.in*

Received 10 January 2003

We have shown in this report the application of projection operator method of group theory in deriving the wavefunctions for the surface state in Cu(110) which had been used in calculating photocurrent This approach gives a qualitative characterization of surface states simply on the basis of existing bulk-band structure calculations.

1. Introduction

Photoemission involved the interaction of radiation with electron of the solid. The electrons which are in the valence band or lying at the Fermi level or below it, are perturbed and photoexcited. Some of these photoexcited electrons which gains sufficient kinetic energy are able to overcome the work function and hence are excited to the vacuum. They in fact contribute to the photocurrent which are measured by the detector. Theoretically photocurrent is calculated by evaluating the matrix element $\langle \Psi_f | H' | \Psi_i \rangle$ involved in the photocurrent density formula as given by Fermi golden rule. Due to the presence of the surface, the calculations of electronic states $|\Psi_i\rangle$ is a complicated problem. Ordinarily, a crystal state of an electron is defined by a Bloch wavefunction. Hence there may be generally two types of electron states which are of importance namely,

(i) Incident-reflected pair of bulk Bloch waves which are propagating within the crystal but evanescent in the vacuum. Such states have the same energy as that of the bulk.

*Author for correspondence

(ii) A surface electron wave which propagates along the boundary with **k** parallel to the surface/interface. This wave is concentrated in the surface and is evanescent both in the bulk and the vacuum regions.

The identification of such states to those lying in the bulk band gaps leads to complex wavevector. These states pertain to surface states. In this report, we are presenting a model calculation of electronic state defined by Ψ_i which represents the surface electronic states and is calculated by employing the projector operator technique of group theory. This had been applied[1] to calculate photocurrent from the Cu(110) surface states.

2. Formalism

The photocurrent density formula from golden rule approximation can be written as

$$\frac{dj(E)}{d\Omega} = \frac{2\pi}{\hbar}\sum |\langle\psi_f|H'|\psi_i\rangle|^2\delta(E-E_f)\delta(E_f-E_i-\hbar\omega)f_0(E-\hbar\omega)[1-f_0(E)] \quad (1)$$

where $\Psi_i(\Psi_f)$ refer to the initial (final) state wavefunctions and the perturbation H' can be written as

$$H' = \left(\frac{e}{2m_e c}\right)\cdot(\mathbf{A}\cdot\mathbf{p}+\mathbf{p}\cdot\mathbf{A})$$

with m_e the mass of the electron, $\mathbf{p}$ the one-electron momentum operator and $\mathbf{A}$ the vector potential of the incident photon field. To compute the photon field we have used the simple dielectric model, which has also been used earlier.[3,4] With simple modifications the photon field used in our calculations for three regions can be written as

$$\tilde{A}_\omega(\omega,z) = \begin{cases} A_1 & z<-d \quad (bulk) \\ \dfrac{A_1\varepsilon(\omega)d}{[1-\varepsilon(\omega)]z+a} & -d\le z\le 0 \ (surface) \\ A_1\varepsilon(\omega) & z\ge 0 \quad (vacuum) \end{cases} \quad (2)$$

where A_1 is a constant depending on the dielectric function $\varepsilon(\omega)$, photon energy $\hbar\omega$ and angle of incidence θ_i.

The final state wavefunction $|\Psi_f\rangle$ used is the scattering state of the step potential which is encountered by the electron. Step potential is defined by $V(z) = V_0\theta(z)$ where $\theta(z)$ is unit function such that $\theta(z) = 1(0)$ for $z > 0$ ($z < 0$).

The final state wavefunction which is the solution of the step potential is given by (in atomic units):

$$\psi_f(z) = \begin{cases} \left(\dfrac{1}{2\pi q_f}\right)^{\frac{1}{2}} \dfrac{2q_f}{q_f+k_f} e^{\imath k_f z} e^{-\alpha|z|} & z<0 \\ \left(\dfrac{1}{2\pi q_f}\right)^{\frac{1}{2}} \left(e^{\imath q_f z}+\dfrac{q_f-k_f}{q_f+k_f}\right) e^{-\imath q_f z} & z>0 \end{cases} \quad (3)$$

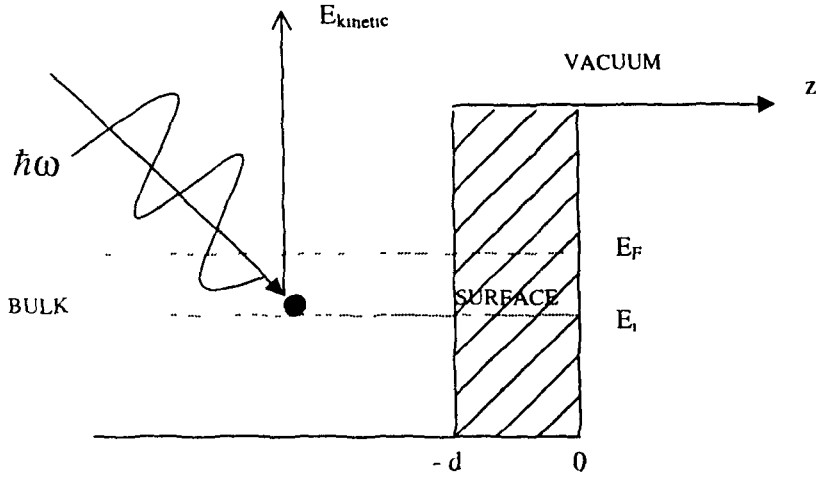

Fig. 1. Model potential diagram for calculating Ψ_i defining the bulk, surface (of width d) and vacuum regions

where

$$k_f^2 = 2E_f\,, \qquad q_f^2 = 2(E_f - V_0) \quad \text{and} \quad E_f = E_i + \hbar\omega\,.$$

In Eq. (3), the factor $e^{-\alpha|z|}$ is included on the surface and bulk to take into account of the inelastic scattering of the electrons. To calculate initial state wavefunction Ψ_i, we have assumed empty lattice potential as shown in Fig. 1. In one dimension, one can write Ψ_i as

$$\Psi_i(z) = \begin{cases} \phi(z)(e^{ik_i z} + Re^{-ik_i z})e^{\mu z} & \text{surface \& bulk} \quad z < 0 \\ Te^{-\chi z} & \text{vacuum} \qquad\qquad z > 0 \end{cases} \tag{4}$$

where $\phi(z)$ is the atomic orbitals which is calculated using projection operator *method of group theory*. The coefficients $\mathbf{R}$ and $\mathbf{T}$ are evaluated by matching the wavefunctions and its derivative at $z = 0$ and are given by

$$\begin{aligned} R &= -\frac{(1+k_i) - i(\chi+\mu)}{(1-k_i) - i(\chi+\mu)}\,, \\ T &= -\frac{2k_i}{(1-k_i) - i(\chi+\mu)}\,. \end{aligned} \tag{5}$$

For Cu(110), surface state occurs[4] in the $L_{2'} - L_1$ band gap. The LCAO representation for $L_{2'}$ point is $(x+y+z)/\sqrt{3}$. We have therefore considered the point $L_{2'}$ for which the point group is C_{2v}. We have obtained the basis function for the C_{2v} point group corresponding to Cu(110) surface state using the projection operator formula[5]

$$P^p_{mn} = \frac{l_p}{g} \sum_T \Gamma^p(T)^*_{mn} P(T)\,. \tag{6}$$

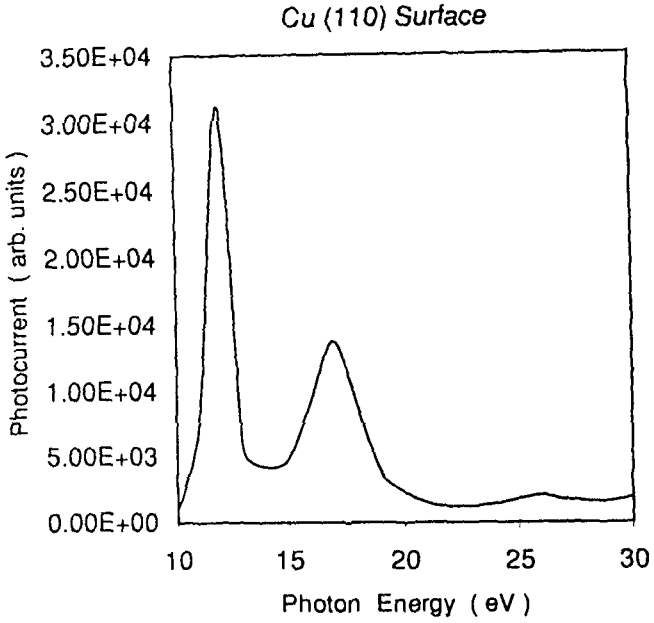

Fig. 2. Plot of photocurrent as a function of photon energy for surface state located at 2.72 eV below Fermi level (surface width $d = 10$ a.u.)

Here l_p is the dimension of the unitary irreducible representation of the group G of Schrödinger equation, g is the order of G and $\sum_T$ is the summation over all transformation of T on G. The final form of Ψ_i obtained in one dimension can be written as

$$\Psi_i(z) = \begin{cases} e^{i\mathbf{k}_\parallel \mathbf{R}_\parallel} e^{\mu z}(e^{ik_i z} + Re^{-ik_i z}) \\ Te^{i\mathbf{k}_\parallel \mathbf{R}_\parallel} e^{-\chi z} \end{cases}, \tag{7}$$

where $k_i^2 = 2E_i$, $\chi^2 = 2(V_0 - E_i)$, $\mu = k_i - \pi/a$ and a is the lattice constant.

Evaluation of photocurrent density given by Eq. (1) now reduces to the evaluation of the integral

$$I = \int_{-\infty}^{-a} \Psi_f^* \tilde{A}_\omega \Psi_i dz + \int_{-a}^{0} \Psi_f^* \tilde{A}_\omega \frac{d}{dz} \Psi_i dz + \frac{1}{2} \int_{-a}^{0} \Psi_f^* \frac{d\tilde{A}_\omega}{dz} \Psi_i dz + \int_0^\infty \Psi_f^* \tilde{A}_\omega \varepsilon(\omega) \Psi_i dz . \tag{8}$$

Integrals in Eq. (8) are evaluated numerically.

3. Results and Discussions

We have applied the model wavefunction developed for calculating photocurrent from Cu(110) surface, where two surface states have been observed experimentally in photoemission[6,7] and inverse photoemission[8,9] measurements. Surface states[4]

were found to exist in the band gap $L_{2'} - L_1$ and we have considered in our calculations only the surface state occurring at symmetry point $L_{2'}$. As it is a model calculation and also we are interested in the effect of wavefunction Ψ_i on the matrix element for photocurrent evaluation, hence an empty potential was assumed to exist for Cu. Experimentally determined dielectric constants were used to calculate the photon field vector in Eq. (2), and the lattice constant for Cu was chosen to be $a = 3.61$ Å. We have assumed the surface state to be located at 2.72 eV below the Fermi level of Cu. The variation of photocurrent against photon energy pertaining to this surface state is shown in Fig. 2. We find that photocurrent is maximum when photon energy ($\hbar\omega$) is 12 eV, and it decreases to a minimum at $\hbar\omega = 14$ eV. Further increase in photon energy causes it to rise to a second maximum at around $\hbar\omega = 17$ eV, after which the photocurrent decreases towards minimum. This decrease in the photocurrent is due to the presence of the term α associated with the wavefunction. We find that the dielectric model used in this calculation, which incorporates the wavefunction Ψ_i in the matrix element, gives photocurrent results which showed similar variation as that found in metals like[2,3] Be, W etc. Furthermore, the photocurrent data in the case of the Cu(110) surface state showed better qualitative agreement than that obtained using the Mathieu potential[10] model. However the wavefunction Ψ_i used in the model calculation defines both the bulk and the surface electronic states which in fact is not appropriate. We need a specific type of wavefunction separately for the surface and the bulk regions. Furthermore we have not considered the effect of crystal potential and it had been assumed to be an empty potential type which is not correct as Cu belongs to *d*-band type metals where the potential is very strong. However, as shown by Bertel,[4] we find that projection operator technique can be used to obtain a symmetry analysis of surface states to generate symmetry-adapted surface state wavefunctions which can also be used for photoemission calculations.

Acknowledgments

RKT and PKP acknowledges a research grant, and LZ a fellowship from Department of Atomic Energy (Mumbai). RKT also thanks Prof. S. Mukherji (North Bengal University, Darjeeling) for permitting him to avail facilities of IUCAA. B. Z. acknowledges a senior research fellowship from Directorate of Higher and Technical Education, Govt. of Mizoram, Aizawl.

References

1. B. Zoliana, Zaithanzauva Pachuau, P. K. Patra, D. T. Khating and R. K. Thapa, *3rd Regional Conference on Physics Research in North East*, Dibrugarh University, Dibrugarh, Assam, India, 9th Nov. 2002.
2. R. K. Thapa and N. Kar, *Mod. Phys. Letts.* **B8**, 361 (1994).
3. R. K. Thapa and N. Kar, *Phys. Rev.* **B51**, 17980 (1995).
4. E. Bertel, *Phys. Rev.* **B50**, 4925 (1995).

5. J. F. Cornwell, Group Theory and Electronic Energy Bands in Solids, Amsterdam-London (North-Holland, 1969), p. 54.
6. P. Heimann, J. Hermann, H. Miosga and H. Neddermeyer, *Surf. Sci.* **85**, 263 (1979).
7. S. D. Kevan, *Phys. Rev.* **B28**, 4822 (1983).
8. P. Sandl and E. Bertel, *Surf. Sci. Lett.* **302**, L325 (1994).
9. W. Jacob, V. Dose, U. Kolac, Th. Fauster and A. Goldmann, *Z. Phys.* **B63**, 459 (1986).
10. Zaithanzauva Pachuau, B. Zoliana, P. K. Patra, D. T. Khathing and R. K. Thapa, *Phys. Letts.* **A294**, 52 (2002).

Indian J Phys 77A (4), 393–396 (2003)

Note

AN INTERNATIONAL JOURNAL
IJPA

Photoemission studies of metals by using Mathieu potential

B Zoliana[1], Zaithanzauva Pachuau[1], Lalthakimi Zadeng, P K Patra[2], D T Khathing[3] and R K Thapa*

Condensed Matter Theory Research Group, Department of Physics, Pachhunga University College, Mizoram University, Aizawl, Mizoram 796 001, India

[1]Department of Physics, Govt Zirtiri Residential Science College, Aizawl, Mizoram-796 001, India

[2]Science Education Centre, North Eastern Hill University, Shillong-793 003, Meghalay, India

[3]Department of Physics, North-Eastern Hill University, Shillong-793 022, Meghalay, India

E mail rktt@sancharnet in

Received 25 February 2003 accepted 7 March 2003

Abstract Photocurrent results from ferromagnetic materials Fe and Ni and *d*-band metals Pd and Cr is discussed which is calculated by using the Mathieu potential for the crystal A local dielectric functions have been used to calculate the electromagnetic field for the bulk, surface and vacuum regions of the metals

Keywords Photoemission, metals, Mathieu potential

PACS Nos 79 60 Bm 77 22 Ch

Mathieu potential had been applied to photoemission calculations by Pachuau *et al* [1] in the case of empty potential and a strong potential [2] These cases had been applied to free-electron type metals like Al and Be for empty potentials and *d*-band type metals Cu, W, Mo and also Si It has been seen that surface photoeffect had been exhibited in these metals for values of incident photon energies below and above the plasmon energy but within low photon energy range With this view in mind, we present in this Note, the extension of Mathieu potential model developed to the calculations of photocurrent from ferromagnetic metals Ni and Fe and transition metals Pd and Cr

The photocurrent density formula [1] from golden rule approximation can be written as

$$\frac{dj(E)}{d\Omega} = \frac{2\pi}{\hbar}\sum\left|\langle\psi_f\left|H'\right|\psi_i\rangle\right|^2\delta(E-E_f) \times\delta(E_f-E_i-\hbar\omega)f_0(E-\hbar\omega)[1-f_0(E)], \quad (1)$$

where $\Psi_i(\Psi_f)$ refer to the initial (final) state wavefunctions, perturbation H' can be written as

$$H' = \left(\frac{e}{2m_e c}\right)(A\,p + p\,A),$$

where m_e is the mass of the electron, p the one-electron momentum operator and A is the vector potential of the incident photon field With simple modifications, the photon field used in our calculations for three regions can be written as

$$\tilde{A}_\omega(\omega,x) = \begin{cases} A_1, & x<-d \quad \text{(bulk)}, \\ \dfrac{A_1.\varepsilon(\omega)\,d}{[1-\varepsilon(\omega)]x+d}, & -d\le x\le 0 \quad \text{(surface)}, \\ A_1\,\varepsilon(\omega), & x\ge 0 \quad \text{(vacuum)}, \end{cases} \quad (2)$$

where A_1 is a constant depending on the dielectric function $\varepsilon(\omega)$, photon energy $\hbar\omega$ and angle of incidence θ, $\varepsilon(\omega)$ is defined locally and interpolates linearly between the bulk

*Corresponding Author

and the vacuum values Considering one-dimensional crystal, its potential is represented by $V(x) = V_a \cos 2\pi x/a$, where a, is the period of the crystal potential and maximum (repulsive) value is V_a at $x = 0$. The one dimensional Schroedinger's equation can now be written as

$$\frac{d^2\Psi}{dz^2} + (a 2q \cos 2z)\Psi = 0, \tag{3}$$

where $2q = \frac{V_a}{a}$, $z = \frac{\pi x}{a}$, $T = \left(\frac{\pi}{a}\right)^2$, $a = \frac{E}{T}$. Here, q is the magnitude of the potential which measured its strength. Eq (3) can be solved for obtaining initial state wavefunction $\Psi_i(x)$ for the bulk and surface regions ($x \le 0$) and also for the vacuum regions These wavefunctions as derived are given by (in atomic units) :

$$\Psi_i(x,q) = \begin{cases} \left(\frac{1}{4\pi k_i}\right)^{1/2}\left(1 - \frac{q}{16} + \frac{11}{640}q^2\right)e^{-\mu(x_0' - x)}, & x \le x_0', \\ (2\varsigma)^{1/2} e^{-\xi(x - x_0')}, & x > x_0'. \end{cases} \tag{4}$$

The derivation of $\Psi_i(x,q)$ had been discussed in detail by Pachuau [2,3]

The step potential at the surface encountered by an electron is defined by $V(x) = -V_0\theta(x)$, where $\theta(x)$ is unit function such that $\theta(x) = 1(0)$ for $x > 0$ ($x < 0$). The final state wavefunction which is the solution of this step potential and is given by (in atomic units) :

$$\psi_f(x) = \begin{cases} \left(\frac{1}{2\pi q_f}\right)^{1/2} \frac{2q_f}{q_f + k_f} e^{ik_f x} e^{-\alpha|x|}, & x < 0 \text{ (bulk and surface)}, \\ \left(\frac{1}{2\pi q_f}\right)^{1/2}\left(e^{iq_f x} + \frac{q_f - k_f}{q_f + k_f}\right)e^{-iq_f x}, & x > 0 \text{ (vacuum)}, \end{cases} \tag{5}$$

where $k_f^2 = 2E_f$, $q_f^2 = 2(E_f - V_0)$ and $E_f = E_i + \hbar\omega$

In eq. (5), the factor $e^{-\alpha|x|}$ is included on the surface and bulk side to take into account the inelastic scattering of the electrons

Photocurrent was calculated from metals Fe, Ni, Pd and Cr as a function of incident photon energy ($\hbar\omega$) for two different values of surface width d = 10 a.u. and d = 0.0. The real and imaginary parts of dielectric constants were calculated for each of these metals by using the experimentally determined values [4] of refractive indices and absorption coefficients (extinction constant). However, we have used the same surface parameters $E_i, \theta, \ldots$, for all the metals as was used in the case of Cu

Refering to Figure 1, we have plotted photocurrent as a function of photon energy ($\hbar\omega$) in the case of Fe. It is observed that maximum in photocurrent is obtained at $\hbar\omega = 15$ eV for d = 10 a.u. For further increase in photon energy, photocurrent decreases and becomes minimum at $\hbar\omega = 19$ eV. A second peak of small height in photocurrent is obtained at $\hbar\omega = 24$ eV. Similarly in the case of Ni also,

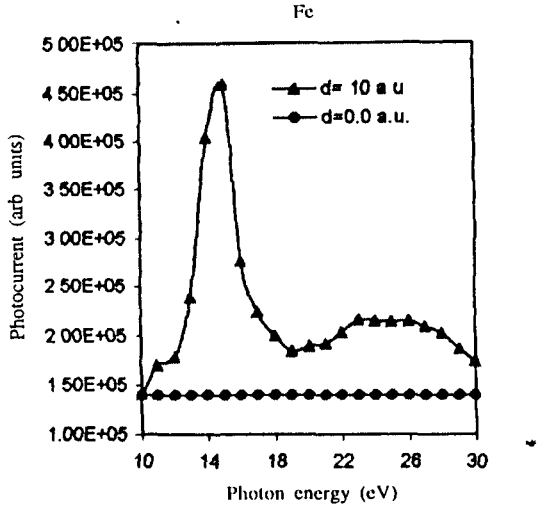

Figure 1. Variation of photocurrent against photon energy for surface width d = 10 0 a u and narrow surface width (d = 0 0 a u) in the case of Fe

we have plotted (Figure 2) photocurrent as a function of photon energy for d = 10 a.u. For Ni, we find a maximum in photocurrent at photon energy $\hbar\omega = 15$ eV, but it decreases towards zero as photon energy is further increased.

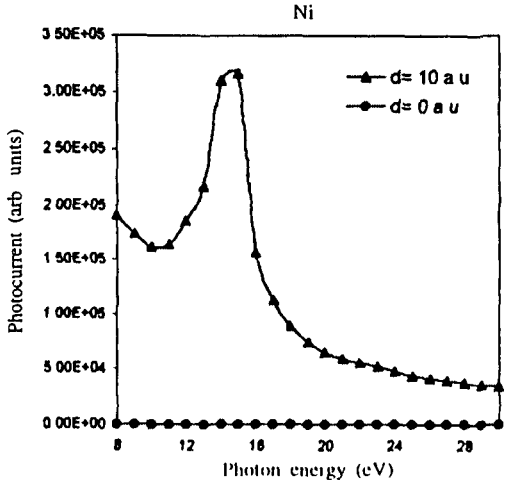

Figure 2. Same as in Figure 1 in the case of Ni

Besides these two magnetic metals, photocurrent was also calculated in the case of Pd and Cr with the same initial parameters as was used in the case of Fe and Ni. The behaviour of photocurrent is shown in Figure 3. For surface width d = 10 a.u., we find that a maximum in photocurrent occurred at $\hbar\omega = 8$ eV, decreased to minimum at

$\hbar\omega = 15$ eV. It showed a small hump in photocurrent for $\hbar\omega = 17$ eV and decreased to minimum again for further increase of photon energy. Photocurrent data of Pd showed behaviour exactly similar to that obtained by Thapa [5] but by using the Kronig-Penney potential model. For narrow surface width, photocurrent data showed a constant value also for Pd when plotted against photon energy.

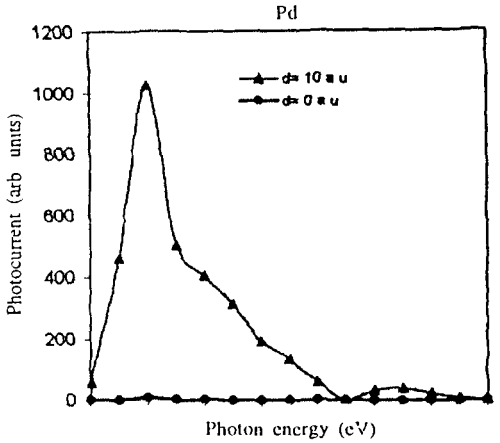

Figure 3. Same as in Figure 1 in the case of Pd.

We show in Figure 4, the plot of photocurrent as a function of photon energy in the case of Cr. For $d = 10$ a.u., there is a peak in photocurrent obtained at $\hbar\omega = 14$ eV. Again, photocurrent decreased to minimum at $\hbar\omega = 19$ eV and showed a second hump of lower magnitude at $\hbar\omega = 27$ eV. Cr also showed similar behaviour for narrow surface width as seen in the case of Fe, Ni and Pd.

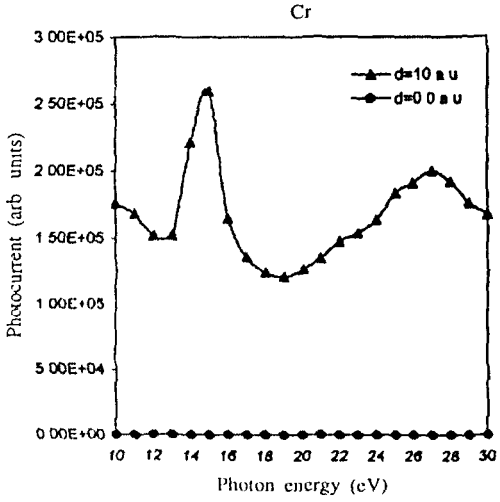

Figure 4. Same as in Figure 1 in the case of Cr.

We find from our results that in the low photon energy range all the metals showed similar trends in the behaviour of photocurrent for both the surface widths. The origin of first peak at $\hbar\omega = 8$ eV in the case of Pd is attributed to surface photoeffect as explained by Thapa [5]. This had been evidenced by the plot of field for photon energy below and above 8 eV. The decrease in photocurrent to minimum after the first peak in all the metals is due to loss of photon energy by excitations of bulk plasmons. Plasmons in metals and semiconductors play a significant role in transport and optical properties. Surface plasmons and in general, the dynamical screen properties at the surface attracted therefore considerable attention [6,7]. Surface plasmons in particular, are of importance as it is linked to the position of the centroid of the screening charge [8] at the surface plasmon frequency. We assume the surface plasmon frequency (ω_S) to be the value of photon frequency at which photocurrent is maximum and this is related to bulk plasmon frequency (ω_B) by $\omega_S = \omega_B\sqrt{2}$. Further, it had been already shown from electrodynamics of surface phenomena [9] that at frequency $\omega \approx \omega_B$, the component of electromagnetic field (vector potential) tends towards minimum which causes the photocurrent to be also minimum. We find that the metals under study, satisfy this condition although bulk plasmon frequency (energy) is not a well-defined quantity. Here, we have considered it to be equal to the value at which $\varepsilon_1 \to 0$.

We have also plotted photocurrent as a function of $\hbar\omega$ for narrow surface width *i.e.* $d = 0$ a.u. by including Fresnel fields for all the metals under study. The behaviour of photocurrent in this case, was found to be quite different. There is no peak in photocurrent found as in the case for $d = 10$ a.u. The photocurrent in this case, is constant and remains parallel with the x-axis. This indicates that inclusion of field is important in photoemission calculations.

We have tried in this report to see the effect of Mathieu type of potential on photoemission calculations. We find that photocurrent results from these metals showed similar behaviour as had been obtained by Thapa *et al* [10] in the case of other metals and semiconductors [11]. However, the main drawback of the model presented here is that the same initial state wavefunction is used both for the surface and the bulk regions of the metal to calculate the photocurrent. We are working to represent the initial state wavefunction accurately for these regions by applying the projection operator method of group theory [12].

Acknowledgments

RKT and PKP thanks University Grants Commission, New Delhi for a research grant. Prof. S G Davison and Prue Davison, Department of Applied Mathematics and Physics, University of Waterloo, Ontario, Canada, have helped with many relevant literature connected with the works reported here.

References

[1] Z Pachuau, B Zoliana, D T Khating, P K Patra and R K Thapa, *Phys Lett* **A275** 459 (2000)

[2] Zaithanzauva Pachuau, B Zoliana, P K Patra, D T Khating and R K Thapa *Phys Lett* **A294** 52 (2002)

[3] Zaithanzauva Pachuau *PhD Thesis* (unpublished) (North-Eastern Hill University, Shillong, India)

[4] J Weaver *Handbook of Chemistry and Physics* (Boca Raton : CRC Press) (1987)

[5] R K Thapa *Phys Stat Sol* **B179** 391 (1993)

[6] P J Feibelman *Prog Surf Sci* **12** 287 (1982)

[7] P Apell, A Ljungbert and S Lundqvist *Phys Scripta* **30** 367 (1984)

[8] M Rocca and F Moresco *Prog Surf Sci* **53** 331 (1996)

[9] Zaithanzauva Pachuau, B Zoliana, P K Patra and R K Thapa *3rd Regional Conference on Physics Research in North-East* (Dibrugarh University, Dibrugarh, India, 9th November 2002)

[10] R K Thapa and N Kar *Phys Rev* **B51** 17980 (1995)

[11] R K Thapa and N Kar *Mod Phys Lett* **B8** 361 (1994)

[12] B Zoliana, Zaithanzauva Pachuau, P K Patra, D T Khating and R K Thapa *3rd Regional Conference on Physics Research in North-East* (Dibrugarh University, Dibrugarh, India, 9th November 2002), B Zoliana, Z Pachuau, R K Thapa, Lalthakimi Zadeng, P K Patra and D T Khathing *Intl J Mod Phys B* (accepted)

Photoemission calculations from transition metals Ni and Fe

R.K.Thapa*, Lalthakimi Zadeng, S.Srivastava, B.Zoliana[a], Z.Pachuau[a] and P.K Patra[b]

Condensed Matter Theory Research Group, Department of Physics
Pachhunga University College, Mizoram University, Aizawl 796 001 Mizoram

[a] Department of Physics, Government Zirtiri Residential Science College,
Aizawl 796 001, Mizoram
[b] Science Education Centre, North Eastern Hill University, Shillong 793 003, Meghalaya

ABSTRACT

We have applied the Kronig - Penney model potential to calculate photocurrent from ferromagnetic metals Ni and Fe. Spatially dependent vector potential had been used to evaluate the relevant matrix elements for calculating photocurrents.

Key Words : Photoemission, photocurrent, vector potential, plasmon, photon energy.

PACS No.: 79.60 Bm

---

*Author for correspondence
E-mail : rktt@sancharnet.in
FAX : 0091-389-2323491
Phone : 0091-389-2328044

Magnetic materials are very important as they play key role in the generation and distribution of electric power, and in communication it finds use in the data storage and retrieving mechanism. This application in information technology has made therefore, the thin film technology as the center of primary interest in Solid State Physics. In order to therefore comprehend the microscopic origin of the novel magnetic effects of thin film and multilayers, the electronic structure, in particular that of surfaces and interfaces needs to be studied. Theoretical study of the electronic structure along with the experiment is important in understanding the properties of magnetic materials. Angle-resolved photoemission technique is now one of the most widely used experimental tools for studying the band structure of metals, semiconductors as well as that of superconductors. In this brief report a simple study of the behavior of photocurrent data is presented for ferromagnetic metals Ni and Fe in the low photon energy range.

In this report, we present a simple treatment of photoemission in which photocurrent is calculated by using the golden rule formula given by

$$\frac{dj(E)}{d\Omega} = \frac{2\pi}{\hbar}\sum |< \psi_f |\Delta| \psi_i >|^2 \, \delta(E - E_f)\delta(E_f - E_i - \hbar\omega) f_o(E - \hbar\omega)[1 - f_o(E)] \qquad (1)$$

where Δ is the perturbation responsible for photoemission by radiation of frequency ω and $\psi_i\ (\psi_f)$ refers to the initial (final) state wavefunction, $E_i(E_f)$ the initial (final) state energy, $f_o(E)$ denotes the Fermi occupation function. We are considering the photoemission to take place along z – axis which is normal to the surface. We may therefore write Δ in one-dimension as

$$\Delta \approx \frac{e}{2mc}\left[\tilde{A}_\omega(z)\frac{d}{dz}+\frac{1}{2}\frac{d}{dz}\tilde{A}_\omega(z)\right] \tag{2}$$

where $\tilde{A}_\omega(z) = A^z_\omega(z)/A_O$ is the component of vector potential along z -axis, A_o is the amplitude of the incident beam. We assume z-direction to be perpendicular to the surface which is chosen as z = 0 plane. The metal is assumed to occupy all space to the left of the z=0 plane. The response of the electromagnetic field is bulk-like everywhere except in the surface region defined by $-a \le z \le 0$. In this region, the model dielectric function is chosen to be local one, which interpolates linearly between the bulk value inside the metal ($z < -a$) and the vacuum value (unity) outside ($z > 0$). The model frequency-dependent dielectric function used is therefore given by,

$$\varepsilon(\omega, z) = \begin{cases} \varepsilon(\omega) \equiv \varepsilon_1(\omega) + i\varepsilon_2(\omega), & z \le -a \\ 1+[1-\varepsilon(\omega)](z/a), & -a \le z \le 0 \\ 1, & z \ge 0 \end{cases} \tag{3}$$

We consider a p - polarized light to be incident on the surface plane making an angle θ_i with the z - axis. The vector potential of interest in the long wavelength $(\omega a/c) \to 0$ is given by

$$\tilde{A}_\omega(z) = \begin{cases} B, & z \le -a \\ B\,a\,\varepsilon(\omega)/\{[1-\varepsilon(\omega)]z + a\}, & -a \le z \le 0 \\ B\,\varepsilon(\omega), & z \ge 0. \end{cases} \tag{4}$$

where $B = -\dfrac{sin2\theta_i}{[\varepsilon\varepsilon(-sin^2\theta_i]^{\frac{1}{2}}+\varepsilon(\omega)cos\theta_i}$.

The initial state wavefunction ψ_i used in Eq. (1) is the one deduced by Thapa and Kar[1] by employing Kronig - Penney potential model and had been applied to various cases [2 - 4]. Photocurrent was calculated form these metals for two values of the surface widths, namely a = 0 (narrow surface width) and a = 10 a.u. for the same values of surface state energy (11.1 eV), potential barrier height = 15.75 eV, $\theta i = 45^{o}$, scattering factor α = 0.5 and phase shift (δ) = - 0.5055. The dielectric constants were calculated from the experimental values[5] of refractive index (n) and absorption coefficient (k). For each of the metal under study we have plotted the values of photocurrent as a function of incident photon energy ($\hbar\omega$) for two different values of surface widths namely a = 10 a. u. and a = 0. 0 a.u. (narrow surface width.)

Fig.1 shows the plot of photocurrent[6] in the case of ferromagnet Ni. For a = 10 a.u. photocurrent showed a maximum at $\hbar\omega \approx$ 10eV and decreased to minimum at 14 eV photon energy. A second hump in photocurrent was obtained at $\hbar\omega$ = 20 eV and decreased with the further increase of photon energy.

We have also plotted the variation of photocurrent against the incident photon energy in the case of narrow surface width (a = 0.0). As the magnitude of photocurrent was too small compared to the values for a = 10 a.u., photocurrent values for each photon energy was multiplied by 5 times to get it magnified and significant too. However the behavior of photocurrent for this case is quite different and did not exhibit any minima at $\hbar\omega_p$ or maxima below $\hbar\omega_p$ (the plasmon energy of Ni).

In Fig. 2 we show the plots of photocurrent in the case of Fe. In this case we find maxima in photocurrent at $\hbar\omega$ = 10 eV followed by a minimum at $\hbar\omega$ = 12 eV for a = 10 a. u. Another hump in photocurrent is seen at $\hbar\omega$ = 15 eV. The photocurrent data for narrow surface width is also plotted but its behavior is similar as in the case of Ni.

Ni is the best understood of the magnetic transition metals, certainly the most studied, and is believed to be an itinerant-electron ferromagnet. The experimental optical density of states (DOS) of ferromagnet Ni consists of high density[7] d-bands extending from E_F to about 5.6 eV. Keeping this in mind, photocurrent in the case of Ni was calculated from its Fermi level. The plasmon energy of Ni as experimentally found is ~ 21 eV and at this photon energy, photocurrent is normally expected to be minimum as also exhibited by other metals like Al[2], W[3], Pd[4], Be[8] etc. However in our case, we get minimum in photocurrent at ~14eV photon energy. The deviation in the occurrence of minimum from 21 eV to 14 eV in the case of Ni can be attributed mainly due to refraction effects in which the electromagnetic field plays the vital role. At plasmon frequency, the component of electromagnetic field perpendicular to the surface is zero due to which photocurrent decreases to minimum. Similar explanations can be attributed to the case of behavior of photocurrent in Fe. However in the case of these two metals, we have assumed plasmon energy to be 12 eV at which photocurrent tends towards a minimum value.

The occurrence of maxima in photocurrent at $\hbar\omega < \hbar\omega_p$ is due to surface effect. This fact had been explained already in the case of other metals[2-6] by considering the location of the surface state wavefunction in and around the surface plane.

We have attempted in this report to present the dependence of photocurrent on the frequency of the incident photon field and the surface thickness. Photocurrent had been calculated in low photon energy range in order not to photoexcite the bulk oscillation. The reason for this being that the excitations are basically due to surface photo effect and the photocurrent peak therefore occurs at $\hbar\omega_s = \hbar\omega_p/\sqrt{2}$ which is the surface plasmons value.

R.K.T. and P.K.P. acknowledges a research grant from University Grants Commission, New Delhi. R.K.T also thanks Prof. S. Mukherji, Inter University Centre for Astronomy and Astrophysics, Physics Department, North Bengal University, Darjeeling (W. B.), for financial support and computational facilities. G. D. acknowledges sanction of fund for a Minor Research Project by University Grants Commission, Guwahati (Assam).

References :

1. R.K. Thapa and N. Kar, *Indian Jour. Pure and Appld. Phys.* 26 (1988) 620.
2. P. Das, R.K. Thapa and N. Kar, *Mod. Phys. Letts.* B5 (1991) 65.
3. R.K. Thapa and N. Kar, *Surf. Sci.*, 138 (1995) 338.
4. R.K. Thapa, *Phys. Stat. Solidi*, 179 (1993) 391.
5. J. Weaver, in *Handbook of Chemistry and Physics of Solids* (CRC Press, Boca Raton, Ohio) 1987, p. E-377.

6. Lalthakimi Zadeng, S. Srivastava, R.K. Thapa, P.K. Patra, B. Zoliana and Z. Pachuau, *3rd Regional Conference on Physics Research in North East*, Dibrugarh University, 9th Nov. 2002.

7. D.E. Eastman, *J. Appld. Phys.* 40 (1969) 1387.

8. R.K.Thapa and N. Kar, Phys. Rev. B51 (1995) 17980.

FIGURE CAPTIONS :

Figure 1 : Variation of photocurrent (in arb. units) against photon energy (eV) for narrow surface width (a = 0.0) and for surface of width a = 10.0 a. u. in the case of Ni.

Figure 2 : Variation of photocurrent (in arb. units) against photon energy (eV) for narrow surface width (a = 0.0) and for surface of width a = 10.0 a. u. in the case of Fe.

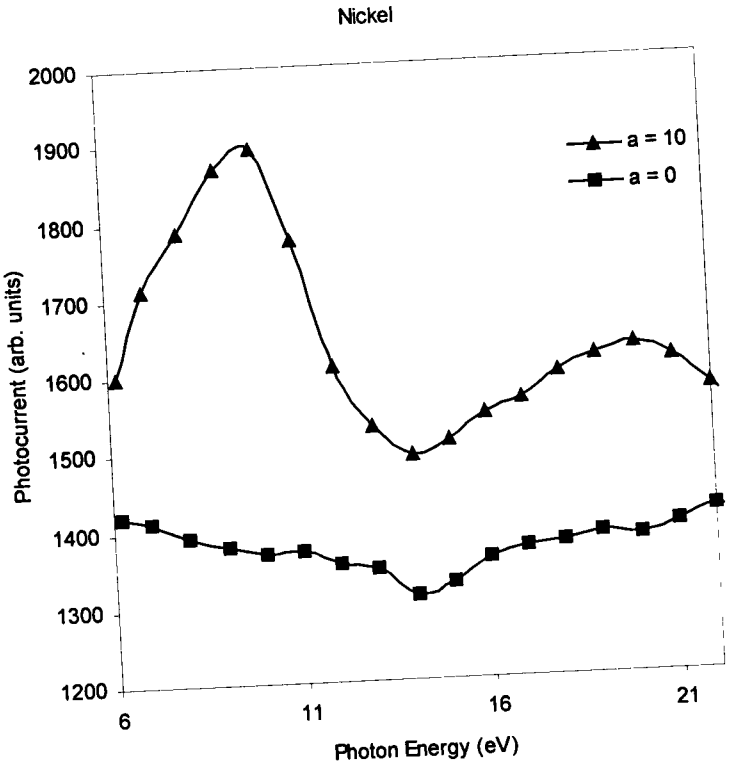
Nickel
2000
1900
1800
1700
1600
1500
1400
1300
1200
Photocurrent (arb. units)
6
11
16
21
Photon Energy (eV)
a = 10
a = 0

Figure 1.

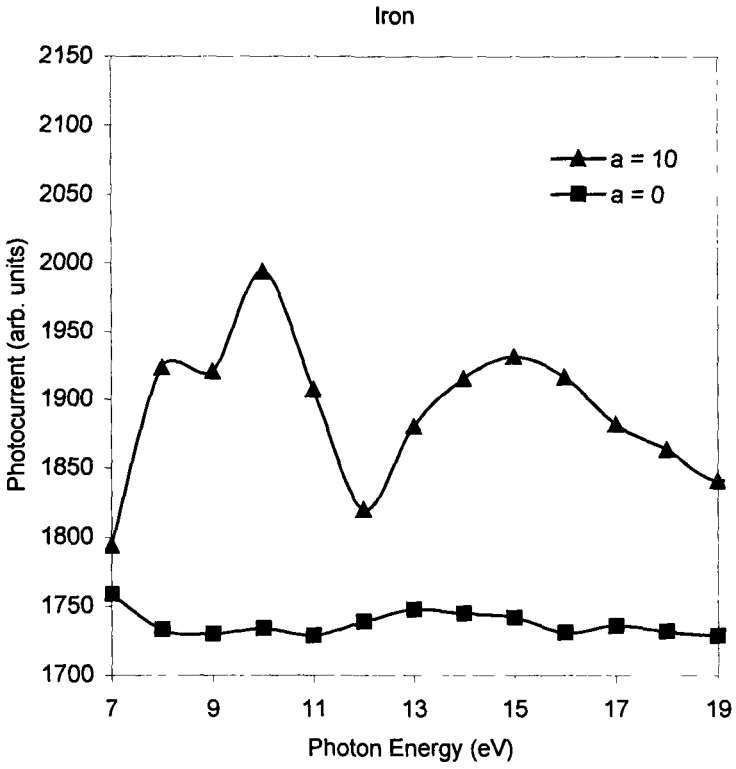

Figure 2.